SUDBURY NEUTRINO OBSERVATORY

Proposal

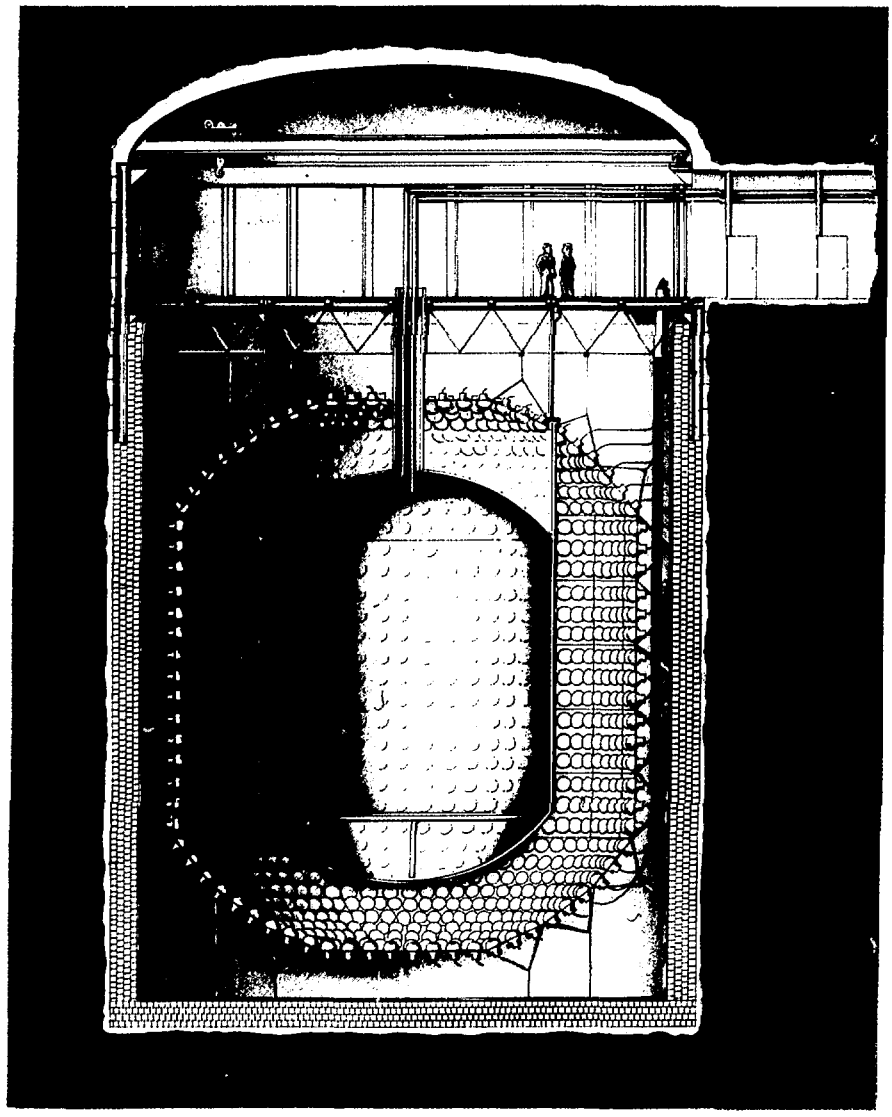

Participating Institutions

Queen's University
University of California at Irvine
Oxford University
National Research Council of Canada
Chalk River Nuclear Laboratories
University of Guelph
Laurentian University
Princeton University
Carleton University

SNO-87-12
1987 October

SUDBURY NEUTRINO OBSERVATORY PROPOSAL

G.T. Ewan, H.C. Evans, H.W. Lee, J.R. Leslie, H.-B. Mak,
W. McLatchie, B.C. Robertson, P. Skensved
Queen's University at Kingston

R.C. Allen, G. Bühler, H.H. Chen, P.J. Doe
University of California at Irvine

D. Sinclair, N.W. Tanner
University of Oxford

J.D. Anglin, M. Bercovitch, W.F. Davidson,
C.K. Hargrove, H. Mes, R.S. Storey
National Research Council of Canada

E.D. Earle, G.M. Milton
Chalk River Nuclear Laboratories, Atomic Energy of Canada Ltd.

P. Jagam, J.J. Simpson
University of Guelph

A.B. McDonald
Princeton University

E.D. Hallman
Laurentian University

A.L. Carter, D. Kessler
Carleton University

October 1987

As of January 15, 1988 the Collaboration has been expanded and includes the following additional members and institution:

University of Pennsylvania: E.W. Beier, W. Frati, F.M. Newcomer, R. Van Berg

Princeton University: R.T. Kouzes, M.M. Lowry

Queen's University: J.D. MacArthur

Laurentian University: R.U. Haq

Shaped by the vision, wisdom, and enthusiasm of Herbert Chen (1942 - 1987), this proposal is dedicated to his memory by his friends and colleagues in the Sudbury Neutrino Observatory collaboration.

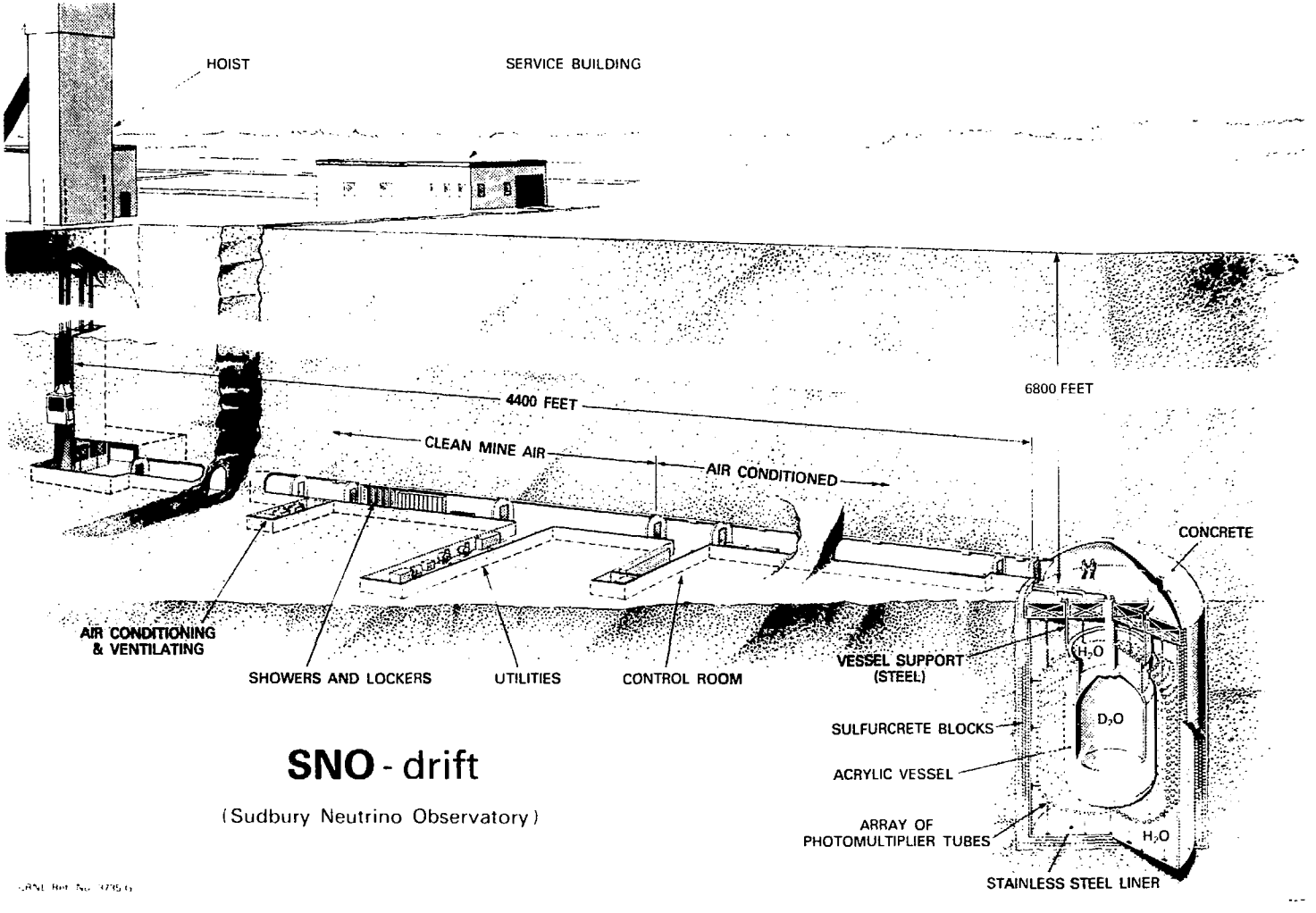

Artistic Conception of the Sudbury Neutrino Observatory at the Creighton Mine.

Contents

Executive Summary

We propose to develop a world class observatory for neutrino astrophysics. This observatory will contribute both to astrophysics by clarifying the basic energy generating processes in the Sun and to nuclear and particle physics by determining fundamental properties of the neutrinos themselves. The observatory will make use of heavy water as its principal sensitive medium. Deuterium has properties which make it an ideal detector material and we propose to exploit the availability, on loan, of 1000 tonnes of heavy water from Canada's reserves to realize a unique and versatile neutrino detector. The detector would be located deep underground in the Creighton Mine (owned by INCO Limited) in the town of Walden, near Sudbury.

A fundamental hypothesis in models of the evolution of the Sun and stars is that energy generation takes place by nuclear fusion in their interiors. The only direct test of this hypothesis is to detect the neutrinos produced in these reactions since neutrinos interact only through the weak interaction and can escape largely unimpeded from the interior. The results of solar neutrino experiments to date indicate that the flux of electron-neutrinos emitted in the decay of ^{8}B in the solar interior is at least a factor of three lower than that calculated with the best models of solar energy generation, a twenty year old discrepancy known as the Solar Neutrino Problem. Two classes of solution to this problem have been suggested; either the model of the Sun is deficient so that the neutrinos are not produced in the expected quantities, or the neutrinos change in some way in transit to Earth so that they are not detected (neutrino oscillations). While both possibilities have been discussed in the literature for many years, it has been realized only recently that there is a mechanism whereby electron-neutrinos produced in the Sun might be converted into other neutrino types with high efficiency in passing through solar matter. This mechanism requires that at least some neutrino types have mass and that there is some mixing of

neutrino states. The observation of this effect would have profound implications for fundamental physics.

New tools are required to resolve the Solar Neutrino Problem. The proposed detector would have a sensitivity more than an order of magnitude greater than those of previous detectors and would make use of three reactions to characterize completely the high-energy solar neutrino flux. The electron-neutrino would be detected by its interaction with the deuteron to form two protons and an electron which carries off most of the energy. By measuring the energy of the electron, the neutrino spectrum could be deduced and any spectral distortion due to neutrino oscillations in the Sun would be measured. All neutrino types can scatter inelastically from the deuteron causing the deuteron to break up into a neutron and a proton. This reaction would be detected by observing the γ-rays from the subsequent capture of the free neutron and is a measure of the total neutrino flux, providing a test of solar models even if neutrino oscillations occur. The relative rates for these two reactions would establish whether or not conversion of neutrinos from electron type to some other type is responsible for the Solar Neutrino Problem. The third reaction to be studied is elastic scattering of neutrinos from electrons. This gives a good measure of the direction of the neutrino flux and would confirm that the observed neutrinos came from the Sun.

The dramatic appearance of supernova Shelton 1987A in February of this year has highlighted the importance of neutrino detection in the understanding of the physics of stellar collapse. The unprecedented sensitivity and versatility of the proposed detector would enable it to play an important role in studying supernovae occuring in our Galaxy. In addition to offering information on the dynamics of the supernova, the sensitivity to the muon- and tau-neutrinos might allow their masses to be measured and, in particular, test the hypothesis that neutrinos form the dark matter known to exist in the Universe.

The unique property of the neutrino which enables it to travel from the Sun's core to Earth without significant interaction also imposes considerable demands on detector design. The detector must be large so that a statistically significant number of neutrino events can be detected in a reasonable time and it must be well shielded from all sources of background. These constraints require that a large volume of heavy water (1000 tonnes) be placed deep underground (to attenuate the cosmic rays). All of the materials used in the detector must meet very stringent requirements on

radioactive purity and much of the research to date by the proposers has been devoted to developing new technologies to detect and remove sources of radioactivity to achieve ultra-low levels of contamination.

This document provides a detailed description of the detector, its anticipated operating characteristics, its sources of background and its construction sequence and costs. A number of Supporting Documents have been prepared for the collaboration by engineering firms, and Annexes detailing the relevant scientific work of the collaboration form a part of this submission. The proposal is the result of three years of intensive effort by a collaboration of scientists from Canada, the USA and the UK. During the past year INCO Limited has cut a 180 metre long access drift to the proposed detector location in preparation for geotechnical measurements. The observatory could be built in four years at a capital cost (including contingencies) of $35 million (Canadian) and would be operated as a National Facility administered under an Institute of Neutrino Physics at an annual cost of $1.8 million. The proposed administrative structure would facilitate the development of other underground experiments at the Creighton mine.

We are proposing that Canadian scientists and engineers, in collaboration with colleagues in the USA and UK, seize the opportunity presented by a temporary surplus of heavy water and a highly favourable underground site, to build a neutrino observatory superior to any presently proposed. The observatory will be at the forefront of neutrino astronomy and would establish a centre for underground science. It will attract scientists and their experiments from many countries, and will provide a National Facility for basic research and education well into the next century.

Résumé de L'Étude

Nous envisageons de construire un observatoire de classe internationale pour l'astrophysique des neutrinos. Cet observatoire apportera une contribution à la fois à l'astrophysique, en élucidant les processus fondamentaux de production d'énergie au sein du Soleil, et à la physique nucléaire et des particules, en déterminant les propriétés fondamentales des neutrinos proprement dits. L'observatoire utilisera l'eau lourde comme principal milieu sensible. Le deutérium a des propriétés qui en font un matériau détecteur idéal et nous nous proposons d'exploiter les 1000 tonnes d'eau lourde provenant des réserves canadiennes, et qui ont été mises à notre disposition à titre de prêt, pour réaliser un détecteur de neutrinos polyvalent et sans équivalent. Ce détecteur serait installé à grande profondeur dans la mine Creighton (appartenant à INCO Limited) à Walden, près de Sudbury.

Une des hypothèses fondamentales utilisées dans les modèles de l'évolution du Soleil et des étoiles est que la production d'énergie résulte d'une fusion nucléaire intervenant à l'intérieur de ces astres. Le seul moyen qui s'offre à nous de démontrer la validité de cette hypothèse de façon directe est de détecter les neutrinos produits au cours de ces réactions étant donné que les neutrinos n'interagissent que par l'entremise de l'interaction faible et qu'ils s'échappent du milieu solaire pratiquement sans interagir. Les résultats des expériences conduites jusqu'à ce jour sur les neutrinos solaires indiquent que le flux de neutrinos électroniques émis au cours de la désintegration de ^{8}B à l'intérieur du Soleil est inférieur d'au moins un facteur de trois à celui qui a été calculé avec les meilleurs modèles existants de production d'énergie solaire. Cette divergence, connue depuis vingt ans, porte le nom de "problème des neutrinos solaires". On a, jusqu'à présent, proposé deux types de solutions à ce problème: ou bien le modèle du Soleil est incorrect et, de ce fait, la production de neutrinos est inférieure à celle escomptée, ou bien les neutrinos changent d'une façon ou d'une autre pen-

dant leur transit vers la Terre de telle sorte qu'ils ne sont plus détectés (oscillations de neutrinos). Ces deux possibilités font l'objet de discussions dans la littérature scientifique depuis de nombreuses années, mais ce n'est que tout récemment qu'on a réalisé qu'il existe un mécanisme par lequel des neutrinos électroniques produits dans le Soleil pourraient bien être convertis en d'autres types de neutrinos avec un rendement élevé au cours de leur traversée de la matière solaire. Ce mécanisme exige toutefois qu'au moins un de ces types de neutrinos ait une masse et que les états des neutrinos soient couplés. L'observation de cet effet aurait de profondes implications pour la physique fondamentale.

La solution du problème des neutrinos solaires exige de nouveaux outils. Le détecteur proposé aurait une sensibilité dépassant d'un ordre de grandeur celle des détecteurs précédents et reposerait sur trois réactions pour caractériser complètement le flux des neutrinos solaires de haute énergie. Le neutrino électronique serait détecté grâce à son interaction avec le deutéron, qui produit deux protons et un électron, ce dernier emportant la majeure partie de l'énergie. En mesurant l'énergie de l'électron, il deviendrait possible de déduire le spectre des neutrinos et de mesurer d'éventuelles distorsions spectrales dues aux oscillations des neutrinos dans le Soleil. Tous les types de neutrinos peuvent interagir de façon inélastique avec le deutéron, qui se dissocie alors en un neutron et un proton. Cette réaction serait détectée par l'observation des rayons-γ résultant de la capture subséquente du neutron libre et apporterait une évaluation du flux total de neutrinos, ce qui permettrait une vérification du modèle du Soleil qui ne serait pas affectée par l'existence d'oscillations de neutrinos. La comparaison des taux relatifs de ces deux réactions permettrait de savoir une fois pour toutes si la conversion de neutrinos du type électronique en un autre type quelconque est à l'origine du problème des neutrinos solaires. La troisième réaction qui serait étudiée est celle de la diffusion élastique des neutrinos avec des électrons. Ceci donne une bonne indication de la direction du flux des neutrinos et permet donc de vérifier que les neutrinos observés proviennent du Soleil.

L'apparition spectaculaire de la supernova Shelton 1987A en février 1987 a révélé l'importance que revêt la détection des neutrinos pour comprendre la physique de l'effondrement stellaire. La sensibilité et la polyvalence inégalées à ce jour du détecteur envisagé lui permettraient de jouer un rôle important dans l'étude des supernovae apparaissant dans notre Galaxie. Non seulement nous permettra-t-il de recueillir des données sur la dynamique des supernovae, mais également, il rendra possible, grâce à

sa sensibilité, une mesure des masses des neutrinos associés au muon et au tau et, en particulier, de vérifier la validité de l'hypothèse selon laquelle les neutrinos constitueraient la masse invisible dont on admet l'existence dans l'Univers.

La propriété unique du neutrino, propriété qui lui permet de se déplacer du centre du Soleil jusqu'à la Terre sans interaction importante, requiert également qu'une attention considérable soit apportée à la conception du détecteur. Ce détecteur doit avoir de grandes dimensions pour permettre la détection d'un nombre statistiquement suffisant d'interactions de neutrinos au cours d'un laps de temps raisonnable et il doit être bien isolé de toutes les sources de bruit de fond. Ces contraintes peuvent être satisfaites en situant une grande quantité d'eau lourde (1000 tonnes) à grande profondeur dans le sol, afin de minimiser la source de bruit de fonds que constitue le rayonnement cosmique. Tous les matériaux utilisés dans la construction du détecteur doivent renfermer un très faible contenu d'impuretés radioactives et l'essentiel de la recherche effectuée à ce jour a visé à développer de nouvelles technologies permettant de produire des matériaux avec un très faible niveau de radioactivité.

Le présent document décrit le détecteur en détail, ses caractéristiques prévues de fonctionnement, ses sources de bruit de fond, ainsi que l'échelonnement et ses coûts de construction. Un certain nombre de documents techniques ont été rédigés en vue d'une collaboration avec des compagnies d'ingénierie et des annexes couvrant le détail des travaux scientifiques afférents à cette collaboration constituent partie intégrante de la présente proposition. Ladite proposition est l'aboutissement de trois années d'efforts intensifs de scientifiques du Canada, des États-Unis et du Royaume-Uni. En vue des mesures géotechniques qui doivent être faites, INCO Limited a creusé au cours de la dernière année une galerie d'accès de 180 mètres de long jusqu'au lieu où sera mis en place le détecteur envisagé. L'observatoire pourrait être construit en quatre années au coût de 35 millions de dollars canadiens (frais accessoires compris) et serait exploité à titre d'installation nationale administrée par un institut de physique des neutrinos au coût annuel de 1,8 million de dollars. La structure administrative envisagée faciliterait la mise en place d'autres expériences souterraines à la mine Creighton.

Nous proposons que les scientifiques et ingénieurs canadiens, en collaboration avec leurs collègues des États-Unis et du Royaume-Uni, saisissent l'occasion présentée par un excédent temporaire d'eau lourde et un site souterrain favorable pour construire un observatoire de neutrinos, supérieur

à tout ce qui a pu être proposé jusqu'à présent. Cet observatoire sera à la fine pointe de l'astronomie des neutrinos et constituera un centre pour la science souterraine. Il attirera des scientifiques de nombreux pays et nous dotera d'une installation nationale vouée à la recherche fondamentale et à l'enseignement qui répondra encore à nos besoins bien au-delà de l'an 2000.

Chapter 1

Introduction

Our present knowledge of the Sun, the stars and the more distant constituents of the Universe, has come mainly from a study of their electromagnetic radiations. However, many of the most fundamental processes such as the nuclear reactions which generate the energy in the Sun, take place in regions completely inaccessible by electromagnetic observations. It was realized more than 20 years ago that the weakly-interacting neutrinos emitted by these nuclear reactions could be used to probe those regions. To date, two measurements of the flux of solar neutrinos have been performed and they both indicate that the flux is two to three times smaller than expected. This discrepancy, which has come to be known as the Solar Neutrino Problem (SNP), may arise because the theories of stellar energy generation are incomplete, or because the electron-neutrinos generated in the Sun have oscillated into another neutrino type before reaching the Earth. The experiments to date were sensitive only to electron-neutrinos and therefore have not provided sufficient information to distinguish between the two possible explanations for the SNP.

We propose to construct a large volume heavy-water detector which has the potential to measure both the electron-neutrino flux from the Sun and the total solar neutrino flux independent of neutrino type. With this observatory it would therefore be possible to test models of solar energy generation and, independently, to search for neutrino oscillations with a sensitivity many orders of magnitude greater than that of terrestrial experiments. In addition, by accurately determining the energy spectrum of electron-neutrinos it will be possible to search for spectral distortion pro-

duced by neutrino oscillations in the dense matter of the Sun, as described recently by Mikheyev and Smirnov. The proposed detector would moreover be sensitive to neutrinos from a stellar collapse and would detect neutrinos of all types, providing detailed information on the dynamics of the collapse and on the masses of muon- and tau-neutrinos. This unique neutrino observatory would provide a powerful instrument for neutrino astronomy and would also provide sensitive tests of the properties of neutrinos themselves, which are central to further progress on fundamental theories of physics.

The ability of neutrinos to penetrate great distances through dense matter means that they are extremely difficult to detect and this has been the fundamental limitation on the development of neutrino physics. To overcome this, it is vital to maximize the mass and sensitivity of the detector while minimizing its backgrounds. Heavy water (D_2O) is an excellent medium from which to construct a neutrino detector. It offers high sensitivity to the energetic electron-neutrinos (ν_e) which are believed to be produced in the Sun. In addition it offers a sensitivity to all of the neutrino types. Water is one of the few materials which can be purged of background-generating radioactivities to the very stringent levels required. In order to escape the intense cosmic-ray background it is necessary to locate the detector deep underground. Moreover, the detector has to be carefully shielded from the effects of radiation coming from the surrounding rock.

We propose to build a neutrino detector using 1000 tonnes of D_2O and to locate it more than 2000 m below ground in the Creighton Mine, owned by INCO Limited, in the town of Walden, near Sudbury. Such a detector can only be realized in Canada; Canada alone has sufficient reserves of D_2O to mount such a project and the technologically advanced Creighton Mine offers a deep, secure site in which this valuable resource can safely be used.

The design of the proposed detector is shown in Figure 1.2. The neutrinos interact in the D_2O producing energetic electrons which emit Čerenkov light. This light passes through the acrylic vessel containing the D_2O to light-sensitive photomultiplier tubes. The pattern of signals in these photomultiplier tubes allows the neutrino interactions to be characterized. The design is determined largely by consideration of the radioactive backgrounds. The D_2O is shielded from the radioactivity in the rock by 0.9 m of low activity "Sulfurcrete" and by 4 m of ultra-pure light water. The photomultiplier tubes must be separated from the D_2O by 2.5 m of water to attenuate the γ-rays from radioactivity in their glass envelopes.

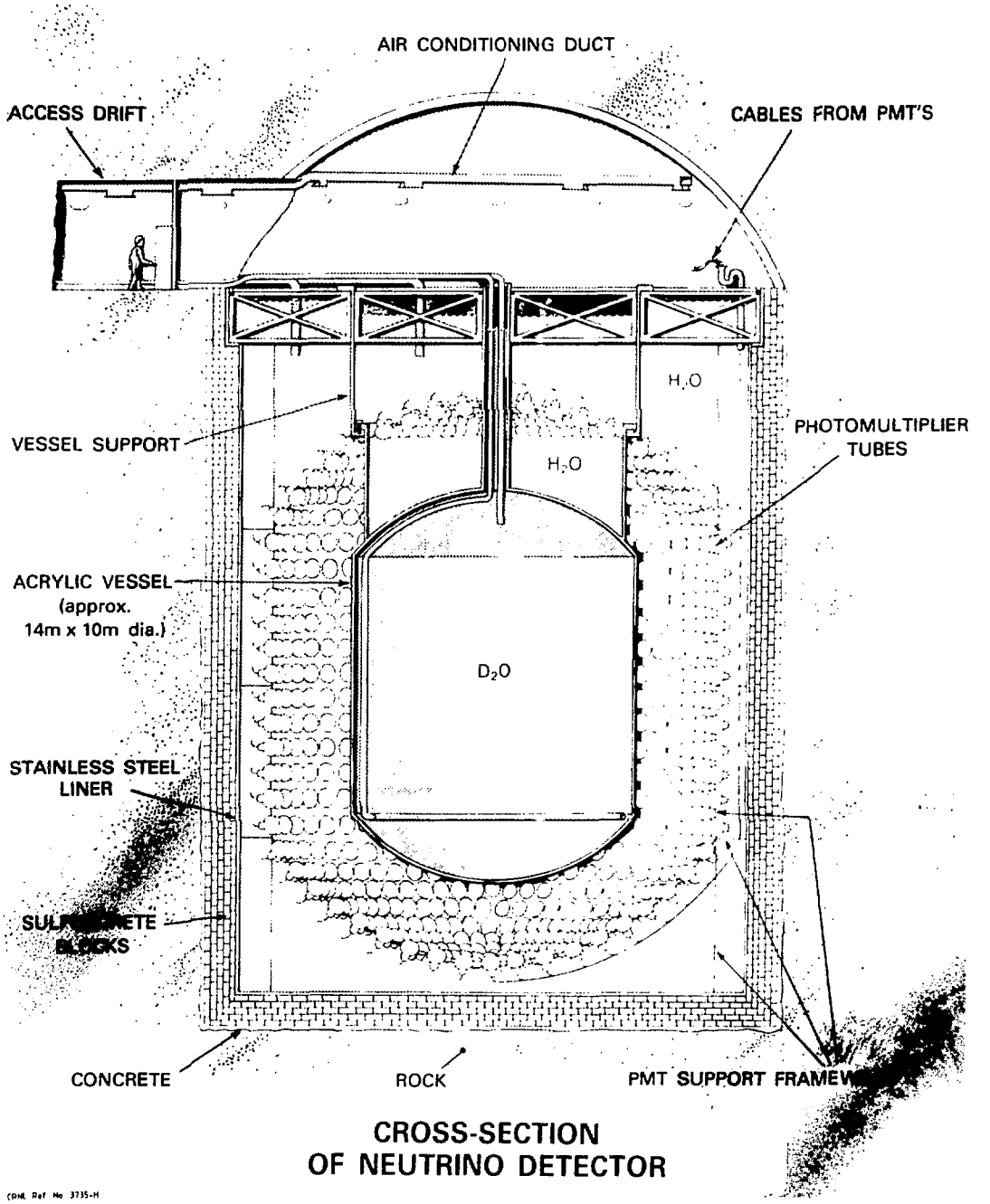

Figure1.1: Design of the Proposed Detector.
The diameter of the cylindrical rock cavity is 20 metres.

This design has evolved over the past three years due to extensive measurements and calculations by a growing collaboration of scientists. The collaboration is now composed of 28 scientists working at 9 institutions in 3 countries. A preliminary feasibility study was prepared in July 1985 [SNO 85-3] and an update to the feasibility study [SNO 86-6] in the following year. During the past three years progress has been made on many fronts. Detailed computer simulations have allowed the detector response to be characterized and the design optimized. A small test detector has been built and operated to learn more about water Čerenkov detectors at low energies. Funds were raised by the participating institutions to commission INCO to excavate a drift into the area chosen for the detector so that the rock properties could be determined, and hence the feasibility of excavating a large cavity could be established. Engineers at Atomic Energy of Canada Limited (AECL), INCO, and Reynolds and Taylor Inc. (the proposed manufacturers of the acrylic vessel) have developed a sound mechanical design for the detector and the laboratory. Perhaps the most dramatic progress has been made in understanding the radioactive background. For example, at the time when the feasibility study was prepared the background expected for the important but difficult, neutral-current measurement was 70 times greater than the expected signal and no data were available for some important background sources. We have now studied all expected background sources and by suitable choice of materials and purification techniques we expect a background below the signal level for this reaction.

The primary physics objective of the proposed observatory will be to study neutrinos from the core of the Sun. The Standard Solar Model (SSM), which has been used extensively to describe stellar evolution, makes clear predictions for the neutrino fluxes. Two experiments have been carried out which were sufficiently sensitive to measure the predicted flux. A radiochemical experiment using a large tank of perchlorethylene was set up by Ray Davis and colleagues to search for neutrinos and has been in operation for almost 20 years. This experiment is primarily sensitive to the neutrinos from the decay of ^{8}B in the Sun but the observed rate implies that this flux is at least three times below the SSM prediction. Very recently the Kamiokande II light water Čerenkov detector, built initially to look for proton decay, has been used to search for these ^{8}B neutrinos. Again the predicted flux is not observed and an upper limit on the flux of about half the SSM prediction has been set. This discrepancy, which has been known for almost 20 years, is widely considered to be a very significant fundamental problem. Two classes of solution have been suggested. If the predicted central temperature of the Sun could be lowered by some change

to the SSM, the production of ^{8}B would be decreased. However, such *ad hoc* modifications made only to accommodate the SNP invariably give rise to other problems. Alternatively, it is possible that the neutrinos are being produced with a flux as calculated by the SSM but that, in transit to Earth they change into some other type of neutrino to which the experiments are not sensitive. Recently Mikheyev and Smirnov used a theory initially developed by Wolfenstein to show that a mechanism may exist which would greatly enhance such a conversion. If this MSW effect is at the origin of the SNP then there should be two observable consequences. First, because the effect is strongly energy dependent the ν_e spectrum will be distorted. Second, the Sun will be an intense source of muon- and tau-neutrinos. The effect requires at least one of the neutrinos to have mass and information about this mass could be extracted from the observations of the solar ν_e spectrum. Confirmation of the MSW effect would have a profound impact on fundamental particle physics.

The proposed experiment will make a unique contribution to the study of neutrinos from the Sun. The charged-current interaction of the neutrino with the deuteron will allow a measurement of the neutrino energy spectrum to show that ^{8}B is being produced in the Sun and to search for the effects predicted by the MSW theory. Since the detector will be some forty times more sensitive than previous detectors, the ^{8}B ν_e flux will be clearly identified. Both the charged-current reaction and the elastic scattering of neutrinos from electrons provide directional information necessary to identify the Sun as the neutrino source.

A unique capability of the proposed detector is the detection of the neutral-current reaction wherein a neutrino breaks up a deuteron into a neutron and a proton. This reaction is independent of the type of neutrino initiating it and hence gives a measure of the total neutrino flux. It is the key experiment to determine whether the neutrinos born as ν_e are converted to other types of neutrinos in transit to Earth. The backgrounds involved in the identification of this reaction are a serious problem but, as mentioned above, we are confident that we have demonstrated that they are tractable.

Although it is now established that supernovae produce neutrinos, the wealth of new data available from the proposed detector would make a valuable and unique contribution to this study. First, it would be the most sensitive detector of the ν_e flux, which current models predict is produced in a short (few milliseconds) burst as the core of the star collapses. It would complement the existing light-water and scintillation detectors which are

primarily sensitive to the $\bar{\nu}_e$ flux. A second unique contribution would be the observation of the other neutrino types (ν_μ, ν_τ) produced in the first few seconds as the supernova evolves. As in the case of solar neutrinos, information significant for both astrophysics and elementary-particle physics would be obtained. A detailed picture of the evolution of the components of the neutrino flux would help to establish the dynamics of the supernova. The supernova gives a very short (few seconds) burst of neutrinos and, if these have mass, the burst will spread in time as it travels to Earth. The observations of neutrinos from SN 1987A confirmed that the mass of the $\bar{\nu}_e$ must be less than 40 eV. A unique capability of the proposed detector would be its sensitivity to masses of the ν_μ and ν_τ to this order. There is no other way to establish these masses to this level. Massive neutrinos have important cosmological consequences, for example, neutrinos might constitute sufficient dark matter to close the Universe.

When the SNP was first identified it was generally expected that a definitive observation would be the measurement of the very low-energy electron-neutrinos which should be produced by the *pp* reaction in the Sun. The flux of these neutrinos is well determined by the solar luminosity and known nuclear reaction cross sections. It was assumed that a measured flux much lower than expected would be strong evidence for neutrino oscillations while if the full flux was observed the resolution of the SNP would lie in the solar physics. This flux can be measured using a radiochemical technique involving gallium as the sensitive material and at present work is underway in Europe on two gallium experiments. However, the MSW effect may cause the oscillations to have a complex energy dependence in which case the gallium experiments would not by themselves, give a definitive answer to the problem. The proposed D_2O detector, with its unique sensitivity to both the ν_e and total ν flux, and to the spectral shape, can distinguish among the different solutions to the solar neutrino problem. Scientifically it is, therefore, a very timely experiment.

There is a practical window of opportunity within which to carry out the experiment. AECL has agreed to lend the D_2O, subject to approval of the final detector design and satisfactory arrangements for insurance. This loan would require a laboratory project schedule which would allow return of the heavy water as required to satisfy AECL's sales demand. Reactor construction schedules imply that the heavy water would be available at least until 1995. Thus if prompt approval is given for the SNO project and if the construction can be kept to schedule then two years data collection with D_2O could be assured. This would be sufficient to complete the solar

neutrino studies proposed although it would be very desirable to run the experimental program longer to improve the accuracy of the data, to watch for variations in the solar flux and to be sensitive to supernovae.

We propose that the laboratory be operated as a National Facility. Not only is this appropriate for a major observatory, but also in building the laboratory we will be creating an ultra-low radioactivity environment in which other scientific experiments could be carried out, and a National Facility will provide the infrastructure to support them.

In the following Chapter the physics which has been outlined above is discussed in more detail. In Chapter 3 we discuss the operation and performance of the proposed detector including an analysis of the backgrounds. This Chapter refers to a number of detailed reports which have been prepared by members of the collaboration and are available as Annexes to this proposal. These cover topics such as measurements of radioactivity in various detector components, calculations of the shielding, measurements of optical properties and detailed simulations of the detector response. We justify in this Chapter our confidence that the charged-current measurement can be performed without further development. The experimental plan to measure the neutral-current reaction involves data taking with and without $NaC\ell$ doping. In Chapter 4 we present the design of the laboratory and address some of the engineering aspects required for its realization. This Chapter is based on a number of reports by organizations outside of the collaboration. These reports, referred to as Supporting Documents, are not available for general circulation. The construction schedules and responsibilities, and the planned program of technical studies by the collaboration are outlined in Chapter 5. In Chapter 6 an administrative structure is suggested which would establish an Institute of Neutrino Physics as a legal entity to take responsibility for constructing and operating the envisaged National Laboratory, and to promote the unique scientific opportunities opened by the facility. Finally, in Chapter 7 the costs of constructing and operating the laboratory are identified. The total capital cost is estimated to be $35M Canadian and the annual operating cost, after construction, would be $1.8M Canadian, including the insurance costs of the heavy water.

Chapter 2

Physics

2.1 Introduction

The only direct information on the reactions which power the Sun is carried by neutrinos escaping from its dense interior. In a pioneering experiment Davis et al. [1] measured a counting rate only one quarter of that calculated using the Standard Solar Model (SSM) [2]. This discrepancy, known as the solar neutrino problem (SNP) is widely considered a major problem in modern physics. Two categories of solutions to the problem have been extensively discussed. The first assigns some deficiency to the SSM and many mechanisms have been suggested to lower the central temperature of the Sun and thus reduce the production of high-energy neutrinos from ^{8}B [3]. The second assigns some deficiency to our knowledge about neutrino propagation. Pontecorvo [4] originally suggested that the reduction in ν_e flux at Earth may be caused by large mixing angle oscillations of neutrinos between weak interaction eigenstates. More recently, Mikheyev and Smirnov [5], following the theoretical framework of Wolfenstein [6] have shown that a mechanism exists whereby, if this mixing of eigenstates is postulated, a large fraction of ν_e created in the solar interior could be converted into $\nu_\mu(\nu_\tau)$, even for very small mixing angles. It is apparent that the Sun is a unique source offering a rare opportunity to search for neutrino oscillations and thereby test unification theories beyond the electroweak sector. Weinberg [7] has pointed out that such theories lead naturally to a prediction of about 10^{-3} eV for the heaviest neutrino mass, a value for which solar experiments, with matter enhancement, are par-

ticularly sensitive. Other suggested solutions to the SNP involve neutrino decay [8] or a finite neutrino magnetic moment [9].

In this Chapter we discuss the neutrino detection potential of the proposed heavy-water Čerenkov detector and how its sensitivity to the solar ^{8}B ν_e flux, spectrum and direction, and to the total solar ^{8}B neutrino flux independently of the neutrino type, could be used to distinguish among the suggested solutions of the SNP. In particular, our experiment allows the Sun to be used as a distant neutrino source for physics experiments free of assumptions of the SSM, and also permits a definitive test of the SSM free of complications from proposed neutrino properties. These aspects of the physics program for the facility are described in Section 2.3. The recent detection of neutrinos from the supernova SN 1987A has focused attention on the physics of stellar collapse. We consider in Section 2.4 the unique capabilities of this detector with respect to detection of neutrinos from stellar collapse. Finally, other physics questions addressable by subsidiary analyses of the data are described in Section 2.5.

2.2 Neutrino Detection

The proposed experimental program would involve the use of five reactions to measure the ν_e flux, energy spectrum and direction, the $\bar{\nu}_e$ flux and energy spectrum, and the total neutrino flux independently of neutrino type. Cross sections for the reactions in the energy range of interest are shown in Figure 2.1.

The ν_e flux, spectrum, and direction would be measured via the charged-current reaction

$$\nu_e + d \rightarrow p + p + e^- .....\text{I}$$

corresponding to 'inverse β-decay of the deuteron'. Monoenergetic neutrinos produce electrons which are almost monoenergetic with kinetic energies of approximately $E_\nu - 1.44$ MeV [10], and hence this reaction is well suited to a direct determination of the energy spectrum of the ν_e. Since the cross section for reaction I is relatively large, several thousand solar induced ν_e events per year are expected for a one kilotonne (kt) heavy-water detector, giving a high statistics energy spectrum. The detected electrons would have an angular distribution with respect to the neutrino direction given

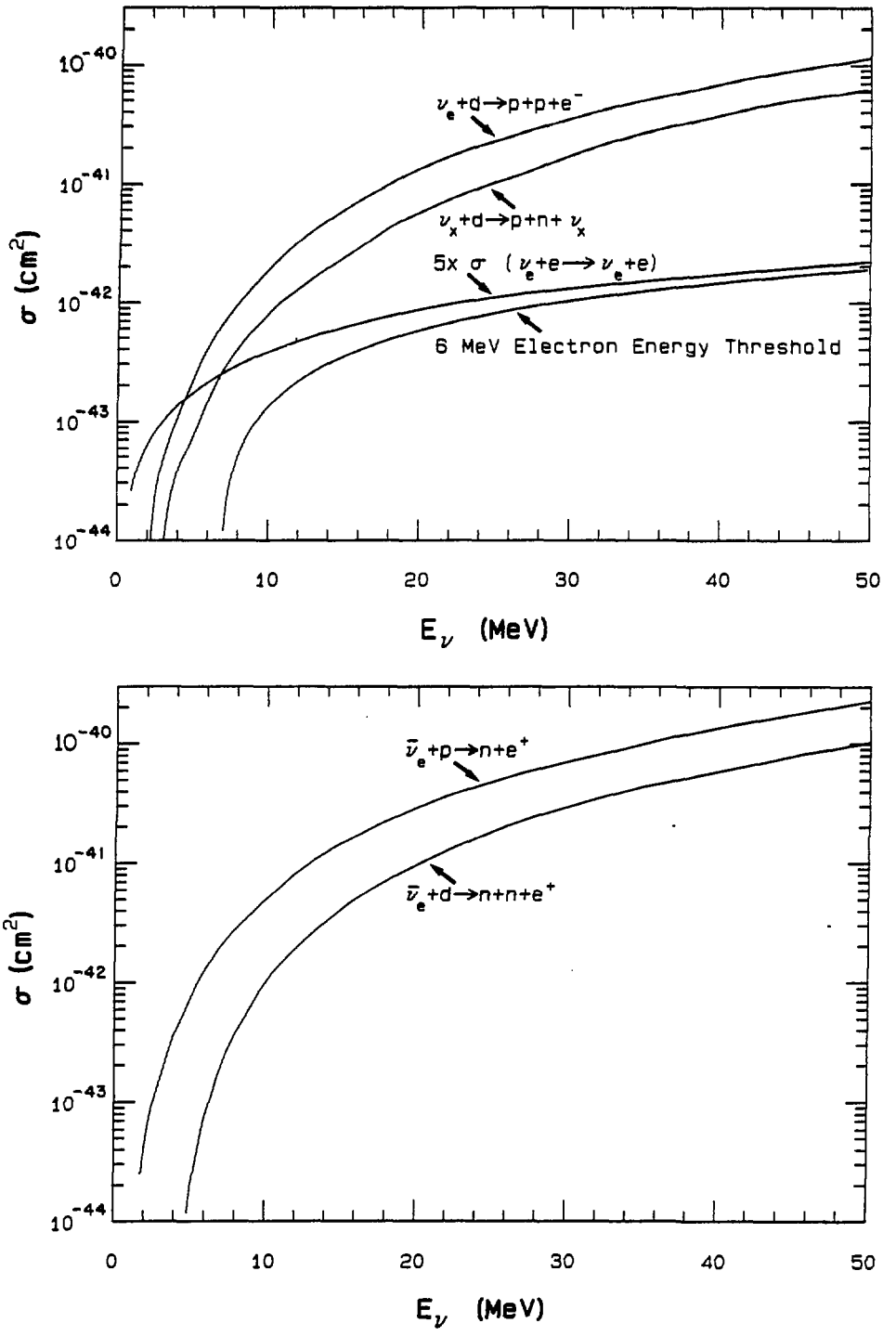

Figure 2.1: The neutrino cross sections for the principal reactions available to the SNO detector are shown as a function of energy. The curves for neutrino-electron scattering show the cross section scaled up by a factor of 5 (the electron/deuteron ratio in D_2O.)

by $W(\theta_e) = 1 - \frac{1}{3}cos\theta_e$, implying a two-to-one backward to forward asymmetry. The accuracy with which the absolute cross section for this reaction can be calculated has been considered by a number of authors. Nozawa et al. [11] report variations of about 6% due to uncertainties in exchange currents and in the deuteron model. Ellis and Bahcall [12], and Bahcall and Ulrich [2] suggest a conservative uncertainty of 10% to reflect the meson exchange effects and forbidden or p-wave corrections which are difficult to treat reliably.

The second reaction producing a detectable signal is neutrino-electron scattering

$$\nu_x + e \rightarrow \nu_x + e.....\text{II}$$

In standard electroweak theory, while all neutrinos scatter from electrons by the neutral-current process, only the electron-neutrinos interact with them through the charged-current process with the result that the scattering cross section for ν_e [13] is 6 - 7 times larger than that for ν_μ [14] or ν_τ. Thus, this reaction is mainly sensitive to the ν_e flux; but with an independent measurement of the ν_e flux from reaction I, the total neutrino flux may also be determined. (The accuracy with which the ν_e component can be subtracted may be limited by the 10% uncertainty in the absolute cross section for reaction I.) For ^{8}B electron-neutrinos, the yield from reaction II is an order of magnitude smaller than that from reaction I. Electrons from reaction II, however, are kinematically constrained to the forward cone, thus providing excellent directional information on the flux. In heavy water, these events can be separated from those of reaction I by their strong forward peaking with respect to the Sun's direction. A clean measurement of reaction II will come from a light water fill, and from the light water surrounding the acrylic vessel, where no events from reaction I will be present. Because the electron spectrum gives an integral of the neutrino flux, and has a lower yield, the neutrino energy spectrum is more difficult to extract than for reaction I.

The total neutrino flux, independent of neutrino type, can be measured by the neutral-current reaction

$$\nu_x + d \rightarrow \nu_x + p + n.....\text{III}$$

The reaction rate would be determined by counting the free neutrons produced. Chen [15] has pointed out *that this reaction is particularly important for resolving the SNP because it gives a direct measure of the solar ^{8}B neutrino production independently of oscillations.* The ratio of the events from

reaction I to reaction III provides a direct determination of the presence of neutrino oscillations, independently of the value of the total solar neutrino flux. Reaction III would be identified by observing the γ-rays produced in the capture of the neutron. A number of possible neutron capture reactions are considered in the detector performance section of this document; the optimal choice at present is to promote capture on $^{35}C\ell$ (introduced into the D_2O in the form of $NaC\ell$) which offers a high-energy γ-ray signal and good capture efficiency.

While the Sun is not expected to be a source of anti-neutrinos, there are interesting $\bar{\nu}_e$ sources in the Universe, e.g. supernovae. These neutrinos can be uniquely detected in the detector in two ways. The flux can be measured in the D_2O through the reaction

$$\bar{\nu}_e + d \rightarrow n + n + e^+ .....\text{IV}$$

The signature for this reaction will be the positron signal followed by two delayed neutron capture γ-rays. The mean neutron capture time in D_2O containing 2500 kg of $NaC\ell$ is 5 ms [Annex-1]. The reaction kinematics are similar to those of reaction I except that the Q-value is -4.03 MeV instead of -1.44 MeV.

The $\bar{\nu}_e$ can also interact in the H_2O surrounding the D_2O via the reaction

$$\bar{\nu}_e + p \rightarrow n + e^+ .....\text{V}$$

The signature will be the Čerenkov light from the positron, of energy $E_\nu - 1.8$ MeV, in the light water. The neutron would be captured in hydrogen giving a 2.2 MeV γ-ray which is below our normal detection threshold. The positron angular distribution is almost isotropic with respect to the neutrino direction.

2.3 Solar Neutrinos

2.3.1 The Standard Solar Model

It is generally accepted that fusion of light nuclei produces the immense amount of energy radiated by stars and synthesizes most of the light elements in the Universe [16]. Since the nuclear furnaces are deep within

the stellar interiors, only the detection of neutrinos from these nuclear reactions can provide direct verification of such processes and detailed information about the physical condition of stellar cores. The Sun is the only star close enough to provide a detectable steady neutrino flux on Earth. Its solar mass, radius, luminosity, surface temperature, surface elemental abundances and rotational speed have been measured accurately [17], and its age can be estimated reliably from natural radioactivities on Earth and from meteorites. These properties pose severe constraints on proposed stellar models.

The SSM [2] assumes that the energy in the Sun is generated by the fusion of four protons into a ^{4}He nucleus, that the Sun is a spherically symmetric plasma in hydrostatic equilibrium maintained by a balance of the gravitational force against the pressure gradient, and that the energy is transported from the core to the surface by radiation and convection. At each point, the pressure, density and temperature are related through an equation of state which is similar to that for an ideal gas, with corrections for degeneracy and incomplete ionization. A large number of input parameters such as opacity, initial elemental abundances and nuclear reaction cross sections are needed in the calculation. Evolutionary sequences of the Sun are constructed beginning with a zero-age main sequence star with a homogeneous composition. What emerges from this is an evolving Sun which, after 4.6×10^9 years, must have all the known features of our present-day Sun.

The SSM predicts that more than 98% of the solar energy is generated by a series of nuclear reactions collectively called the proton-proton, or *pp*, chain [2]. The competing branches within this chain are shown in Figure 2.2. The neutrino spectrum predicted by the SSM is shown in Figure 2.3. The *pp* and *pep* ν_e fluxes, $\Phi(pp)$ and $\Phi(pep)$, are largely determined by solar luminosity and well measured nuclear cross sections; hence they are relatively insensitive to the details of the model. On the other hand, the production rates of ^{7}Be and ^{8}B depend critically on the temperature of the core; hence the ν_e fluxes from their decays, $\Phi(^7\mathrm{Be})$ and $\Phi(^8\mathrm{B})$, are sensitive to changes in the input parameters in the calculations. The rate for the $^3He(p, e^+\nu_e)^4He$ reaction (*hep*), which produces neutrinos with an end-point energy of 18.77 MeV, is the least temperature dependent. As shown in Figure 2.4 the ^{8}B neutrinos come only from the most central and hottest part of the Sun while the ^{7}Be, *pp* and *hep* neutrino fluxes carry information about the solar interior at progressively larger radii.

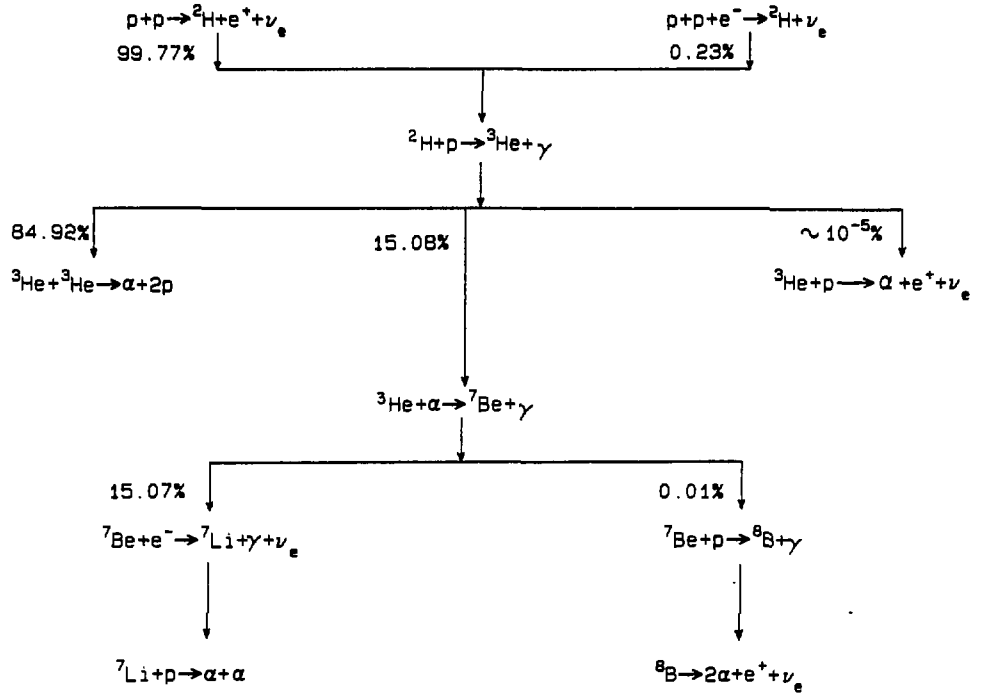

Figure 2.2: Nuclear reactions in the *pp* chain.

Recently, data on helioseismology have provided new tests of solar models [18]. The data are primarily sensitive to the outer regions of the Sun but do probe the mean molecular weight in the solar interior. These studies complement the solar neutrino studies which are sensitive to the interior temperature and energy generating reactions.

2.3.2 The Solar Neutrino Problem

Only two experiments with the requisite detection sensitivity to solar neutrinos have been reported. The first was the $C\ell$/Ar radiochemical experiment of Davis et al. [1] which has been operating at the Homestake Mine in Lead, South Dakota since 1968. The detector contains 2.2×10^{30} atoms of $^{37}C\ell$. The recently updated SSM predicts [2] an ^{37}Ar production rate of 1.6 ± 0.5 atoms per day with the contributions from different solar reactions and decays as listed in Table 2.1. The measured ^{37}Ar production rate [1] above the known background is 0.38 ± 0.05 atoms per day, much lower than expected, and is consistent with a total absence of $\Phi(^8B)$ as can be seen from Table 2.1. The radiochemical extraction efficiency has been *investigated extensively* [19]. *The neutrino capture cross section in* $^{37}C\ell$ *is* deduced from (p,n) experimental results [20] and delayed proton emission rates from ^{37}Ca [21]. Hence it would appear that the detector performance

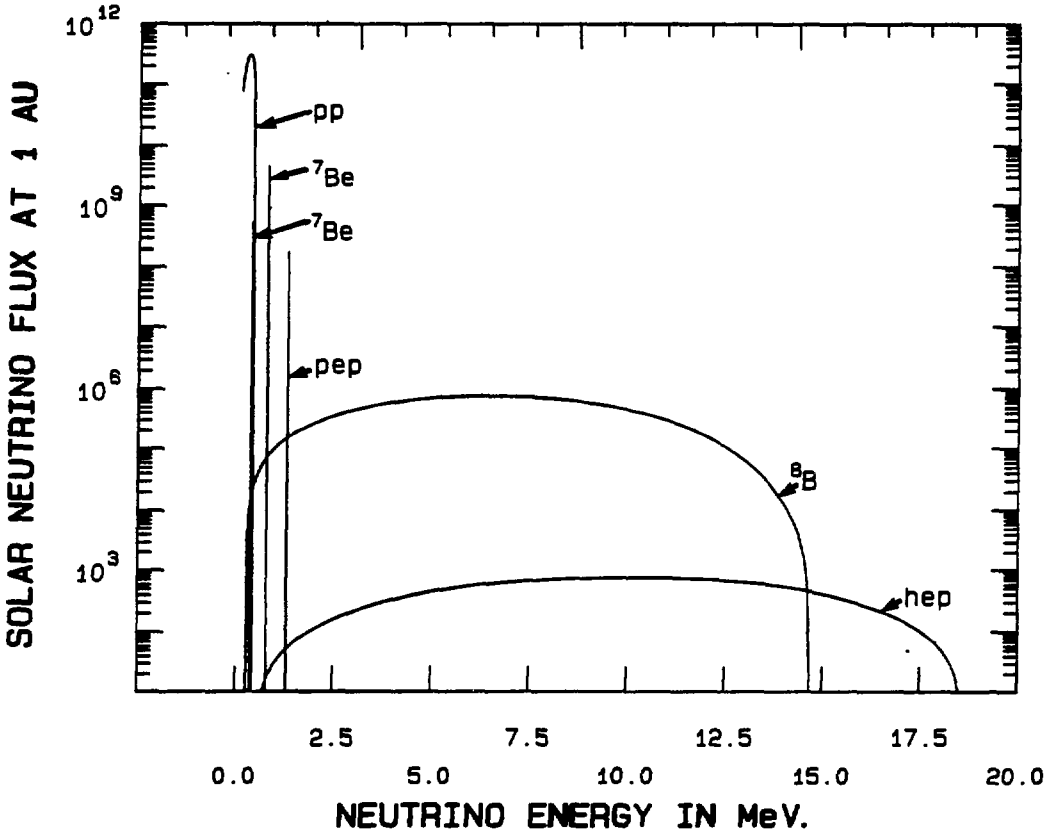

Figure 2.3: The neutrino spectra resulting from the main reactions in the *pp* chain, as predicted by the Standard Solar Model. The SNO detector is sensitive to the ^{8}B and *hep* neutrinos only. The flux unit at Earth for the continuous spectra is $cm^{-2}s^{-1}\text{MeV}^{-1}$, and for the line spectra $cm^{-2}s^{-1}$.

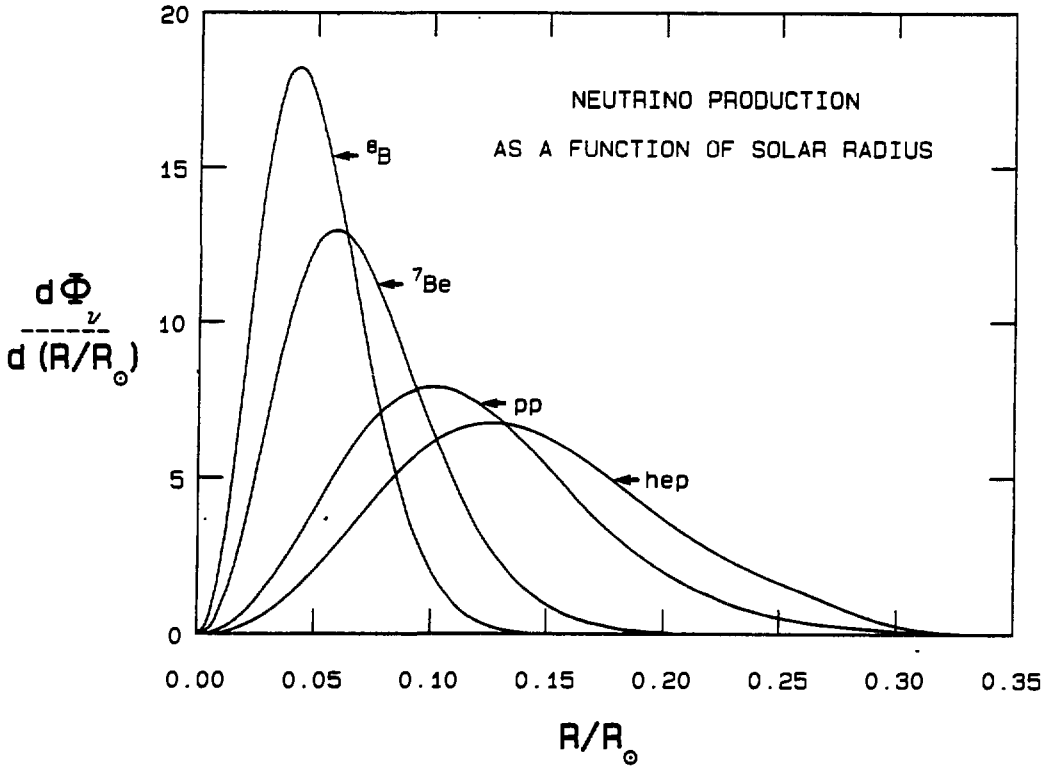

Figure 2.4: The rates of the various modes of neutrino production are given as a function of solar depth. It is seen that the ^{8}B reaction is concentrated in the central, hottest part of the Sun while the *hep* reaction takes place over a much wider and cooler region.

Neutrino source	Flux $cm^{-2}s^{-1}$	^{37}Ar Production atoms/day
pp	6.0×10^{10}	0.
pep	1.4×10^{8}	0.04
^{7}Be	4.7×10^{9}	0.22
^{13}N	6.1×10^{8}	0.02
^{15}O	5.2×10^{8}	0.06
^{8}B	5.8×10^{6}	1.24
hep	8×10^{3}	0.01

Table 2.1: The neutrino fluxes at Earth as predicted by the SSM and the resulting ^{37}Ar production rates predicted for the Cℓ/Ar experiment.

is well understood. Recently, an upper limit on $\Phi(^{8}\mathrm{B})$ of $3.2 \times 10^{6}\, cm^{-2}s^{-1}$ based on a search for $\nu - e$ scattering at Kamiokande II was reported [22]. This gives independent experimental support for a ^{8}B ν_e flux lower than predicted by the SSM.

One way of predicting a low ^{8}B neutrino flux at Earth is to modify the nuclear reaction cross sections and opacity parameters in the SSM so as to reduce the ^{8}B production rate without substantially altering the basic physics in the calculation. However, with the exception of the *pp* and the electron capture reactions, all the important nuclear reaction cross sections in the *pp* chain have been remeasured, independently, at a number of laboratories [23] and large errors in the input nuclear parameters do not appear likely. Lower solar opacity would increase energy transport efficiency, thereby reducing the central temperature. Improvements have been made in the accuracy of the numerical evaluations of solar opacity. This is discussed extensively by Bahcall and Ulrich [2].

Numerous non-standard models have been proposed to solve the SNP by lowering the solar core temperature without affecting the surface chemical composition or luminosity. In the steady state, this can be achieved by including convective mixing, low heavy-element concentrations, strong magnetic fields or a rapidly rotating core [19]. Non-steady state models can lower the energy production rate in the core on a short time scale without affecting the surface luminosity which can only change on a radiation

diffusion time scale (Kelvin-Helmholtz time $\sim 10^7$ years). A lower energy production rate can be caused by thermal instability or periodic mixing of the core [19].

Non-standard nuclear or particle physics effects have also been suggested as possible solutions. Of particular interest is the possibility that the production rate of ^{8}B neutrinos is as expected, but while in transit from the centre of the Sun to Earth, the nature of the left-handed ν_e has been modified. Conversion of ν_e to neutrinos of other types will be discussed in detail in Section 2.3.3. Other suggestions to reduce the ^{8}B production rate include exotic nuclei [24], quark catalysis [25] weakly interacting massive particles [26] and a finite neutrino magnetic moment [9,27].

This list of published suggestions is by no means complete. It does indicate the interest generated by the solar neutrino problem and the range of effort being made to solve it. Most of the proposed non-standard models introduce difficult new problems and none has been generally accepted. Others involve highly speculative properties of nuclei, neutrinos and exotic undiscovered particles.

2.3.3 Neutrino Oscillations

Twenty years ago Pontecorvo [4] suggested that the SNP might be resolved if the neutrinos emitted in weak decay (the neutrino flavour eigenstates) were not mass eigenstates but were linear combinations of neutrino mass eigenstates. Recently Mikheyev and Smirnov [5], working within the theoretical framework developed by Wolfenstein [6], have shown that such oscillations may be greatly enhanced in the solar interior even if the mixing in vacuum is rather small. Such a possibility is plausible since this mixing is just what happens in the quark sector where the s and d quarks are mixed, and because the neutrino masses consistent with SNP explanations arise naturally in some grand unification theories. However, such oscillations imply both that neutrinos have mass and that lepton number conservation is violated. Both possibilities are of fundamental importance. We still have no way to distinguish this type of solution to the SNP from some deficiency in the solar model. The Sun may prove to be the only source which can be used to study these aspects of particle physics.

The theory of vacuum oscillations of neutrinos can be found in ele-

mentary texts on particle physics [28]. We assume that the mass eigenstates are ν_1 and ν_2 with masses m_1 and m_2 (for simplicity we restrict the arguments to two neutrino types). The electron- and muon-flavour states can then be written

$$\nu_e = \nu_1 cos\theta + \nu_2 sin\theta$$

$$\nu_\mu = -\nu_1 sin\theta + \nu_2 cos\theta$$

If a ν_e is produced, the probability of it being a ν_e after moving a distance L is

$$P(\nu_e \rightarrow \nu_e) = 1 - \sin^2 2\theta \sin^2 \left(\frac{1.27 \Delta m^2 L}{E} \right)$$

where Δm^2 equals $m_2^2 - m_1^2$ measured in eV^2, E is the energy in MeV and L is the distance in metres.

Two types of experiments have been carried out to search for vacuum oscillations. The flux of $\bar{\nu}_e$ at various distances from a reactor has been examined to see whether the reduction predicted from the above expression could be detected [29]. With distances of order 50 m, these experiments have ruled out values of $\Delta m^2 > 10^{-2}$ eV^2 for large mixing angles as indicated in Figure 2.5. Experiments have also been carried out at accelerators to look for the conversion of high-energy ν_μ's and ν_e's [30]. Again, no definite evidence for neutrino oscillations has been found and the parameter space which can be eliminated is also shown in Figure 2.5.

Because of the large distance from Sun to Earth, oscillations could in principle be measured for values of Δm^2 as low as 10^{-10} eV^2, a range far beyond that achievable in terrestrial experiments. However, a reduction as large as a factor of 3 with only three neutrino families would require maximum mixing angles. By contrast, the Cabibbo angle mixing the s and d quarks is 0.26 radians and the other mixing angles among the three quark families are much smaller.

Under certain conditions when neutrinos pass through matter the oscillations may be greatly enhanced [5,6]. This arises because in matter the ν_e's interact with electrons through the charged-current which does not affect the other neutrino types. Hence the ν_e mass may become degenerate with the ν_μ or ν_τ mass and if there is any vacuum mixing, the conversion between neutrino types can be greatly enhanced. Following the presentation of Bethe [31], the electron-neutrinos in matter experience a potential

$$V = G\sqrt{2}N_e$$

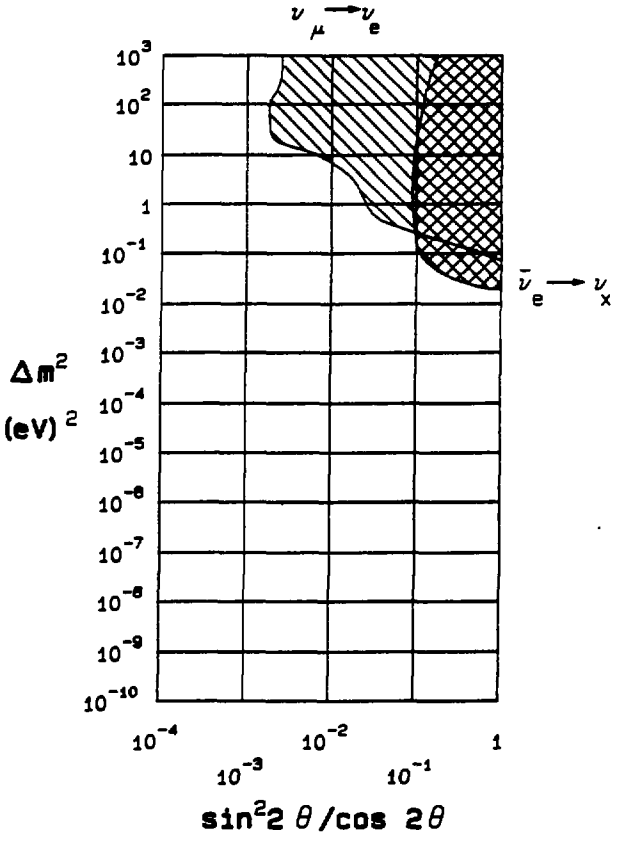

Figure 2.5: The values of the neutrino oscillation parameters Δm^2 and $sin^2 2\theta / cos 2\theta$ excluded by terrestrial experiments are shown. Reactor experiments exclude the cross-hatched region. Accelerator experiments exclude the diagonally-hatched region.

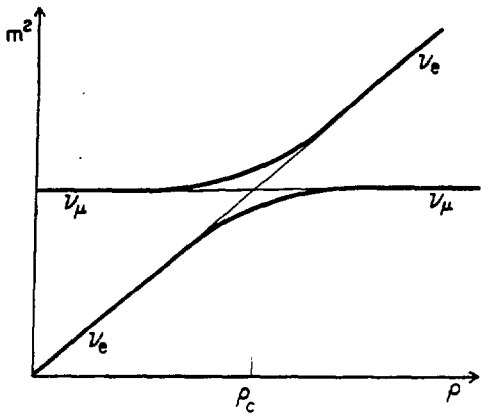

Figure 2.6: A ν_e created in a region of high density (the core of the Sun) converts to a ν_μ in travelling to regions of lower density.

where G is the Fermi constant and N_e is the number density of electrons. In units where $c = \hbar = 1$ we may write

$$m^2 = (E - V)^2 - k^2$$

where k is the neutrino momentum. Thus the change in the mass squared due to the charged-current interaction is

$$\delta m^2 = 2EV = 2E\sqrt{2}GN_e \equiv A$$

This leads to a mass matrix of the form

$$M = \frac{1}{2}(m_1^2 + m_2^2 + A)\begin{pmatrix} 1 & 0 \\ 0 & 1 \end{pmatrix} + \frac{1}{2}\begin{pmatrix} A - \Delta m^2 cos2\theta & \Delta m^2 sin2\theta \\ \Delta m^2 sin2\theta & -A + \Delta m^2 cos2\theta \end{pmatrix}.$$

The manner in which the eigenvalues of this matrix vary with density is shown in Figure 2.6. The important feature is that a crossing occurs at an electron density, ρ_c, where

$$\rho_c \approx 10^7(\Delta m^2/E)cos2\theta.$$

The units of ρ_c are such that it is numerically equal to the normal density (in $g\,cm^{-3}$) for hydrogen and to half the normal density for N=Z atoms. If electron-neutrinos are produced in a high density region to the right of the crossing point in Figure 2.6, and then move through a slowly decreasing density to a region represented by a point to the left of the crossing, an

adiabatic change in the neutrino type from ν_e to ν_μ may occur. For the case of solar neutrinos, the central density of 150 $g\ cm^{-3}$ and hydrogen fraction of 36% imply that there will be a critical value of $E_\nu/\Delta m^2 \approx 10$ MeV/10^{-4} eV^2 just above which essentially all of the ν_e's convert to ν_μ's. Below this critical value, the central density of the Sun is less than ρ_c and no conversion takes place. If the ratio of $E/\Delta m^2$ is much greater than that required to produce oscillations in the solar core then the conversion may take place in the outer part of the Sun where the density is falling exponentially. In this latter case the conversion may not be complete and is referred to as non-adiabatic conversion. Here a decreasing fraction of the ν_e's will be converted to ν_μ's as the energy increases. The range of values of $E/\Delta m^2$ for which efficient conversion takes place is determined by the vacuum mixing angle. Most of the ^{8}B neutrinos could be converted to ν_μ's for values of $sin^2 2\theta$ as small as 10^{-4}.

The Earth also presents a substantial body of reasonably constant density to the neutrinos and must be included in any calculation of the neutrino flux reaching a detector [32]. The effects are particularly important when $sin^2 2\theta$ is greater than 0.04 and Δm^2 is about 10^{-5} eV^2 (where neutrino oscillations resonate in the centre of the Earth). In this case the ν_e flux and spectrum observed at night will differ from that observed during the day.

The fraction of ν_e's created at the centre of the Sun which reach the detector as ν_e is shown in Figure 2.7 as a function of $E/\Delta m^2$ for $sin^2 2\theta$ of 0.04. For a given value of Δm^2, this Figure indicates how the observed ν_e spectrum would be altered by matter oscillations.

A detector sensitive to neutrinos above $E_\nu = 5$ MeV would be particularly sensitive to neutrino oscillations for values of Δm^2 between 10^{-4} eV^2 and 10^{-7} eV^2. It is reasonable to assume that if neutrinos have mass then $m_{\nu_e} << m_{\nu_\mu} << m_{\nu_\tau}$ as a similar ordering holds true for the charged leptons. This implies the ν_e mass can be neglected and our experiment would be sensitive to ν_μ or ν_τ masses of order $10^{-2} - 10^{-4}$ eV. Weinberg [7] has reviewed the implications of grand unification theories. He shows that it is plausible to expect the heaviest neutrino to have a mass of order either m_W^2/M where m_W is the mass of the W boson and M is some large mass such as the grand unification mass about 10^{15} GeV, or m_q^2/M where m_q is a quark mass as in the see-saw model. While these are not quantitative predictions, they do lead to values of the correct order of magnitude to give observable effects for high-energy solar neutrinos. Because

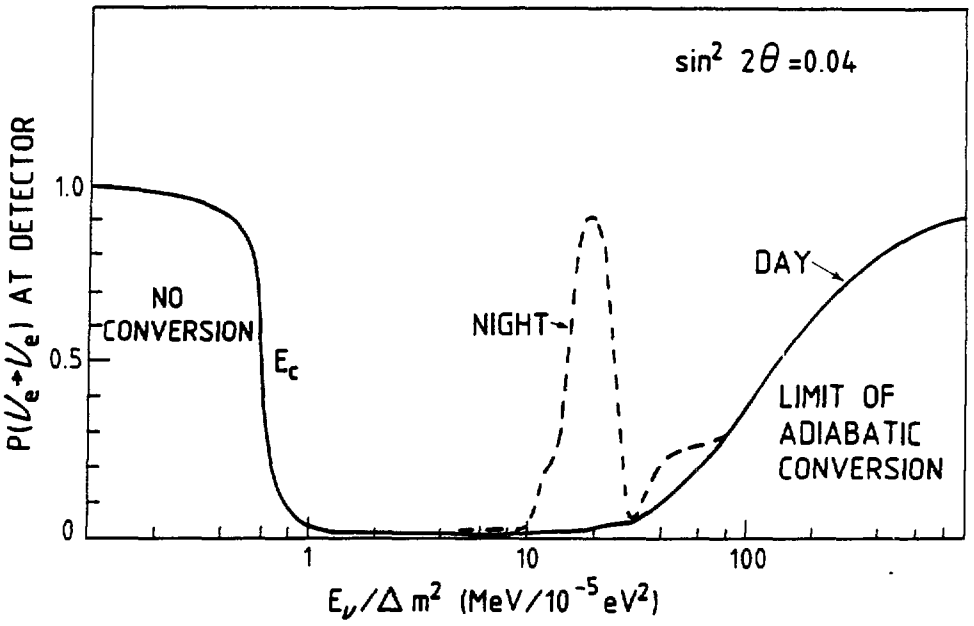

Figure 2.7: The fraction of ν_e's created at the centre of the Sun which reach the detector as ν_e is shown as a function of $E/\Delta m^2$ for $sin^2 2\theta = 0.04$. It can be seen that for certain values of $E_\nu/\Delta m^2$ there is a significant day-night effect as the neutrinos traverse varying thicknesses of terrestrial matter.

resonant oscillations might involve either the muon- or tau-neutrino, a wide range of values for M could be accommodated. Nanopoulos and Olive [33] have recently shown how similar masses might arise from radiative corrections in superstring models although again quantitative predictions are not possible.

2.3.4 Response of SNO to Solar Neutrinos

The proposed heavy water Čerenkov detector would identify solar neutrinos through three complementary reactions: inverse-beta decay of the deuteron, neutrino-electron scattering, and neutrino-disintegration of the deuteron (Section 2.2). The detection thresholds imply that the detector is sensitive to the neutrinos from the ^{8}B and *hep* processes only. In this Section the response of the detector to these neutrinos is examined, first assuming no neutrino oscillations and then showing how such oscillations could be identified.

Solar physics without Neutrino Oscillations

The first objective of the SNO experiment is to establish whether ^{8}B neutrinos are produced in the Sun. The energy spectrum for these neutrinos will be measured using the charged-current reaction (Reaction I). A ^{8}B neutrino flux of $2 \times 10^6\ cm^{-2}s^{-1}$, which is the upper limit consistent with the Cℓ/Ar experiment, would produce about 3260 events per year above an electron detection threshold of 5 MeV. With an energy resolution of better than 20%, this would allow a convincing energy spectrum to be obtained.

The sensitivity of the proposed detector is high relative to all other planned or active detectors and will make it possible to observe the ^{8}B neutrino flux at much lower levels than those attainable in any other detector. In this respect it should be reemphasized that the measurement by Davis et al. is compatible with no ^{8}B solar neutrino flux since all of the ^{37}Ar could be produced by other solar neutrino sources, principally from ^{7}Be. As will be shown in Section 3.7, an undistorted $\Phi(^8\mathrm{B}) = 5 \times 10^4\ cm^{-2}s^{-1}$ would produce a signal 3σ above background in one year of data accumulation with the SNO detector. This is 40 times lower than the upper limit to the ^{8}B neutrino flux determined in the Cℓ/Ar experiment and a factor of 10

lower than any solar model prediction in the absence of oscillations.

It will be possible to confirm that the Sun is the source of the neutrinos by examining the angular distribution of the electrons produced in reactions I and II. As discussed in Section 2.2, electrons from reaction I have a backward-forward asymmetry while those from reaction II are emitted in the forward direction. The angular resolution of the detector is expected to be 25°, making these asymmetries easily observable.

Another advantage of the SNO detector is that the data will be taken in real time. Davis and co-workers [1] have reported possible correlations between their data and those of sunspot activity and solar flares. Since the SNO detector data will be taken in real time with high statistical accuracy we will be able to check for any evidence of such correlations. We will also look for annual variations in the flux which might indicate the existence of a finite neutrino magnetic moment [9].

The ^{7}Be+p reaction rate has a strong energy dependence, hence the ^{8}B neutrino flux is a sensitive probe of the temperature within the solar core. Bahcall and Ulrich [2] have shown that it varies approximately as the 17^{th} power of the temperature. If $\Phi(^8\mathrm{B})$ can be measured to an accuracy of 10%, then the central temperature of the Sun can be determined to an accuracy of 0.6%. Temperature changes could be monitored to 1% on a weekly basis, or to higher accuracy on a longer time scale.

The only other solar neutrinos observable by the proposed detector are those from the

$$^3\mathrm{He} + p \rightarrow {}^4\mathrm{He} + e^+ + \nu_e$$

reaction. It has an endpoint energy of 18.77 MeV and therefore is well above the energy threshold of the SNO detector. However, $\Phi(hep)$ is expected to be very low, namely about 8000 $cm^{-2}s^{-1}$. This reaction is a very sensitive test of solar models since it takes place further out in the Sun than the ^{8}B producing reactions as shown in Figure 2.4. The *hep* reaction, therefore, gives important information on the ^{3}He density and the temperature at a larger radius. There are some conditions under which $\Phi(hep)$ can be measured. If the ^{8}B neutrino flux is much lower than that predicted by the SSM the *hep* induced events will stand out, giving 52 events per year distributed in an electron spectrum with a maximum energy of 17.33 MeV. The second possibility is that $\Phi(hep)$ is greater than that predicted by the SSM, as expected from some non-standard models in which convective mixing increases the amount of ^{3}He in the solar core. In this case events

from this reaction could be measured even in the presence of a substantial ^{8}B neutrino flux since the endpoint of the spectrum lies significantly above that of the ^{8}B neutrino spectrum.

Experimental Tests for Neutrino Oscillations

The essential prediction of all oscillation hypotheses for solving the SNP is that there is a substantial $\nu_\mu(\nu_\tau)$ flux corresponding to a reduction in the ν_e flux from that of the SSM prediction. In addition, many of the hypotheses predict gross distortions in the shape of the ν_e energy spectrum. Not only is this true for matter oscillations but it may also occur for a narrow range of very small Δm^2 for vacuum oscillations. Furthermore, if oscillations in the Earth are important, day- and night-time counting rates will be different.

The SNO detector is well suited to search for neutrino oscillation effects. The charged-current reaction I will give high statistics data on the ν_e spectrum. The flux of ν_μ or ν_τ may give a significant increase in the $\nu_x + e$ scattering yield over what is expected from the measured ν_e flux. The neutral-current reaction III gives the total neutrino flux independently of any oscillation scenario and, combined with the measurement of the ν_e flux from reaction I, determines in a completely model independent way whether neutrino oscillations are responsible for the SNP.

Many authors [34] have discussed neutrino oscillations and extensive numerical calculations have been carried out. The parameter space is large; two unknown mass differences and three unknown mixing angles. Three typical cases, each of which would explain the SNP, are discussed below to illustrate how oscillations could be identified with the proposed detector. Counting rates for the different reactions are given in Table 2.2 and the predicted spectra are illustrated in Figure 2.8. Reconstruction efficiencies and backgrounds are not included in these spectra but are discussed in Chapter 3 where it is indicated that projected backgrounds may prevent the identification of events below 6 MeV.

Case A: Vacuum oscillations of three neutrino types with large mixing angles and with mass-squared differences (Δm^2) greater than 10^{-10} eV^2. The spectral shape would be unchanged unless Δm^2 is near 10^{-10} eV^2; in which case the oscillation length becomes comparable with the Sun-Earth dis-

Table 2.2: Response of the detector to solar neutrinos. The rates above the indicated threshold are given in events per kilotonne year ($kt - y$) assuming a ^{8}B neutrino flux [2] of 6×10^6 cm^{-2} s^{-1} except in the last row, as indicated. The total scattering rate is given together with the $\nu_{\mu,\tau}$ component, in parenthesis, to indicate the increase in rate for reaction II over the value expected from a measurement of reaction I.

Case	$\nu_e d \rightarrow ppe$		$\nu_x e \rightarrow \nu_x e$		$\nu_x d \rightarrow \nu_x pn$[a]
	$> 5MeV$	$> 9MeV$	$> 5MeV$	$> 9MeV$	
Standard solar model	9750	2300	1100 (0)	180 (0)	2800
A. Vacuum oscillations	3260	765	480 (120)	78 (18)	2800
B. Matter oscillations					
$E_c = 9MeV$	3750	75	645 (80)	45 (21)	2800
$E_c = 2MeV$	98	22	173 (165)	27 (25)	2800
C. Non adiabatic limit in ^{8}B energy range	3750	975	488 (108)	87 (15)	2800
Standard Solar Model wrong, flux 2×10^6 cm^{-2} s^{-1}	3255	765	360 (0)	60 (0)	933

(a) Assumes neutron capture in $C\ell$ and a 5 MeV detection threshold.

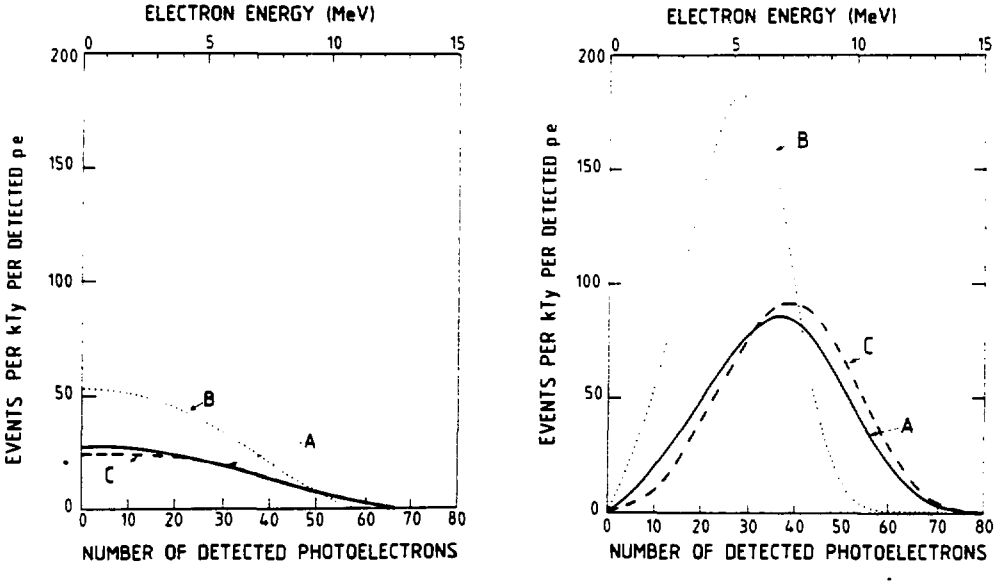

Figure 2.8: Detected ν_e spectra for various neutrino oscillation hypotheses. The left-hand figure gives the spectra for the ν-e scattering while the right-hand figure gives the spectra for the charged-current reaction. The detector sensitivity and resolution have been included in these figures. Curves A refer to the case for vacuum oscillations, curves B refer to conversion of high-energy ν_e while curves C are for non-adiabatic conversion, as described in the text.

tance and complex spectra might result. The cleanest signature for this case would be the high rate for the neutral-current dissociation reaction III, supported by a higher rate for reaction II, relative to what would be expected from a pure ν_e flux as measured by reaction I.

Case B: For values of Δm^2 in the range $(0.33 - 1.5) \times 10^{-4}$ eV^2, the high-energy ^{8}B electron-neutrinos above an energy E_c are converted to $\nu_\mu(\nu_\tau)$ [31]. The SNP could be explained by E_c between 2 and 9 MeV. E_c near 9 MeV leads to a gross change in the ν_e spectrum measured with reaction I as shown in Figure 2.8. If E_c is below the experimental threshold then an identifying feature is a modest counting rate for reaction II with a very low rate for reaction I, as indicated in Table 2.2 for E_c of 2 MeV. In such a case, the possibility of measuring the spectrum and direction of $\nu_\mu(\nu_\tau)$ through reaction II would be important in identifying the Sun as a source of ^{8}B neutrinos. Again a high event rate for reaction III would confirm the existence of neutrino oscillations.

Case C: The neutrinos from ^{8}B decay undergo non-adiabatic conversion. In this case, more low-energy ν_e's are converted than high-energy ν_e's. Changes in the ν_e spectrum are gradual and therefore are not easy to measure as shown in Figure 2.8. However, the counting rates for reactions II and III can also be used to identify this case (Table 2.2). Most of the non-adiabatic solutions which resolve the SNP give similar counting rates and spectra.

Any of the suggested modes of neutrino oscillations which explain the SNP can be identified unambiguously by the proposed detector. The adiabatic conversion gives an easily recognizable change in the energy spectrum which can be measured via reaction I. The non-adiabatic solutions are harder to distinguish on the basis of the spectrum but many of these solutions lead to some day-night differences. They would also have a profound effect on the lower energy neutrinos, and hence on the event rates in the gallium radiochemical experiments. All modes of oscillation can be detected through the ratio of neutral-current to charged-current counting rates.

The wide range of values for Δm^2 and mixing angle to which the D_2O detector would be sensitive can be appreciated by inspection of the results of calculations by Baltz and Weneser[35], shown in Figure 2.9. Part (a) of this Figure gives the counting rate per year above 5 MeV in one kilotonne of D_2O expected for the SSM flux. The ratio of charged-current events to neutral-current events would have the same form and is independent

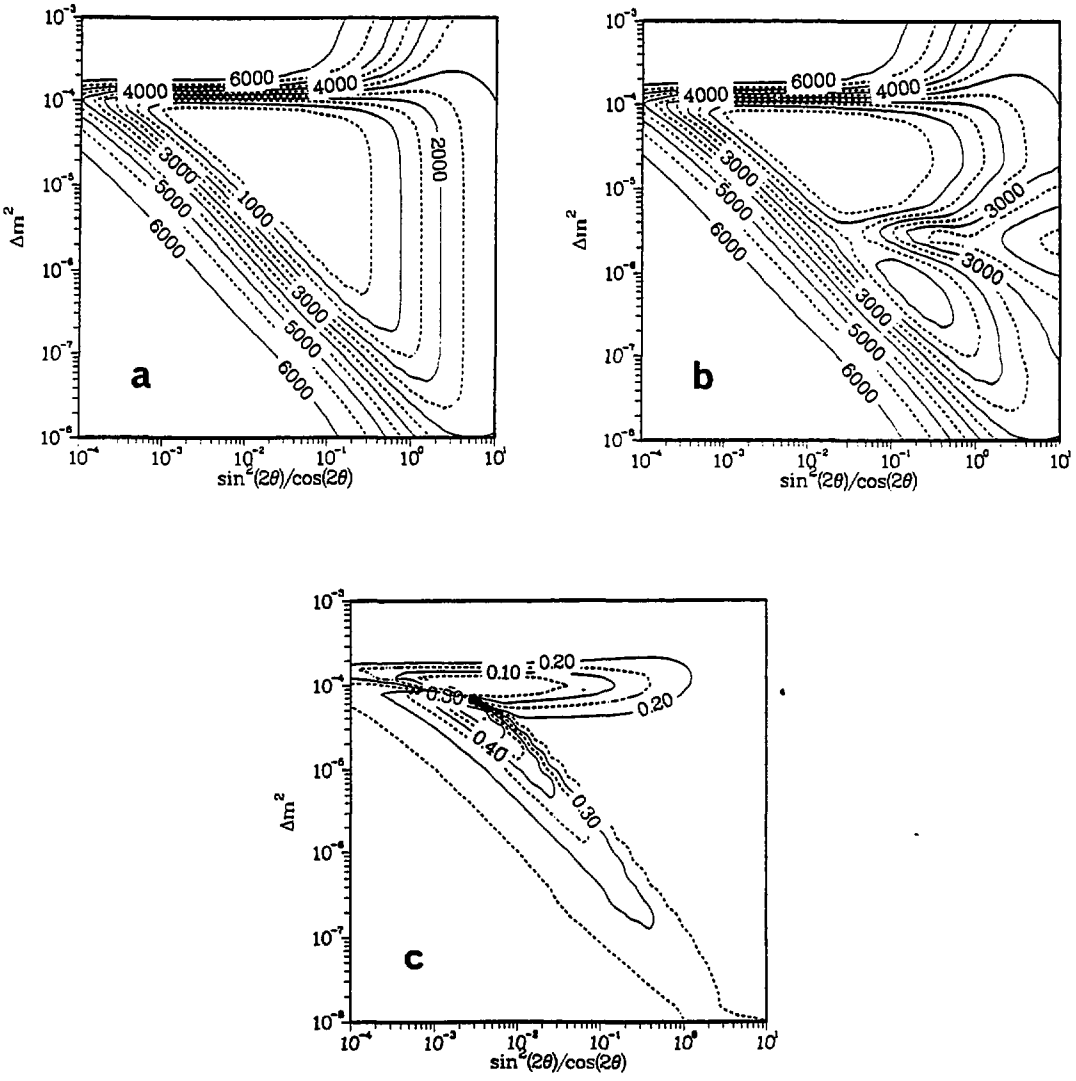

Figure 2.9: The calculations by Baltz and Weneser[35] illustrate how neutrino oscillations might be identified in the SNO detector. The upper figures give the day-time (**a**) and night-time (**b**) counting rates per $kt - y$ above 5 MeV for the SSM ^{8}B neutrino flux. While the numerical values on the contours are model dependent, the model independent ratio of charged-current to neutral-current events would have the same form. The lower figure (**c**) gives the ratio of events above 9 MeV to events above 5 MeV to indicate regions in which the ν_e spectrum is sensitive to oscillations.

of the solar model. Part (b) of the Figure gives the same information for neutrinos which have passed through the Earth. It is clear that for values of Δm^2 and $sin^2 2\theta / ccs 2\theta$ near 4×10^{-6} eV^2 and 0.5 respectively there are large differences between the day-time and night-time counting rates. As discussed with reference to Figure 2.7 the spectrum shape as measured with the SNO detector is sensitive to the oscillation parameters. Figure 2.9(c) depicts the predicted ratio of events above 9 MeV to events above 5 MeV.

2.3.5 Other Solar Neutrino Detectors

Friedlander and Weneser [36] have recently published a review of possible solar neutrino experiments. In addition to the Cℓ/Ar experiment, two other direct counting experiments and three radiochemical experiments, are operating or are being planned.

Recently, the 3000 tonne Kamiokande II light water proton decay detector has been upgraded to observe solar neutrinos [22] using the ν_x+e elastic scattering reaction. The Čerenkov photons emitted by the recoiling electron are collected by 1000 50 cm diameter photomultipliers which provide a coverage of 20% of the detector surface area. The detector was designed for observing high-energy events from proton decay; hence it is not well shielded from low-energy background events. Background from radioactivity in the surrounding materials limits the fiducial volume of the detector for detecting solar neutrinos to the central 680 tonnes and background from radioactivity in the water limits the detection threshold to 10 MeV. These effects and the low event rate from the elastic scattering reaction limit the detector's sensitivity to $\Phi(^8\mathrm{B})$. Nevertheless a result of $\Phi(^8B) \leq 3.2 \times 10^6 cm^{-2} s^{-1}$ (90% confidence level) has been reported [22] after 208 days of data taking. This is about half the value, $\Phi(^8B) = (6.0 \pm 2.0) \times 10^6\ cm^{-2} s^{-1}$, predicted by the SSM, but is significantly higher than the value deduced from the Cℓ/Ar experiment ($2.0 \pm 0.3\ \times 10^6\ cm^{-2} s^{-1}$).

A 3600 tonne liquid-argon time-projection chamber which might be used to detect solar neutrinos is being planned for the Gran Sasso Laboratory in Italy [37]. This detector is designed to measure the intensity and energies of ν_e by the charged-current reaction

$$\nu_e + {}^{40}\mathrm{Ar} \longrightarrow {}^{40}\mathrm{K} + e^-$$

As the transition to the analogue state has a threshold energy of 5.885

MeV, this detector is only sensitive to $\Phi(^8\mathrm{B})$. The $\nu_x + e$ elastic scattering reaction can also be used as in other real time experiments. No estimates of background for this detector have been published.

Two Ga/Ge radiochemical experiments have been funded. A U.S.S.R.-U.S.A collaboration [38] is constructing a 60 tonne detector in the Baksan Laboratory, and a Germany-France-Italy-Israel-U.S.A. collaboration [39] is building a 30 tonne detector in the Gran Sasso Laboratory. The $^{71}\mathrm{Ga}(\nu_e,\mathrm{e})^{71}\mathrm{Ge}$ reaction has a threshold of 233 keV, hence these detectors are sensitive to neutrinos from the *pp* reaction (55% of the capture events are from $\Phi(pp)+\Phi(pep)$). If there are no neutrino oscillations, these experiments would provide important confirmation that hydrogen fusion is the energy source in main sequence stars, a basic assumption in the theory of stellar evolution not yet verified experimentally. Because the Ga/Ge experiments can only measure the integrated ν_e capture rate, it will not, by itself, provide a model-independent solution to the solar neutrino problem. However, these experiments will provide information about the low-energy neutrino flux.

A search for $^{98}\mathrm{Tc}$ in deeply buried molybdenum deposits is underway in the United States [40]. The long half-life of $^{98}\mathrm{Tc}$, 4.2×10^6 years, allows a measurement of the long term average neutrino production in the Sun. The $^{98}\mathrm{Mo}(\nu_e, e^-)^{98}\mathrm{Tc}$ reaction is sensitive mainly to the $^8\mathrm{B}$ and *hep* neutrinos. First data from this experiment should be available soon but interpretation may be difficult because the cross section for neutrino absorption in $^{98}\mathrm{Mo}$ is uncertain by a factor of 2.

2.4 Stellar Collapse

2.4.1 Introduction

The dramatic appearance of Supernova SN 1987A in the Large Magellanic Cloud in February 1987 [41] was notable as the nearest optically observed stellar collapse in 400 years and as the first stellar collapse from which neutrinos were directly observed [42]. The light water Čerenkov detectors of the Kamiokande II and Irvine-Michigan-Brookhaven (IMB) collaborations each observed about 10 neutrino events, primarily from $\bar{\nu}_e$, grouped within a time period of 12 seconds. The number and the energy

distribution of neutrinos observed is consistent with theories of stellar collapse and the total time spread is consistent with the expected production times for neutrinos [43,44,45]. In addition, the large distance from SN 1987A (50 *kpc*) and the short time duration of the events enable an upper limit to be set [46] on the $\bar{\nu}_e$ mass, a limit which is comparable to that obtained from terrestrial experiments [47].

Events such as SN 1987A are rarely seen because most nearby supernovae (particularly those within our Galaxy) are thought to be obscured from optical observation by interstellar dust. Neutrinos are not affected by this material and could be detected from supernovae in any part of our Galaxy. Reasonable estimates of the number of stellar collapses within our Galaxy, based on the number of medium and massive stars observed and their expected evolution lifetimes, indicate that one collapse may occur on average every 10 years [48]. If such an event occurs, the SNO detector, with active volumes of both light and heavy water, will provide extensive information on the neutrino fluxes. The D_2O volume provides much higher sensitivity to $\nu_e, \nu_\mu, \nu_\tau, \bar{\nu}_\mu$ and $\bar{\nu}_\tau$ than is possible in existing detectors and hence, important new information would be obtained. In addition, the $\bar{\nu}_e$ flux could be monitored in both the light and heavy water.

The theory of stellar collapse has been discussed by many authors and the following scenario is proposed. After a star has exhausted its hydrogen fuel and evolved away from the main sequence, the ^{4}He core will contract. The eventual fate of the star will depend largely on its initial mass, M_{MS}, and on how much of its mass has been ejected during different stages of its development [49]. In a massive star, ($10M_\odot \leq M_{MS} \leq 70M_\odot$), the carbon core contracts and ignites non-degenerately. It evolves through the different stages of nuclear burning and develops an iron core which eventually collapses, producing a type II supernova and leaving behind a remnant neutron star or black hole.

Recent theoretical investigations of pre-supernova and supernova formation have led to qualitative understandings of the physical processes involved. Once an iron core is developed, no more nuclear energy can be generated within the core; hence it must undergo gravitational contraction until it is supported by a degenerate electron gas. Addition of iron group nuclei from outer shells which are still processing nuclear fuel increases the core mass until it exceeds the Chandrasekhar limit, $M_{CH}=5.76Y_e^2M_\odot$, where Y_e is the electron to nucleon ratio. At this point, the degenerate electron gas can no longer resist the gravitational force and the core starts its fi-

nal infall. The temperature and density increase, leading to inverse beta decay and neutrino loss as well as photodisintegration of the iron group nuclei. These processes further reduce the core energy and pressure, resulting in a supersonic implosion. The inner core (mass $\leq 1.1 M_{\odot}$, radius $\leq 10\ km$) stiffens at nuclear matter density, $\rho_N \sim 2.7 \times 10^{14}\ g\ cm^{-3}$, and causes the infalling material to bounce, resulting in an outgoing shock wave [43]. Electron capture and ν_e loss lead to the formation of a neutron star [50]. The protoneutron star cools down by the emission of neutrinos and anti-neutrinos of all types which are produced by neutral-current processes [51]. In the cooling phase, for a sufficiently massive core, the emission of neutrinos and anti-neutrinos may stop abruptly as the protoneutron star collapses into a black hole. The mechanism of transferring the energy from gravitational collapse to the outer mantle in a supernova explosion remain controversial. Some models suggest that the shock wave from the core-bounce can blow the outer layers apart while others suggest that nuclear dissociation and neutrino loss will remove sufficient energy from the shock wave to stall its outward motion, and additional deposition of energy by neutrinos diffusing out of the hot collapsed core is needed in order to drive off the outer mantle. Core collapse of a star that has ejected most of its outer shell material earlier may not produce a bright visual display (quiet collapse).

2.4.2 Neutrino Production in Stellar Collapse

Neutrinos play an important role in the early stages of the collapse in reducing the lepton density as well as removing energy from the core. Independently of the details of the collapse, to form a $\sim 1 M_{\odot}$ neutronstar from an iron core which contains roughly equal numbers of protons and neutrons, $\sim 10^{57}$ protons have to be converted into neutrons by the electron capture reaction

$$p + e^{-} \rightarrow n + \nu_e \ .$$

In addition, $\sim 4 \times 10^{53}$ ergs of gravitational energy must be released in the formation of a neutron star. The total observed electromagnetic and kinetic energy of a supernova outburst is $\leq 10^{51}$ ergs, and gravitational radiation will remove at most 1% of the available energy [52]. Thus almost all the energy must be carried away by neutrinos and anti-neutrinos created by electron capture and neutral-current processes. If the energies of these neutrinos are in the range 5→20 MeV, as is currently believed, a total of $\sim 10^{58}$ neutrinos and anti-neutrinos of different types will be emitted.

This simple picture has been confirmed by the recent observations from SN 1987A [42].

While the general features of stellar collapse are qualitatively understood, detailed dynamics of the collapse, which depend on the pre-supernova model used, on the physics of neutrino interactions and on the properties of nuclear matter, have not been firmly established. Various numerical codes with different models for neutrino transport, nuclear matter equations of state and zoning techniques produce different scenarios for the formation of supernovae; hence different neutrino emission time structures and energy spectra [45,53,54]. Direct observation of neutrinos from supernovae will provide valuable insight into the physical processes which are taking place in this extremely high density and high temperature environment.

It is generally accepted that a short burst of ν_e will be generated by the electron capture reaction during the initial collapse. Their average energy is $\sim$15 MeV, and the burst lasts for a few tens of milliseconds. Emission of neutrinos and anti-neutrinos in the cooling phase of the protoneutron core lasts from a few seconds to a few tens of seconds. A typical prediction of the time distribution of neutrino luminosity [45] is shown in Figure 2.10. Roughly equal numbers of neutrinos and anti-neutrinos of all types are produced by the neutral-current processes. At a density of $10^{11} \rightarrow 10^{12}\, g\, cm^{-3}$, the neutrino mean free paths are $\sim 10^5 \rightarrow 10^6 \cdot cm$. Hence most of the neutrinos and anti-neutrinos are trapped inside the core, blocking electron capture and slowing down the process. The average energies of these neutrinos and anti-neutrinos, which leak out by diffusion, are in the range 10$\rightarrow$30 MeV. Because of their longer mean free paths, ν_μ ($\bar{\nu}_\mu$) and ν_τ ($\bar{\nu}_\tau$) can escape from higher density regions in the core; hence they may have higher average energies than ν_e ($\bar{\nu}_e$). However, convection within the protoneutron star may increase the energies of all neutrinos and anti-neutrinos substantially [55]. The energy spectra calculated by Mayle et al. [44] are shown in Figure 2.11. A sudden termination of neutrino events over a time period of milliseconds during this diffusion cooling phase would strongly suggest the formation of a black hole.

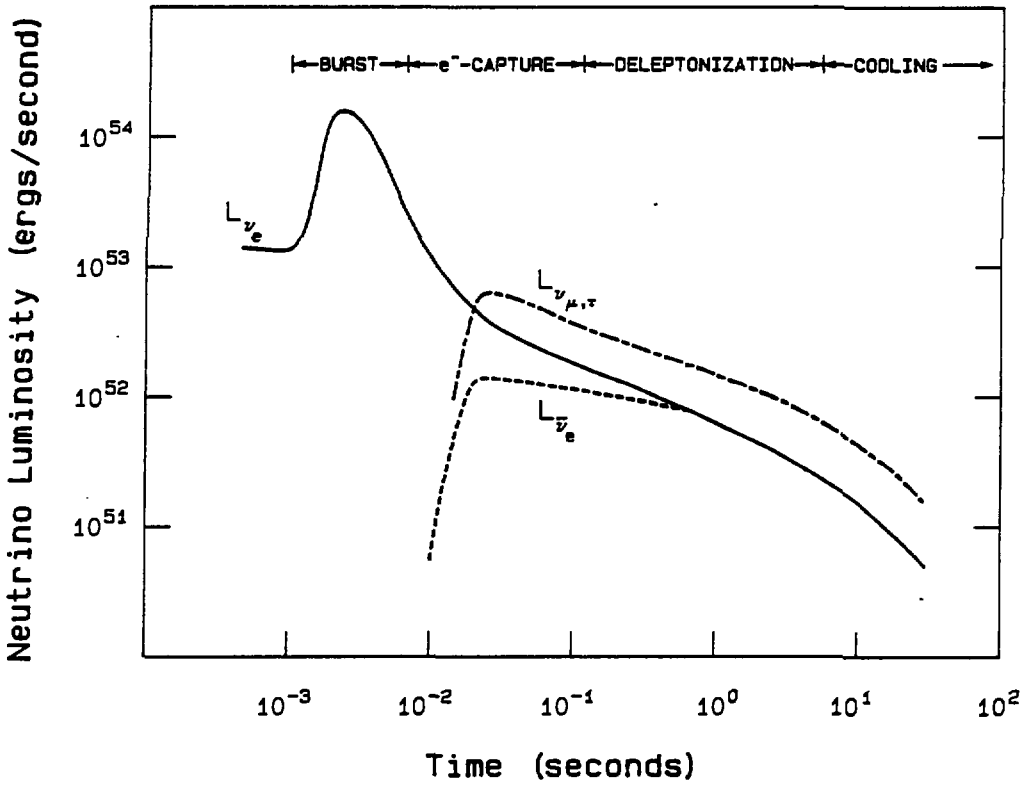

Figure 2.10: The production of the different types of neutrino is shown in relation to the stages of a supernova development. (Adapted from the work of Burrows [45].) If the neutrino flux were to cease after a few milliseconds the formation of a black hole would be strongly indicated.

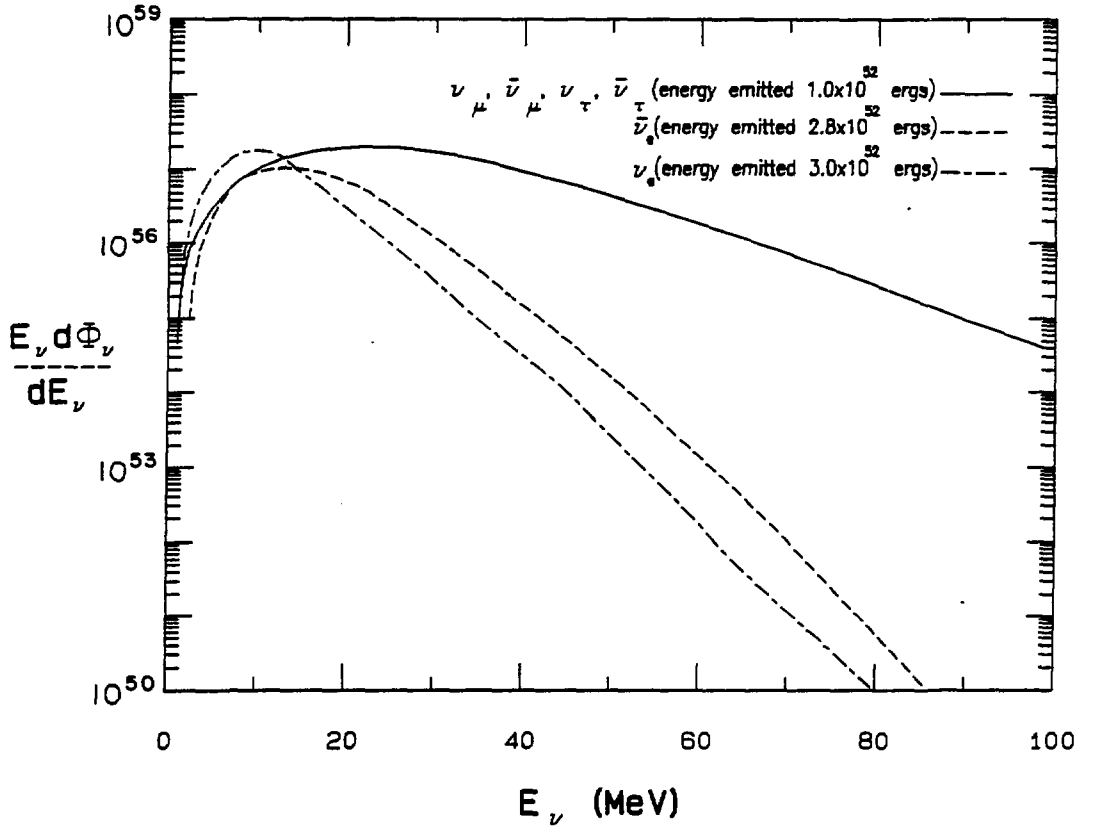

Figure 2.11: The time-integrated neutrino spectra for a supernova of a 12 $M_\odot$ star as calculated by Mayle et al. [44].

2.4.3 Detection of Supernovae Neutrinos in SNO

Following the prediction that a large number of neutrinos will be radiated from the collapse of the iron core and the cooling of protoneutron stars, several experiments were proposed to observe these neutrino bursts. A number of real time underground scintillator-based experiments [56] have been built to search for $\bar{\nu}_e$ from stellar collapse. These detectors have small fiducial volumes; hence their sensitivities are limited. The large volume water Čerenkov detectors have proven their value in this field by the detection of neutrinos from SN 1987A.

The proposed SNO detector will make a unique contribution to the study of these neutrinos because of its sensitivity to all neutrino types, because of its low-energy threshold, and because it can distinguish the various components of the neutrino flux. This detector, existing light water Čerenkov detectors and scintillator detectors all have high sensitivity for $\bar{\nu}_e$ through the charged-current reaction V, $\bar{\nu}_e + p \rightarrow n + e^+$. The heavy water detector has much higher sensitivity to the ν_e flux than any other detector through reaction I, $\nu_e + d \rightarrow p + p + e^-$. After reconstruction, the spatial distribution of events can be be used to determine the ν_e and $\bar{\nu}_e$ fluxes; the majority of the charged-current events in the D_2O are from ν_e while most of the events in the H_2O are from $\bar{\nu}_e$. It is expected that the contributions from elastic scattering reactions will be less than 10% of the total event rates. In addition, the neutral-current reaction III, $\nu_x + d \rightarrow \nu_x + p + n$, in the heavy water can be used to measure the total neutrino intensity. Since the ν_e and $\bar{\nu}_e$ fluxes are determined independently, it is possible to deduce the total flux of other types of neutrinos. For a stellar collapse at 10 kpc, the numbers of neutrino induced events in a 1 kt detector are listed in Table 2.3. In this calculation, the distributions published by Bowers and Wilson [43] are used. In the cooling phase the average energies of ν_e, $\bar{\nu}_e$ and other neutrinos are ~10 MeV, ~11 MeV and ~25 MeV respectively. The ν_e in the initial burst are assumed to have an average energy of 15 MeV [51] and the burst is assumed to be $\sim 10\,ms$ long. The neutrino intensities and time distributions are taken from Burrows [45].

	Reaction	Target medium	Events in ν_e burst kt^{-1}	Events in cooling phase kt^{-1}
I	$\nu_e + d \longrightarrow p + p + e^-$	D_2O	10	33
II	$\nu_x + e \longrightarrow \nu_x + e$	D_2O/H_2O	1	16
III	$\nu_x + d \longrightarrow \nu_x + p + n$	D_2O	6	760
IV	$\bar{\nu}_e + d \longrightarrow n + n + e^+$	D_2O	0	20
V	$\bar{\nu}_e + p \longrightarrow n + e^+$	H_2O	0	120

Table 2.3: Predicted number of events in the SNO detector from a stellar collapse at 10 *kpc*, at 100% detection efficiency.

As mentioned above, one of the important results from SN 1987A was the upper limit on the mass of the $\bar{\nu}_e$. As is clear from Table 2.3, reaction III provides a large sensitivity to $\nu_{\mu,\tau}$ and consequently it is possible that interesting mass measurements could be obtained. The present limits (Aguilar-Benitez et al. in ref. [47]) are 0.25 MeV for ν_μ and 70 MeV for ν_τ. For a collapse at 10 *kpc*, a mass of 50 eV would give a delay of 3 seconds in the ν_μ or ν_τ events. Although the cooling phase may last for 10 seconds, a shift of this magnitude with respect to the ν_e and $\bar{\nu}_e$ events would be easily seen. A neutrino mass in the range 50 eV $< m_\nu <$ 100 keV could be measured readily. If the mass were as high as 200 keV, the events would come a year late and would be spread over half a year. This would be hard to detect against the solar neutrino background. Moreover, the missing neutral-current events in the burst would allow one to conclude that either the neutrinos have a large mass or they decayed or indeed, they were never produced. This sensitivity to the $\nu_{\mu,\tau}$ mass is a distinct advantage of the D_2O detector. In the event of a stellar collapse within our Galaxy it would permit the observation of finite $\nu_{\mu,\tau}$ mass with a sensitivity far better than terrestrial experiments and, perhaps, sufficient to determine whether the total mass of neutrinos is large enough to close the Universe. The required mass is estimated to be about 40 eV [57]. In addition, although the number of ν_e events from the initial burst is relatively small, the inherent timing accuracy is very good. For example, if the 10 expected events were to occur within a 20 *msec* period, this would imply an upper limit of about 3 eV for the mass of the ν_e, a sensitivity substantially better than present limits in terrestrial experiments.

Although the rate of stellar collapse within our Galaxy is expected to be not more than one every ten years, the information obtainable from such a collapse would be substantial. The SNO detector is capable of measuring the numbers and time distributions of different neutrino types. This information will provide a very detailed picture of stellar collapse and it will be possible to measure masses for all neutrino types with greatly improved accuracy. Moreover, the detector will provide continuous and automatic monitoring for neutrino bursts, either as a stand-alone facility or as a part of an international network of neutrino detectors. The early detection of a neutrino burst may lead to the discovery of a new supernova, hours before any optical display can be expected. This would make it possible for astronomers to study the very important early phases of the explosion in the electromagnetic domain.

2.5 Other Physics

There are a number of other areas of physics where the proposed detector would make a significant contribution. Three such examples are outlined below.

The design of the detector follows that of the successful light water detectors built to search for proton decay and the use of heavy water allows a new dimension for such a search. Baryon non-conservation has been discussed extensively in the literature [58]. Minimal SU(5) theory [59] which predicted a proton decay lifetime of about 10^{30} y, with $e^+ + \pi^\circ$ as the main decay mode, has been contradicted by experiments [60,61,62] and stringent limits on several of the other decay modes have been set. With the heavy-water detector this search could be extended to give limits on the proton lifetime which are independent of decay mode [63]. This extension is possible because, after the decay, the spectator neutron would be captured giving a signal which is independent of the decay process. Two possible search modes are suggested. If just the signal from the free neutron is used there will be a background from the solar neutrino charged- and neutral-current signals which would limit sensitivity to a limit of 5×10^{27} y; a factor of 20 better than the present lower limit of 2.2×10^{26} y from a radiochemical experiment [64]. The sensitivity can be greatly improved if in the proton decay a prompt Čerenkov signal is detected. The signature of the decay would be this signal followed by the delayed neutron capture signal. The main background to such a process would come from the flux of atmospheric neutrinos which is estimated to be 30 per kt-y; corresponding to a sensitivity limit on the proton lifetime of 2×10^{30}

It has been suggested than magnetic monopoles may exist and that they may catalyze nucleon decay [65,66]. It has also been suggested that these monopoles might get swept up by the Sun, inducing nucleon decay into pions which subsequently decay producing electron-neutrinos in the energy range 20 MeV$< E_\nu <$ 50 MeV. The Kamiokande experiment has set an upper limit of $10^4\, cm^{-2}s^{-1}$ on the flux of these neutrinos [67]. The cross section for reaction I in the SNO detector is 70 times larger than for the $\nu_e + e$ scattering reaction detected at Kamiokande. This would permit a flux as low as $100\, cm^{-2}s^{-1}$ to be detected, allowing for the slightly higher background expected at Sudbury from atmospheric ν_μ interactions.

Some grand unification theories predict ΔB=2 $n - \bar{n}$ oscillations [68].

Such oscillations are suppressed in nuclear matter because the n and $\bar{n}$ experience different potentials. If such an oscillation did occur the $\bar{n}$ would soon annihilate with a nucleon producing mesons. The deuterons in the D_2O offer an attractive medium in which to search for this effect. The suppression is predicted to be smaller in deuterium than in heavier nuclei [69] and more importantly, the suppression calculations are less uncertain than for more complex nuclei. In addition, the subsequent annihilation is free from complications such as Fermi motion or nuclear absorption. Scaling from the Kamiokande measurement [70] we estimate that the SNO detector would be sensitive to oscillation periods in the deuteron of order 7×10^{31} years which implies an oscillation time of 3×10^8 s for the free neutron.

Chapter 3

The SNO Detector

3.1 Introduction

An outline of the proposed detector is shown in Figure 1.1. It consists of 1000 tonnes of heavy water (D_2O), of purity greater than 99.85%, contained in an acrylic vessel. This vessel, constructed from 5 *cm* thick panels, is surrounded by 4 *m* of high purity H_2O and 0.9 *m* of low activity concrete. Mounted uniformly around the acrylic vessel, at a distance of 2.5 *m*, are 1955 Hamamatsu R1449 50 *cm* diameter photomultiplier tubes (PMTs), providing 40% photocathode coverage. The PMT array is sensitive to Čerenkov light produced by relativistic electrons and muons in the central regions of the detector. The electrons are produced by neutrino interactions as discussed in Chapter 2, and by background sources. The cavity for the detector will be located at a depth of 2070 *m* (6800 foot level) in the "hanging wall" of the Creighton mine of INCO Limited, near Sudbury, Ontario.

The laboratory site was chosen in the "hanging wall" rock since it is composed of norite which has a lower Th and U content than the gabbro, granite and diorite which make up the "footwall" rocks, and because its homogeneous nature is more suited to the construction of a large cavity. The 6800 foot level provides a 5900 metre water equivalent (*mwe*) flat overburden, sufficient to make the cosmic-ray muon rate negligible. In addition, anticipated mining activities at this level ensure adequate servicing over the projected lifetime of the laboratory.

All other detector parameters are subject to external constraints and to optimization of the detailed design. For the present, INCO requires that the excavation for the detector must not exceed 20 m in diameter. The results of the geotechnical survey, to be completed by the end of 1987, and reported in a Supporting Document [SD-1], could alter this dimension. Initial discussions with Atomic Energy of Canada Limited (AECL) concerning the D_2O indicated that a loan of more than 1000 tonnes was unlikely to be approved. Furthermore, estimates of the background from the norite suggest that 4 to 5 m of H_2O are required to shield the D_2O and hence 1000 tonnes is as much as can be accommodated within the confines of a 20 m cavity. The reference design presented here is a design for which feasibility of construction and operation can be assured, based on presently available data.

The measured radioactivity in the PMTs requires that they be placed 2.5 m from the D_2O containment vessel and the activity of the host rock requires that approximately 1 m of low activity concrete (with 1% boron) and 1 m of H_2O be installed between the norite and PMTs to reduce the contribution from external γ-rays to a level which is low compared with the contribution from internal sources.

The present design specifies an ultra-violet transmitting (UVT) acrylic vessel of 5 cm thickness to contain the D_2O. This design, in which the vessel is supported under tension, allows a large margin of safety against failure. The non-spherical shape is required to maintain a 5 m distance from the norite. The choice of 40% photocathode coverage is dictated by a consideration of the desired efficiency, energy threshold and resolution of the detector.

In this Chapter we describe the operation of the proposed detector placing particular emphasis on the characteristics relevant to the detection of solar neutrinos. In Section 3.2 the performance of each detector component which affects the light transmission or detection is described together with an outline of the electronics required to process the resulting signals. The experiment requires an exceedingly low radioactive environment and much of the experimental work done for this proposal has been devoted to searching for materials from which to create this environment. The results of these studies are discussed in Section 3.3. In Section 3.4 we report on Monte Carlo simulations of all aspects of the detector response, both to the expected neutrino signals and to the various background sources. Because there exist little experimental data on the response of Čerenkov detectors

to low-energy electrons, a small test detector has been developed and some of the results obtained with it are given in this Section. In Section 3.5 we discuss the detection of the neutral-current reaction and its backgrounds. In Section 3.6 we examine the effects of changing the photocathode coverage on detector response to the charged-current and neutral-current reactions. The experimental program is outlined in Section 3.7. A number of important engineering details required to realize a practical detector are covered in the following Chapter on laboratory design (Chapter 4).

To provide a constant reference, for all calculations we have assumed a ^{8}B ν_e flux of $2 \times 10^6\ cm^{-2}s^{-1}$, the maximum flux consistent with the results of the Cℓ/Ar experiment, and a total flux of all neutrino types of $6 \times 10^6\ cm^{-2}s^{-1}$ as predicted by the SSM.

3.2 Detector Operation

As discussed in the previous Chapter, neutrinos interact in the detector producing either relativistic electrons or free neutrons. The neutrons are subsequently captured generating γ-rays which in turn produce relativistic electrons through the Compton scattering and pair production processes. The electrons will produce Čerenkov photons which pass through the D_2O, acrylic, and H_2O to be detected by the PMTs. The signals from the PMTs are interpreted to give the location, energy and direction of the electron based on the time of arrival of the photons at the PMTs and the locations of the particular PMTs hit. In this Section the properties of each component which directly influence the ultimate performance of the detector are examined.

3.2.1 Optical Properties

Charged particles (electrons) travelling in a transparent medium at velocities greater than the group velocity of light in that medium radiate Čerenkov light. These photons have a continuous spectral distribution which is constant in frequency over the spectral range to which the PMTs are sensitive. The photons are emitted in a forward cone whose axis is the

medium	n	T_T (MeV)
D_2O	1.333	0.262
H_2O	1.338	0.258
acrylic	1.461	0.190
pyrex	1.474	0.185

Table 3.1: The refractive index (n) and the corresponding kinetic energy threshold (T_T) for Čerenkov radiation are listed for the relevant materials in the detector.

direction of the electron and whose opening angle (θ) is given by

$$cos\ \theta = (n\beta)^{-1}$$

where n is the index of refraction in the medium and β is the electron's speed relative to the speed of light. In D_2O, θ equals 41° for relativistic electrons. Because the electron direction is constantly changing due to scattering, the detected light will not, in general, correspond to a simple ring pattern. The index of refraction for various media and the corresponding kinetic energy thresholds T_T (below which electrons have speeds less than c/n) are given in Table 3.1. The number of photons $N(\gamma)$ emitted by the electrons is approximately proportional to the electron track length (and hence energy) and is ~358 photons per cm [71] in the spectral range to which the PMTs are sensitive (λ = 300 to 650 nm). The electron track length in D_2O is approximately 0.45 cm per MeV [72] for electrons of kinetic energy between 5 and 15 MeV. Thus about 1140 photons are produced by a 7 MeV electron.

When the SNO detector was first proposed, the published literature [73] indicated that light attenuation was significantly greater in D_2O than in H_2O. Indeed, the quoted attenuation in the blue part of the spectrum was so large that operation of the detector would have been severely compromised. Therefore, we measured [74] the light transmittance in D_2O and H_2O, and found that, as expected on theoretical grounds, the attenuations in the blue part of the spectrum are similar (Figure 3.1). The D_2O sample was as provided by AECL while the H_2O was freshly purified at NRCC. The differences between the H_2O and D_2O at the high frequency end may reflect the higher purity of the H_2O.

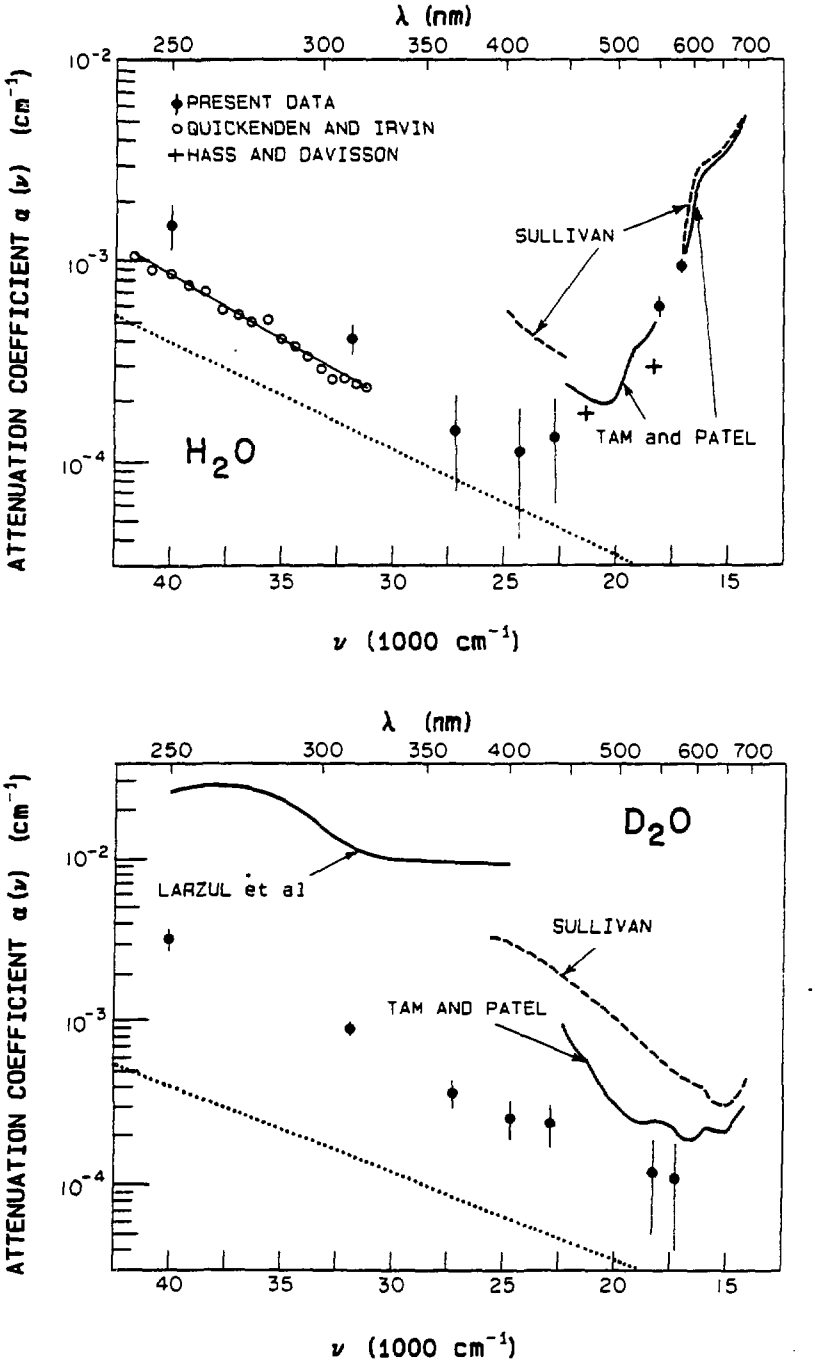

Figure 3.1: Experimental attenuation coefficients for H_2O and D_2O as a function of frequency. The solid circles with error bars represent our data [74]. The data from some other experiments [73] are also given for comparison. The dotted line represents the Rayleigh scattering contribution to the attenuation.

The proposed detector differs from the IMB and Kamiokande II detectors in that the sensitive volume is contained within an acrylic vessel. Careful attention has consequently been paid to the optical properties of acrylic and the results of a series of measurements are described in Annex-2. The most serious problem is absorption in the ultraviolet (UV) region; reflection from the water-acrylic interfaces is also important and is addressed in the Monte Carlo calculations (Section 3.4.3). Considerable variation has been observed in the optical quality of UV transmitting acrylics. The Polycast [75] material which is assumed in the present design would attenuate the light by 21% while samples from other manufacturers gave attenuations between 15% and 29%. Good light transmission is one of several important properties of the acrylic which must be optimised in the design. Radioactive content, size of sheet, cost, strength and bonding properties are additional important factors.

Another important feature of the acrylic is its long term behaviour either when immersed in ultra-pure H_2O and D_2O or with an additive in the D_2O. A series of tests, described in Annex-3, are being carried out involving immersion of acrylic samples in quartz vessels containing H_2O, D_2O or a 2.5% solution of $NaC\ell$. Maintaining these samples at a temperature of 65°C accelerates substantially any chemical activity that might adversely affect properties of the acrylic so that noticeable changes might be achieved after several weeks of immersion. Initial results indicate that the long term deterioration in transmittance in the UV below 400 nm is about 4% in 15 years, which would not seriously affect the performance of the proposed detector.

The transmittances of Čerenkov photons through 5 m of D_2O, 5 cm of Polycast acrylic and 3 m of H_2O are plotted as a function of photon frequency in Figure 3.2. The quantum efficiency of the Hamamatsu R1449 PMTs over the same frequency range is also shown in Figure 3.2. The average quantum efficiency over this frequency range is 17% and the attenuation reduces this to an effective 11%. Finally, the detection efficiency is reduced to 4.4% by the 40% photocathode coverage. This estimate does not take into account the geometric effects of the hemispherical PMT design although this is considered in the Monte Carlo calculations described in Section 3.4.

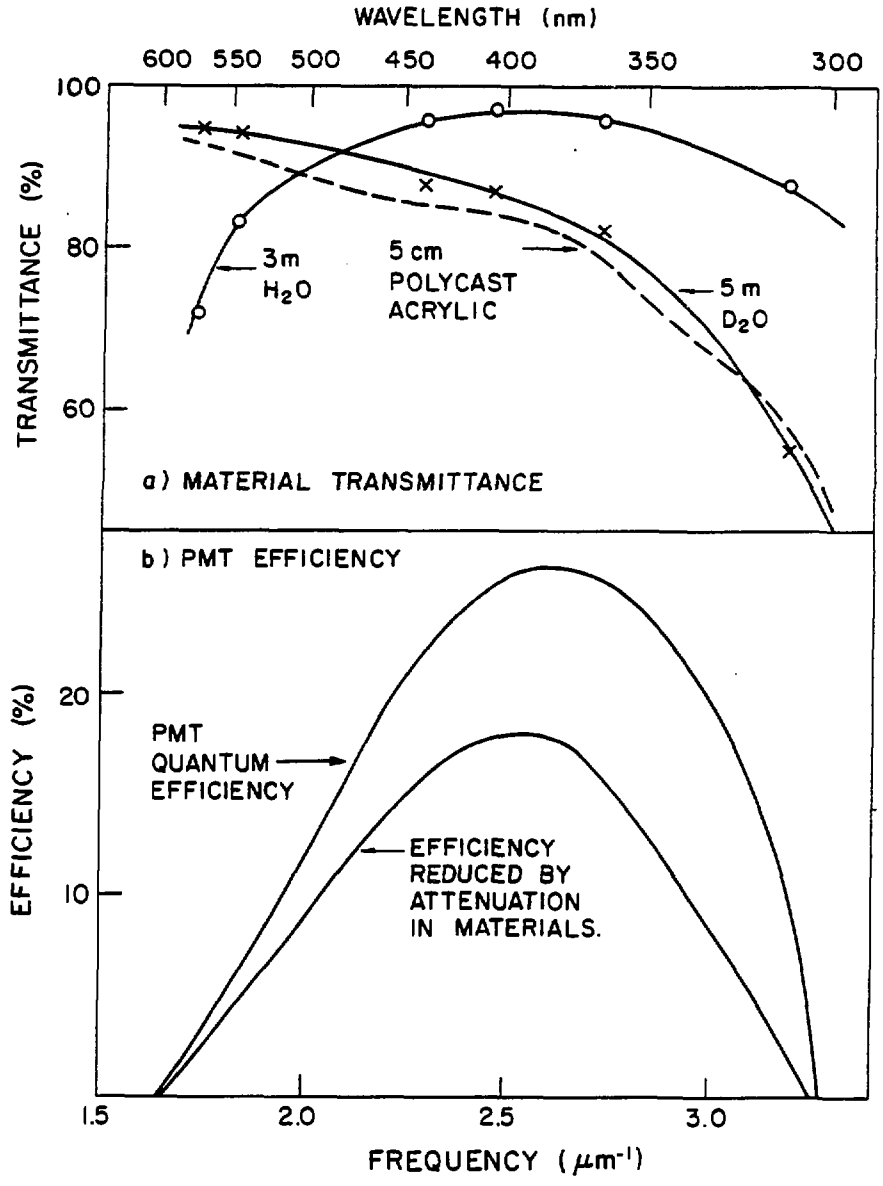

Figure 3.2: The frequency dependence of the transmittance of light through various detector components from the centre of the detector to the PMTs is shown in the upper part of the Figure while the quantum efficiency of the PMTs is shown in the lower part.

3.2.2 Photomultiplier Tubes

In the reference design of the detector it is assumed that Hamamatsu R1449 [76] 50 *cm* PMTs will be used to detect the Čerenkov light. These PMTs offer the lowest cost per unit photocathode area of any PMT currently commercially available and, moreover, their reliability has been demonstrated in the Kamiokande II water Čerenkov detector. A possible alternative is the R1449Z PMT, a recent variant of the R1449 PMT, employing a smaller dynode structure to give improved timing characteristics.

The properties of these PMTs which have been investigated are linearity, gain, sensitivity to single photon illumination, photocathode uniformity, sensitivity to the Earth's magnetic field and electron transit time spreads for various starting points on the photocathode. A detailed account of these studies is given in Annex-4.

The linearity of a sample R1449 PMT was tested by illuminating its photocathode with light from an optical pulser and attenuating the light with neutral density filters. At the lowest levels the anode pulse height did not depend on intensity indicating single photoelectron counting while, at higher levels, a clear peak was observed whose amplitude was proportional to the intensity up to an amplitude corresponding to 300 detected photoelectrons. The gain at an anode voltage of 2350 *Volts* was found to be 4×10^6.

The R1449 PMT was illuminated with low light levels from a LED source in an operating regime where single photoelectrons are expected to be dominantly produced. The resulting spectrum is shown in Figure 3.3. It is clear that it is not possible to distinguish these pulses from the noise. The efficiency for counting single photoelectron pulses depends on the form of the response and was estimated to be 85% at a detection threshold of 0.25 photoelectrons. The quantum efficiency was measured to be 23% at 390 *nm* compared with 26% reported elsewhere [76].

The large PMTs are sensitive to the Earth's magnetic field and this is particularly true of the R1449Z PMT due to the smaller target area of the first dynode. The sensitivity of this photomultiplier tube to magnetic fields was determined by placing it in the magnetic field of a rectangular coil (80 $cm \times 100$ cm) oriented so that the axis of the coil was parallel to the Earth's magnetic field and centred on the first dynode of the photomultiplier tube.

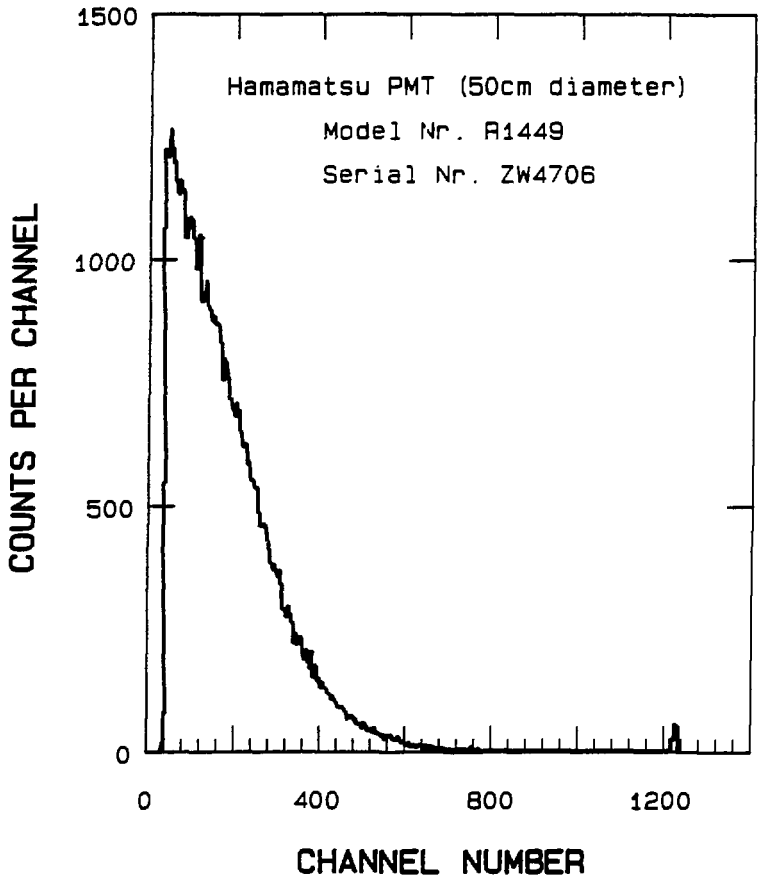

Figure 3.3: Single photoelectron spectrum for a Hamamatsu R1449 PMT.

These measurements show that the photocathode sensitivity varies by less than 5% from its optimally compensated value if the field is reduced to a magnitude of 10% of the Earth's field. Such a field can be achieved in the SNO detector using a set of horizontal and vertical coils located behind the "Sulfurcrete" shielding blocks. Our measurements [Annex-4] imply that it will not be necessary to use μ-metal shielding on the PMTs. The final design of the field compensation system can only be done after a magnetic survey of the cavity has been carried out.

The electron transit time spread (TTS) was measured for three R1449 PMTs and one R1449Z PMT. The TTS was measured to be 8.0 to 9.5 *ns* FWHM for the R1449 PMTs and 6.5 *ns* for the R1449Z PMT. The centroid of the TTS varied by less than 1.5 *ns* for all points on the photocathode.

While the R1449 PMT is the optimum photomultiplier tube available at the moment, work is proceeding with Burle Industries (formerly RCA - New Products Division) on the design of a 20 *cm* PMT which would have a number of advantages for the SNO detector. The timing resolution might be about 5 *ns* which would allow better event reconstruction accuracy. The PMTs would provide better pulse-height resolution at low levels allowing the single photoelectron peak to be identified. In addition, the 20 *cm* PMT would have a flat photocathode and less glass per unit area than the 50 *cm* PMT, which would give the SNO detector a more uniform sensitivity [Annex-7] and a lower background from radioactivity in the glass. We are also working on a less radioactive glass from which to fabricate the PMT envelopes; our findings have been summarized in Annex-5. It is expected that the cost per unit photocathode area of the 20 *cm* PMTs would be similar to that of the R1449 PMTs.

3.2.3 Electronics and Data Acquisition

The electronics has to be able to identify significant events and to record, for each event, the "hit" pattern of PMTs detecting photons, the amplitude of the anode signal in each PMT and the arrival time of the photons at each PMT. The average coincidence rate is expected to be low ($\sim$100 Hz at a threshold of 20 PMTs hit) and poses no problem although the burst rate in the case of gravitational collapse of a star (supernova) could be as high as a few thousand events in a second. In addition, we require a short dead time after each signal so that an event such as a stopping

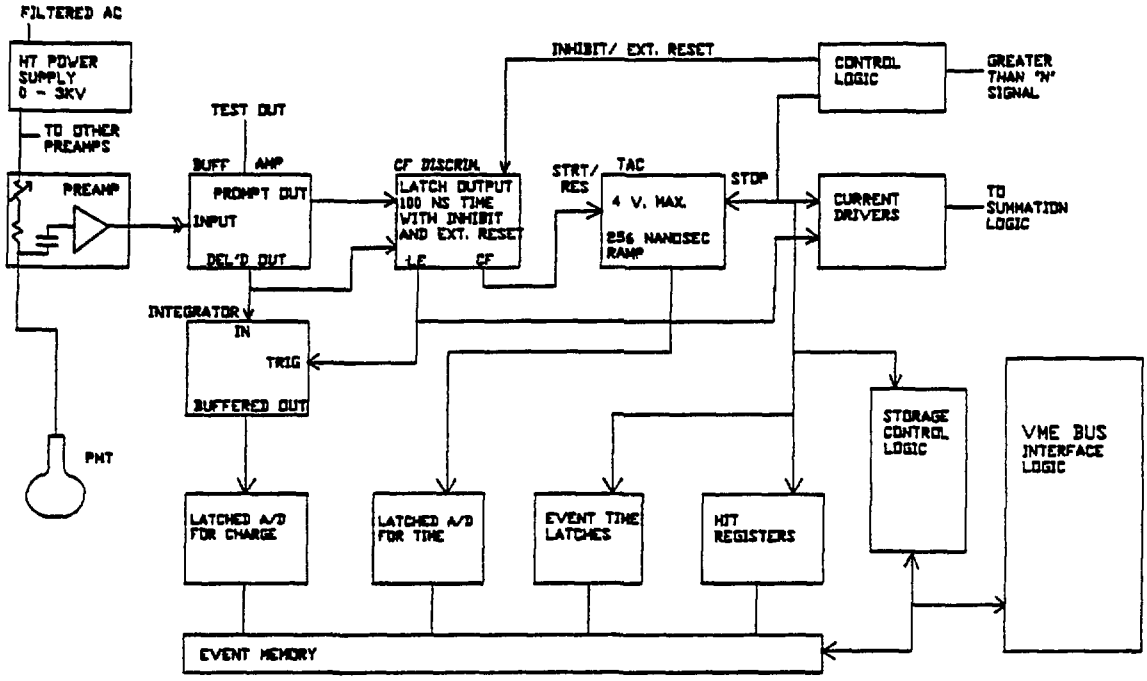

Figure 3.4: Schematic diagram of the electronics required for each PMT.

muon and its subsequent decay may be recorded as two sequential signals. A block diagram of a system which meets these requirements is shown in Figure 3.4. A detailed description of the electronics is given in Annex-4.

Each PMT is connected to a preamplifier/high tension card through a single length of coaxial cable. A suitable preamplifier circuit giving a gain of 30 and risetime less than 2 *ns* has been constructed using surface-mounted components. The preamplifier feeds a fast timing discriminator and a gated current integrator. The discriminator signal goes to the start of a time-to-amplitude converter (TAC), and to the trigger logic. The trigger logic determines whether the number of PMTs firing within a time interval Δt is greater than a preset threshold, N, and if this is the case, it generates a signal called 'Greater than N'. This signal stops the TACs and causes the integrated anode charge and the TAC signal to be digitized, using 50 *ns* flash ADCs with the results stored in a first-in/first-out (FIFO) memory. The time interval Δt required for the trigger is 80 *ns* to allow for the spread in the transit times of the photons from the event to the PMTs. Thus the total time required to accept the data from an event is under

200 *ns* after which the system is ready to accept another event. The data are removed from the local memories via a VME bus and a system of microprocessors assembles the data for individual events and passes these to the data acquisition system. The burst rate capability is set by the size of the FIFO. If each channel's memory is capable of storing up to 200 words of information, then 5000 events of 10 MeV average energy could be accumulated in a time limited by the 200 *ns* event processing time. Data characterizing a 10 MeV event could be moved from the PMT electronics to the data acquisition computer at a rate of 4000 events per second.

Specific details of the electronics will depend to some extent on the final choice of PMT. The system described in Annex-4 is based on the assumption that the R1449 PMT will be chosen. This system uses a non-linear 8 bit ADC for the amplitude signal to give the equivalent of 10 bit dispersion at the low end and 6 bit dispersion at the high end. The amplitude information is required to correct the timing signals for walk and to give a measure of the number of photons being detected. The TAC is digitized to 8 bits over a 256 *ns* range with 1 *ns* dispersion. This is ample for the PMTs which have a resolution of about 9 *ns*. If PMTs having better timing and amplitude resolution are chosen, then this system may not be adequate. Furthermore, if a larger number of smaller PMTs are used, the luxury of having a separate ADC for each PMT may prove to be too expensive an option.

All of the electronics would be located in the access drift as close to the detector as possible. Four racks are required for the high voltage supplies and preamplifier cards while four others are required to hold the 16 VME crates containing the remaining electronics. A master VME crate would merge the data and perhaps carry out an initial filtering of the data to remove unwanted noise events. This would allow a lower trigger threshold to be set by hardware. The use of the VME bus will permit the Advanced Computer Project (ACP) multiprocessor technology developed at Fermilab by Nash and associates [77] to be used for this filtering. Finally, the data would be transferred to the main data acquisition computer for storage. This computer would be located either on the surface or in the drift with information transferred to a surface station through a fibre optic link.

3.2.4 Calibration

The data from the detector can only be reliably interpreted only if the response of the detector as a function of energy and the efficiency for neutron capture within the sensitive region of the detector are known. These quantities will be determined by source calibration, neutron transport calculations and Monte Carlo simulations of the detector properties. Calculations and simulations already performed are discussed in Annexes 1, 6 and 7. Experience with the Kamiokande II detector and a small test detector (STD) at NRCC [Annex-15] underlines the uncertainties of calculating the response of the detector and the importance of physical calibration.

Two forms of calibration are required. The relative response of the PMTs and of the electronic channels must be established and the light-diffusing spheres successfully used at IMB [79] and Kamiokande [78] will be used. The more problematic calibration is the absolute response in terms of photoelectrons detected per unit of energy. Various methods of producing calibration information are reviewed in Annex-8.

The electrons produced by solar neutrinos to which the SNO detector is sensitive will range in energy from 5 to 20 MeV. At the low end of this range it is possible to use (n,γ) sources for calibration. It is more difficult to find sources to cover the high-energy end of the range and hence development work is required. Other large water Čerenkov detectors have used the electron spectrum from the decay of stopped muons for calibration. Since the SNO detector is located at greater depth than these others, the stopped muon rate is too low to provide a useful calibration point.

High-energy γ-rays can be produced by the capture of neutrons, from a source such as californium, on a variety of targets placed with the source inside the detector. At Kamiokande II, the neutron capture reaction in nickel provided important information for the interpretation of the observation of neutrinos from SN 1987A. Neutrons can also be captured in ^{2}H or in additives (such as Cℓ) to give spectra which will not only produce calibration data but also reproduce the spectra from neutrino induced deuteron disintegration. In general, the energy released is about 8 MeV and the γ-ray spectrum following capture is complex. Light nuclei have simple decay schemes, but tend to have low capture cross sections. Some of the possible targets together with their cross sections and the energy released are listed in Table 3.2.

Target	$\sigma_{capture}$	Excitation Energy
^{2}H	0.53 mb	6.25 MeV
^{3}He	0.04 mb	~21 MeV
$^{35}C\ell$	43 b	8.6 MeV
nat Fe	2.5 b	7.6,9.3 MeV
nat Ni	4.4 b	7.8,8.9 MeV

Table 3.2: Selected neutron capture calibration sources.

A higher energy calibration point might be achieved using fast neutron capture on ^{3}He. (Thermal neutron capture is masked by the much more prolific ^{3}He(n,p) reaction.) The (n,γ) cross section has been measured to be 42μb [80] at a neutron kinetic energy of 4 MeV and, if this value is assumed to be constant over the energy range of fission neutrons from Cf, the counting rate for this reaction is of the order of 4500 per day for a neutron source strength of $2 \times 10^{5} n\,s^{-1}$ surrounded by a spherical container of 8.7 litres of ^{3}He at 3 MPa. The energy of γ-rays from this reaction will be (20.6 MeV + 0.75 $\times$ E), where E is the energy of the incident neutron. From a typical fission neutron spectrum, with most probable energy of 0.75 MeV and FWHM of 2.2 MeV [81], the γ-ray energies will range from 21 to 22.2 MeV. The feasibility of using such a source in the detector is being investigated. The most serious difficulty with it will be the high rate of lower energy γ-rays from neutron capture in materials other than ^{3}He.

Another possible γ-ray source would come from the use of the ^{11}B(p,γ) reaction. There is a strong resonance in this reaction at a proton energy of 163 keV which gives rise to coincident γ-rays of 11.7 and 4.4 MeV. The main difficulty of employing this source would be finding a way to introduce the proton beam into the centre of the D_2O volume.

Sources of β-rays of sufficiently high energy to be useful are short-lived although one possible source, ^{8}Li (half-life 0.84 s, endpoint energy 13.1 MeV) is being investigated. A source based on the circulation of a solution of lithium salt between a thermal neutron source and a transparent reservoir inside the detector is feasible in principle although it would be necessary to use lithium highly depleted in ^{6}Li. Cf sources of 3×10^{6} n s^{-1} are readily available and could produce ^{8}Li at the rate of 310 atoms $s^{-1}g^{-1}$ of pure ^{7}Li. One remarkable feature of this approach is that the β-spectrum produced

by this source would resemble very closely the ^{8}B neutrino spectrum which we are proposing to determine.

3.3 Radioactive Background and Shielding

3.3.1 Introduction

The expected solar neutrino signal rates of a few tens of events per day necessitate an extremely low background environment for the D_2O. There are two sources of background that must be guarded against. These sources are cosmic rays and radiation produced by naturally occurring radionuclides, and are the main consideration in determining the siting and the design of the detector.

The detector is to be located in a cavity in the Creighton Mine, near Sudbury, Ontario at a depth underground of 2070 m. At this depth the only surviving cosmic-ray components are muons and neutrinos. Muon-induced ^{16}O spallation products, such as ^{8}B, ^{12}B and ^{12}N which are high-energy β emitters (13 to 16 MeV endpoint energies) with relatively long half-lives (10-800 ms) could be particularly troublesome. These have been observed by Kamiokande II experimenters [22] who find that about 1% of the muons produce detected spallation products above a 10 MeV threshold. However, as can be observed from the relationship of muon intensity versus depth (Figure 3.5), the muon intensity at the SNO detector site is a factor of 200 lower than that at Kamiokande II. This leads to an estimate of just 24 muons per day passing through the D_2O containment vessel of which about 1.5 per day will produce detectable spallation events above the detector energy threshold. These events will be identified by their characteristic time signature, a high-energy muon signal followed by a β-decay signal.

A more pervasive source of background is radiation induced by the naturally occurring radionuclides, ^{40}K, ^{232}Th, ^{235}U and ^{238}U. The decay chains of ^{232}Th and ^{238}U are shown in Figures 3.6 and 3.7, respectively. Besides the direct radiations produced by these radionuclides there are those indirectly produced by α-particles and neutrons. The α-particles can interact with nuclei in the host material, the most important reactions being (α,pγ) and (α,n) reactions on various light elements, in particular ^{29}Si, ^{30}Si,

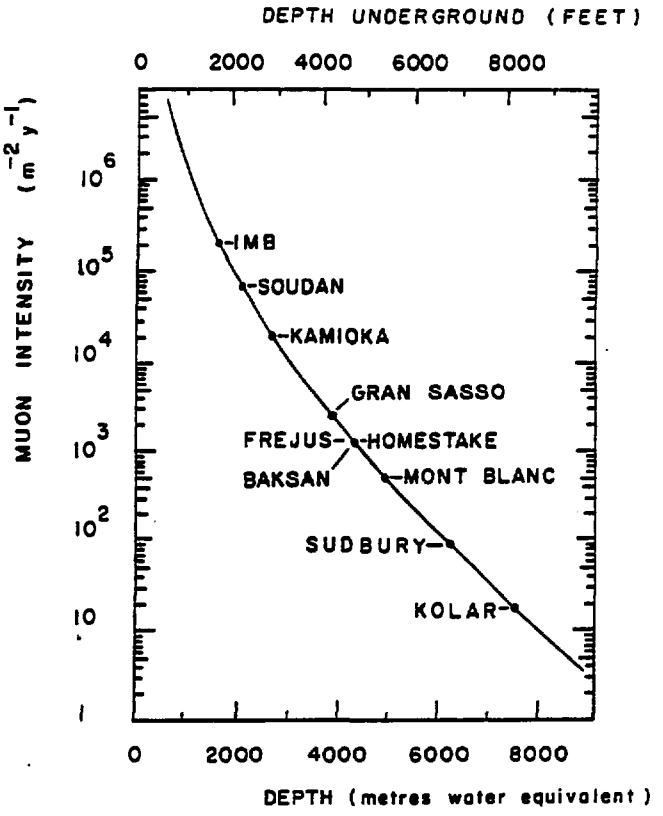

Figure 3.5: Cosmic-ray muon flux as a function of overburden (mwe) or depth underground (feet in standard rock) for the Sudbury laboratory and underground laboratories in existence around the world.

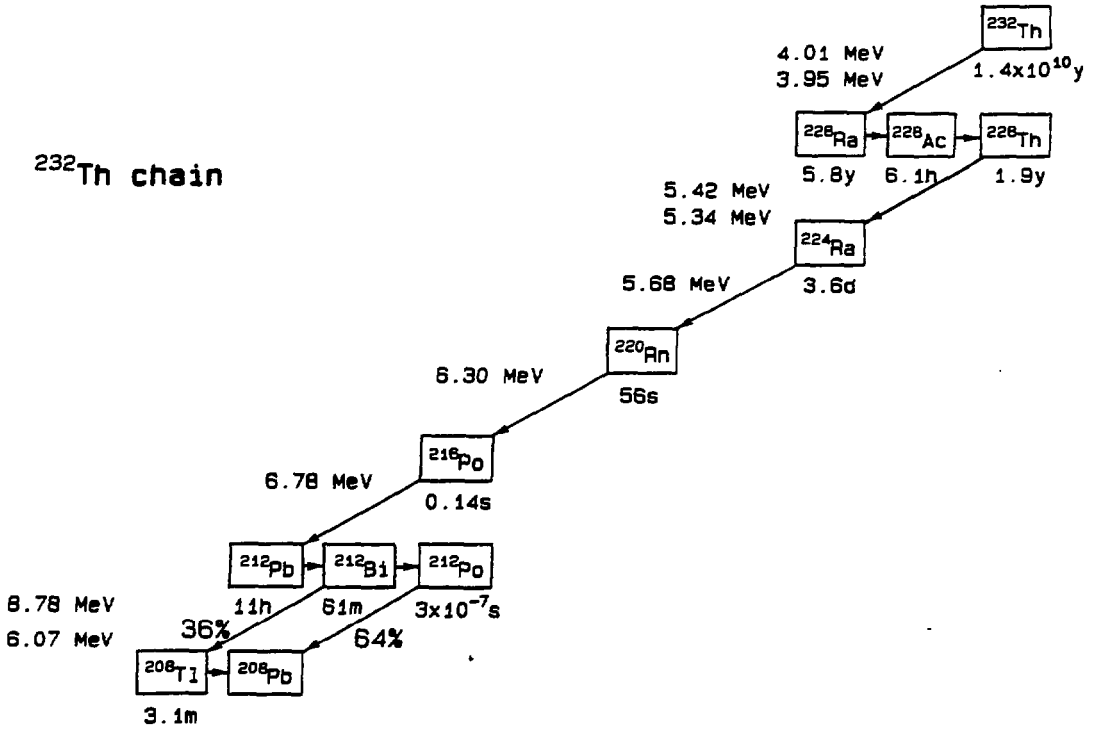

Figure 3.6: The decay chain for ^{232}Th. The long-lived ^{228}Ra and ^{228}Th daughters allow the chain to be out of equilibrium. The troublesome 2.615 MeV γ-transition is at the bottom of the chain, as shown in Figure 3.8.

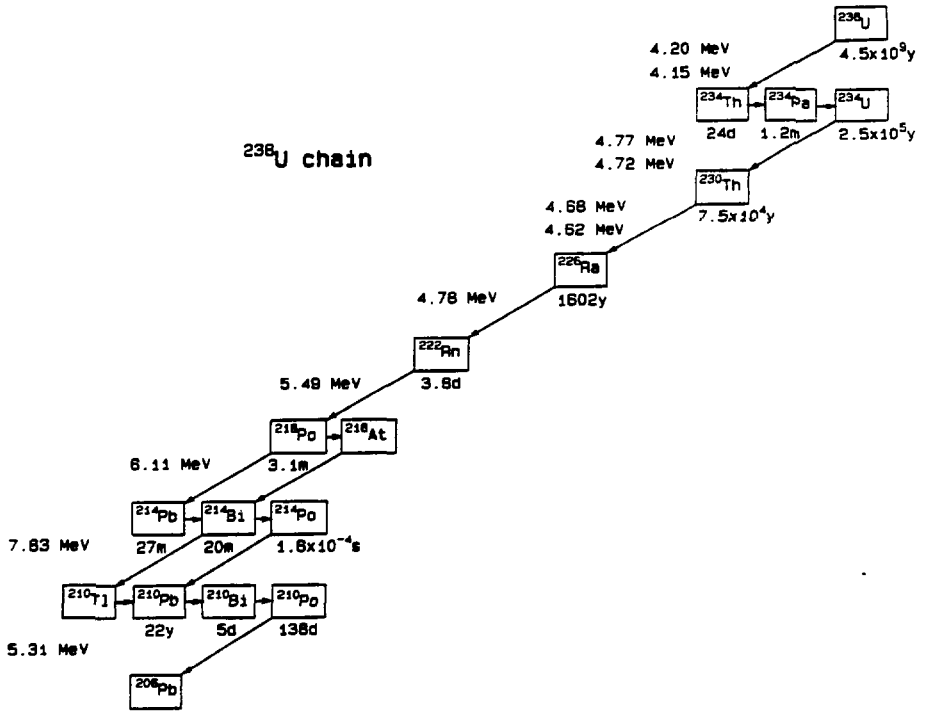

Figure 3.7: The ^{238}U decay chain. The long-lived daughters ^{234}U, ^{230}Th and ^{226}Ra may cause disequilibrium and preceed the troublesome ^{214}Bi.

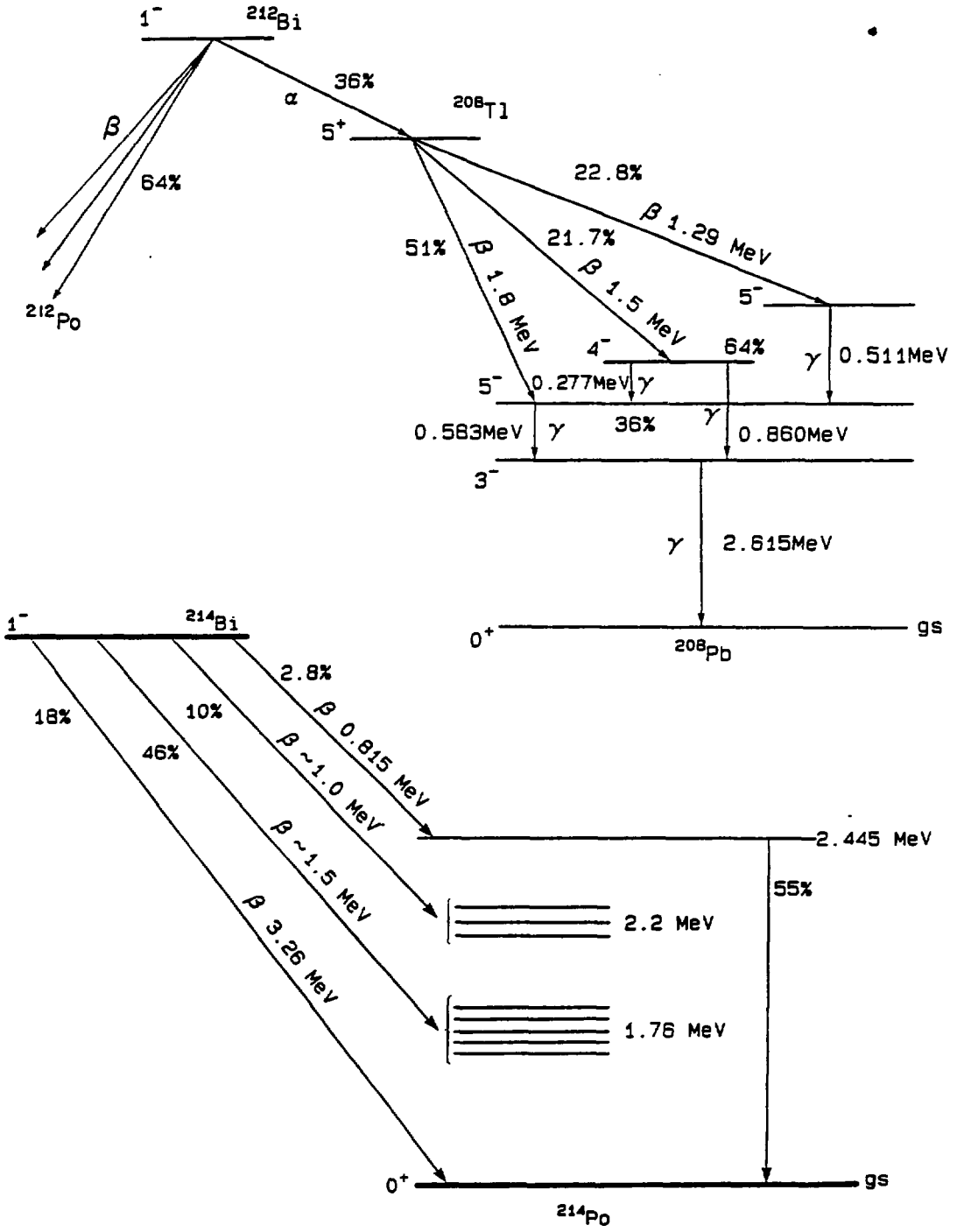

Figure 3.8: Simplified decay schemes for ^{212}Bi and ^{214}Bi.

^{27}Al, ^{25}Mg, ^{26}Mg, and ^{23}Na. The neutrons released in these reactions or those from spontaneous fission can be captured to produce γ-rays whose energy extends up to nearly 10 MeV and which are the main source of background emanating from the rock walls of the detector cavity.

The radioactivities identified above are present in the rock and, at some concentration, in all materials. Consequently, a detector for (^{8}B solar) neutrinos must incorporate adequate shielding from external radiation and be constructed of materials which are specially selected to have low concentrations of radioactive elements. In fact, the design of the proposed detector is dictated largely by shielding and radioactivity considerations.

The neutral-current reaction, $\nu_x + d \rightarrow \nu_x + p + n$, with the release of a detectable neutron is unique to this detector and has its correspondingly unique backgrounds. Neutrons entering the D_2O constitutes a source of background and γ-rays greater than 2.223 MeV in the D_2O can cause deuteron photodisintegration, mimicking the neutrino disintegration of the deuteron.

The charged-current, $\nu_e + d \rightarrow p + p + e$, and elastic-scattering, $\nu_x + e \rightarrow \nu_x + e$, reactions have backgrounds similar to those in H_2O Čerenkov detectors i.e. energetic electrons due to β-decay and Compton-scattered γ-rays, such as those shown in Figure 3.8. In addition, neutrons from the neutral-current reaction, from photodisintegration of the deuteron and from outside the D_2O vessel can be captured by the deuteron producing a 6.25 MeV γ-ray which is a charged-current reaction background unique to D_2O.

In this Section we first discuss the precautions necessary to reduce the high-energy γ-ray flux in the active volume of the detector (inside the surface defined by the PMTs) to an acceptable level. This γ-ray flux is primarily a background to the events associated with the charged-current and elastic-scattering reactions. We then discuss the internally generated backgrounds. The sharp rise in the radioactive γ-ray background below 3 MeV gives two problems. First, it limits the low-energy threshold at which charged-current reaction data can be extracted. This will be discussed in Section 3.4.5 where the Monte Carlo simulation of the detector response to various backgrounds is reported. Second, those γ-rays of more than 2.223 MeV (chiefly the 2.615 MeV γ-ray from the decay of ^{208}Tℓ and the 2.445 MeV γ-ray from the decay of ^{214}Bi) can give rise to neutrons in the D_2O which may give a background to both the charged- and neutral-current reactions.

3.3.2 External Radiation

The first problem to be addressed is the shielding of the detector from the external background γ-rays. The critical backgrounds are high-energy γ-rays from ^{238}U fission and neutron capture in the norite rock, and in the construction materials (concrete and stainless steel liner) adjacent to the norite. Once a neutron enters the H_2O it no longer poses a problem since it is captured by hydrogen yielding a low-energy (2.223 MeV) γ-ray. The source of neutrons is the (α, n) reaction primarily in light elements with the α-particles originating from the ^{232}Th and ^{238}U radionuclei and their daughters. The norite rock near the proposed detector location has been found [Annex-9] to contain about 3.3 $\times 10^{-6} g/g$ ^{232}Th and 1.2 $\times 10^{-6} g/g$ ^{238}U. A graded shield has been designed to achieve low background within the active volume as defined by the PMTs.

Measurements of γ-Ray and Neutron Flux

The γ-ray flux from norite at the 5400 foot level of the Creighton mine (a location different from the final site) has been measured with NaI(Tℓ) and BGO detectors [Annex-10] and is given in Table 3.3. In conjunction with shielding calculations [Annex-9] to be described in Section 3.3.3, the γ-ray flux from neutron capture in the rock has been estimated from the measured composition of norite (given in Table 3.4) and the results appear in Table 3.3. This γ-ray flux is generated predominantly by neutron capture in Fe. It is noteworthy that the concentration of ^{232}Th at the 5400 foot level ($5.3 \times 10^{-6}\ g/g$) is higher than that measured near the proposed site. The neutron flux in a drift in the norite at the 5400 foot level has been measured with a BF_3 counter [Annex-10] and has also been calculated [Annex-9] in conjunction with the shielding calculations. The measured counting rate was 0.0064 s^{-1} and the calculated rate, assuming that the wooden supports installed in that drift reduced the flux by a factor of two [Annex-10], is 0.007 s^{-1} from two independent calculations. The good agreement among the calculations and measurements for both the γ-ray and neutron fluxes gives confidence in the reliability of the shielding calculations.

E_γ (MeV)	Measured Flux $\gamma\ m^{-2}d^{-1}$	Calculated Flux $\gamma\ m^{-2}d^{-1}$
4.5-5	510±200	
5-7	360±220	320
> 7	180±90	250
> 8	<20	15

Table 3.3: High-energy γ-ray fluxes from norite. The flux was measured using a 10 cm × 12.5 cm NaI(Tℓ) detector with various thicknesses of Pb shielding. The calculations are based on neutron capture in the elements of norite with a neutron flux predicted from the measured Th and U concentrations in the rock.

Element	% composition by weight
H	0.15
C	0.04
O	46.0
Na	2.2
Mg	3.3
Aℓ	9.0
Si	26.2
K	1.2
Ca	5.2
Mn	0.1
Fe	6.2
Ti	0.5

Table 3.4: Elemental composition of norite.

Element	% Composition by weight
H	0.03
C	11.4
O	45.0
Na	0.04
Mg	11.1
Aℓ	0.04
Si	0.08
S	13.0
K	0.01
Ca	19.3
Mn	0.04
Fe	0.09
Zn	0.04
B	1.0

Table 3.5: Elemental composition of the proposed "Sulfurcrete" shielding.

Shielding Composition

The outermost layer of shielding is the 0.9 m of low background boron loaded "Sulfurcrete" lining the cavity (Figure 1.1). "Sulfurcrete" is a type of concrete made with sulphur and a SRX polymer as the binder. Normal concretes are seldom better than rock for radioactivity levels and even special concretes made with low activity aggregates, such as dunites or certain dolomites, are usually only about a factor of 5 to 10 lower because available Portland cements are high in Th and U content. The present solution is to stack a 90 cm layer of precast blocks of borated "Sulfurcrete" made with dolomite from the Timminco Metals quarry at Haley, Ontario. The elemental composition [Annex-9] of the proposed "Sulfurcrete" blocks and the activity of the components are given in Tables 3.5 and 3.6, and would produce concrete blocks with concentrations about $11 \times 10^{-9}\ g/g$ ^{232}Th and $9 \times 10^{-9}\ g/g$ ^{238}U concentrations (more than a factor of 200 lower than in norite). The roughly 10 cm gap between the cavity wall and the "Sulfurcrete" blocks (due to the inevitable unevenness of the wall) will be filled with a Portland cement-Haley dolomite concrete as required. The dome of the cavity will be covered with a 40 cm layer of the latter concrete or with borated "Sulfurcrete" blocks.

Component	% "Sulfurcrete"	^{232}Th $\times 10^{-9}\ g/g$	^{238}U $\times 10^{-9}\ g/g$
Dolomite	86.8	9±3	9±1
Sulphur	12.0	14±7	8±3
SRX Polymer	1.2	120±40	43±8

Table 3.6: Activity of "Sulfurcrete" components.

The next layer of shielding is the H_2O filling the stainless steel liner and surrounding the acrylic vessel. Its minimum thickness is 4.0 m at the waist of the acrylic vessel and at the bottom. The thinner concrete lining the dome of the cavity is compensated for by an extra metre of H_2O above the highest point of the domed top of the acrylic vessel. The H_2O shield serves several purposes. First, it prevents neutrons from reaching the D_2O, because of the relatively high capture cross section of ^{1}H. Second, it reduces the flux of high-energy γ-rays, primarily from neutron capture in the stainless steel and concrete, into the D_2O. Third, it attenuates the high flux of 2.615 MeV γ-rays from the "Sulfurcrete" and PMTs (see Section 3.3.3). "Sulfurcrete" with 11 $\times 10^{-9}\ g/g$ ^{232}Th will produce a flux of 2.615 MeV γ-rays of about $1.1 \times 10^5\ m^{-2}d^{-1}$. The water between the PMTs and the stainless steel tank will attenuate this flux by a factor of more than 3000 making the flux negligible compared to that from the PMTs.

3.3.3 Shielding Calculations

Two independent sets of shielding calculations [Annex-9] have been carried out based on a model of the cavity consisting of 2 m thick norite, 1 m of low background concrete, 0.64 cm of stainless steel and 4.0 m of water surrounding the 5.0 m radius cylindrical acrylic vessel. In the first the discrete ordinate neutron transport code ANISN [83] was used for a geometry in which the rock, concrete, stainless steel and H_2O were assumed to be infinitely long cylinders. The neutrons are produced by (α,n) reactions and spontaneous ^{238}U fission in the norite and concrete. Neutron capture then leads to the production of γ-rays. The calculations utilized the elemental abundances of the norite, concrete and stainless steel and the appropriate neutron capture cross sections. The γ-ray flux was calculated, using a

Monte Carlo code SANDYL [84] and neutron capture tabulations [85], for a right cylindrical geometry, with a height of 24 m. The effects of adding 0.5% and 1% B to the concrete, or using B-loaded polyethylene sheets next to the stainless steel, were also calculated. In the second calculation, a Monte Carlo code was used to track neutrons produced in the rock and concrete by (α,n) reactions. The resultant capture γ-rays produced in the norite, concrete and stainless steel were tracked through these materials and the water using the EGS4 Monte Carlo code [86]. Right circular cylinders were used for both neutron and γ-ray tracking.

The results of the two calculations are essentially in agreement [Annex-9]. They indicate that 36 high-energy γ-rays per day cross the PMT surface, about 0.4 per day cross a surface 1 m outside the acrylic vessel (which is roughly the reconstruction accuracy [Annex-6,-7]) and only about 0.02 γ-rays per day of energy greater than 5 MeV reach the acrylic vessel. These calculations have been refined to include the results of the most recent radioactivity measurements, and the details of the design such as the 1 m wide entry pipe into the D_2O. No significant changes in the predictions have emerged.

Calculations were also carried out using a model in which the PMTs were supported by a stainless steel structure, and high-energy γ-rays were produced by neutron capture in the stainless steel following (α,n) reactions in the glass (with allowance for the presence of H_2O). This calculation shows that stainless steel should not be used for the PMT support structure with the measured concentration of Th and U in the present Hamamatsu PMTs [Annex-11] (see Section 3.3.4), as it would contribute significantly to the background (about 6 γ-rays per day) within 1 m of the D_2O. However, glass of lower radioactivity for the PMTs is being sought [Annex-5], and such glass might permit the use of stainless steel for the support structure.

The PMTs are also a source of high-energy γ-rays produced by the (α,pγ) reaction, primarily on $^{27}A\ell$. It would be very difficult to measure this flux, but a crude estimate based on measurements in granite by Pomansky [87] is given in Annex-9. From these measurements the 1955 PMTs are estimated to emit about 120 γ-rays greater than 7 MeV per day toward the D_2O. Using the attenuation coefficient of 3 m^{-1} which allows for down-scattering to 5 MeV, about 1.6 γ-rays per day of energy greater than 5 MeV cross a boundary 1 m from the D_2O and about 0.08 γ-rays per day penetrate the acrylic, i.e. about four times the rate as that from the walls of the detector.

Since the average distance travelled by neutrons in H_2O from fission to thermal and thermal to capture is 14 and 7 *cm*, respectively [Annex-1], essentially all neutrons from the walls or the PMTs will be captured before reaching the D_2O.

In summary, for the present design, high-energy γ-rays from the walls of the detector and the PMTs are estimated to contribute fewer than 0.2 γ-rays per day above 5 MeV into the D_2O, which is a negligible rate compared to other sources of background discussed in Section 3.3.4. This low rate of high-energy γ-rays will permit a portion of the H_2O to be used for detecting the neutrino elastic scattering reaction, as fewer than 4 background γ-rays per day cross a boundary 1 *m* outside the D_2O. Reducing the amount of water shielding by one metre puts the backgrounds up by about one order of magnitude and this would seriously compromise the ultimate sensitivity of the detector to ^8B neutrinos.

3.3.4 Internal Background

After the H_2O, acrylic vessel and its contained D_2O have been shielded from external radiation by the rock overburden, the "Sulfurcrete" and the water, the remaining important sources of background lie within the components of the detector itself, i.e. the D_2O, H_2O, acrylic, PMTs and their support structure, and electronic units and cabling attached to the PMTs.

A serious background produced by the internal radioactivity is that due to the production of a free neutron anywhere inside the volume of the D_2O where it is a background to the neutrons produced by the neutral-current reaction. The most important source of these background neutrons is the photodisintegration of the deuteron by γ-rays of energy greater than 2.223 MeV which come mainly from daughters in the decay chains of ^{232}Th and ^{238}U. By comparison, the other possible source, spontaneous fission neutrons from ^{238}U, is negligible.

In order to be able to measure the neutral-current reaction and to ensure a low threshold for measurements of the charged-current reaction, it is necessary to reduce the thorium and radium contamination of the detector materials. The contamination levels desired, and those presently achieved, in order to perform the neutral-current measurement will be discussed next. The major thrust of the activities of the collaboration has been and, as de-

tailed in Chapter 5, will continue to be directed towards measuring and reducing contamination levels.

Heavy Water

The medium which must have the lowest concentration of radionuclei is the D_2O. In the ^{232}Th decay chain, the isotope ^{208}Tl, produced in 36% of the ^{232}Th disintegrations when in secular equilibrium, decays to ^{208}Pb with the emission of a 2.615 MeV γ-ray (Figure 3.8). This γ-ray has a cross section for photodisintegration of the deuteron of 1.2 mb [88] and a cross section for collision with an electron of 125 mb. Since every D_2O molecule has two deuterons and ten electrons, the ratio of the probabilities of a Compton collision to a photodisintegration is 520 to 1. However, some of the Compton-scattered photons (about 11.5%) have enough residual energy to cause photodisintegration and, correcting for this, one neutron is produced per 470 2.615 MeV γ-rays. Using the fact that ^{232}Th in secular equilibrium gives 126 γ-rays $\mu g^{-1} d^{-1}$ of 2.615 MeV, we estimate that 3.7 μg of ^{232}Th in the D_2O produces one neutron per day, compared to a neutrino neutral-current rate of 18 per day predicted by the Standard Solar Model. This amount of ^{232}Th in 1000 tonnes of D_2O corresponds to a concentration of $3.7 \times 10^{-15}\ g/g$.

In the ^{238}U series, a 2.445 MeV γ-ray (Figure 3.8) from the decay of ^{214}Bi is emitted at a rate of 16.8 γ-rays $\mu g^{-1} d^{-1}$ of ^{238}U in secular equilibrium. At this energy the photodisintegration cross section is about 0.8 mb [88] and the Compton cross section is 130 mb. Using an analysis similar to that for the 2.615 MeV γ-ray, and allowing for the fact that, after scattering, about 7.2% have enough energy to cause photodisintegration, 750 of these γ-rays produce one neutron in the D_2O. Thus one neutron per day is produced by 45 μg of ^{238}U, equivalent to a concentration of $4.5 \times 10^{-14}\ g/g$ in the D_2O.

The results of measurements of ^{232}Th and ^{238}U in AECL and Ontario Hydro D_2O, and distilled H_2O, are given in Table 3.7. The best measurements have been made by inductively coupled plasma mass spectrometry (ICPMS) and thermal ionization mass spectrometry (TIMS) on highly reduced samples, and details are provided in Annex-12. The lowest value of ^{232}Th currently obtained for D_2O (without resorting to further purification) is about $32 \times 10^{-15}\ g/g$ (the average of the measurements on the

	Source	^{232}Th	^{238}U	Author
D_2O	AECL	0.04±0.01		McLaren
	AECL	0.027	0.031	Kelly
	Ont. Hydro	0.15±0.05	0.3	McLaren
	Ont. Hydro	0.39	0.22	Kelly
H_2O	Distilled	<2		Aardsma et al.
	Distilled	0.14	0.016	Kelly
	Double Distilled	0.0064	0.0027	Kelly

Table 3.7: Measurements on ^{232}Th and ^{238}U in water. The measurements are given in 10^{-12} g/g. Full details are given in Annex-12

AECL D_2O). This would produce about 8.6 neutrons per day in the SNO detector. The ^{238}U in the same sample would produce 0.7 neutrons per day. By comparison, if the ^{232}Th and ^{238}U concentrations in the D_2O were reduced to the levels measured in doubly distilled H_2O then 2 neutrons per day would be produced.

The above estimates of the number of neutrons produced by ^{232}Th and ^{238}U present in the D_2O depend on the assumption of secular equilibrium in the radioactive decay series. In both series the troublesome γ-ray emitting isotopes are preceded by long-lived isotopes of radium, ^{228}Ra (5.75 y) and ^{226}Ra (1602 y) [see Figures 3.6 and 3.7. The ^{226}Ra in the ^{238}U series is also preceded by a long-lived isotope of thorium, ^{230}Th (8×10^4 y). Chemical processes can alter the ratio of radium to the parent thorium or uranium from the value at secular equilibrium, thus altering the number of 2.615 or 2.445 MeV γ-rays to be expected. This is especially true in the ^{238}U series where the long half-lives of ^{226}Ra and ^{230}Th can prevent secular equilibrium from being established over a millennium.

A system is being developed [Annex-12] to extract radium and thorium by filtering the water with Mn-coated acrylic fibres or beads. This technique has been widely used for studying Ra and Th in environmental water [89,90,91]. Based on measurements of the activity of the Mn-coated acrylic [Annex-12] and the distribution coefficient for both Ra and Th on the Mn-coated fibre [89], we estimate that 1000 tonnes of D_2O can be re-

duced to an activity of about 1.4×10^3 of 2.615 MeV γ-rays per day, which would correspondingly produce about 3 neutrons per day. This method of extracting the Ra and Th has the potential of providing a means to monitor whether there is serious disequilibrium in the ^{232}Th chain to a ^{232}Th equivalent level of $11 \times 10^{-15}\ g/g$.

We are, at present, constructing a water purification test facility to establish the performance of the Mn-coated acrylic fibres (and other Ra removal techniques) in ultra-pure water and at very low levels of radioactive contamination. The facility consists of two tanks, each of 9 tonne capacity, which can be filled with ultra-pure water. Clean pumps allow the water to be passed from one tank, through a filter, and into the other. The tanks and interconnecting piping work are made of polypropylene. The amount of Ra on the filters is measured by de-emanating the Rn gas and counting the α-activity. As the Rn gas test is non-destructive, measurements on the filters can be made before and after water passes over them. An important question to be addressed is whether some Th is in a chemical complex which is not extractable in the Mn-coated fibres. This can be resolved by looking for a buildup of ^{224}Ra in the water after filtering. Because the Ra will recoil out of the chemical environment of the Th, the same filter can be used to remove the Ra and, indirectly, the Th, and the levels of purity achieved can be monitored by de-emanating the Rn gas into a proportional counter. A sensitivity of better than 1 disintegration per day per tonne of water, corresponding to a ^{232}Th concentration of $3 \times 10^{-15}\ g/g$ (which would produce 0.8 neutrons per day in the SNO detector) is anticipated.

A potential problem in using D_2O in a Čerenkov detector is the low level light production due to tritium decay. The bulk of the D_2O stockpiled by AECL is 'low trit' which has a typical tritium activity of $\sim 300\ \mu Ci\ kg^{-1}$. As shown in Annex-13, this would be too active by two orders of magnitude for use in the detector. On the other hand, in virgin D_2O (^{3}H $< 0.05\ \mu Ci\ kg^{-1}$) produced by distillation, the tritium would not give a significant increase in noise above the expected PMT noise. Such water is available from Ontario Hydro.

In summary, the D_2O as presently measured would be a source of about 10 neutrons per day as background to the neutral-current neutrino reactions. Based on radioactivity measurements on H_2O and knowledge of the effectiveness of Mn-coated fibres, it is expected that this can be reduced to 3 neutrons per day uniformly distributed throughout the D_2O volume.

Acrylic

The acrylic vessel is also a source of 2.615 and 2.445 MeV γ-rays which can photodisintegrate deuterons of the D_2O. Because only about one-half of the γ-rays originating in the acrylic penetrate into the D_2O, the amounts of ^{232}Th and ^{238}U in the acrylic which can lead to one neutron generated per day are 7.4 μg and 90 μg respectively. Since the mass of acrylic is about 30 tonnes, in order to produce less than one neutron per day the ^{232}Th concentration must be less than $2.5 \times 10^{-13}\, g/g$ while the concentration of ^{238}U must be less than $3.0 \times 10^{-12}\, g/g$.

A number of acrylic samples and components of acrylic have been examined for Th and U [Annex-14]. A technique has been developed [93] to measure ^{232}Th and ^{238}U by instrumental neutron-activation analysis which can routinely determine levels down to $15 \times 10^{-12}\, g/g$ and $30 \times 10^{-12}\, g/g$, respectively. The chief limitation of the technique arises from trace impurities in the acrylic, such as Fe and Zn, which are strongly activated by neutrons to form radionuclei having long half-lives. Standard acrylics are found to have ^{232}Th concentrations ranging from 20 to $60 \times 10^{-12} g/g$, but in samples prepared without UV absorber or dye, limits of $^{232}\text{Th} < 11 \times 10^{-12}\, g/g$ and $^{238}\text{U} < 28 \times 10^{-12}\, g/g$ were obtained, as noted in Table 3.8. At present this technique is limited to scanning samples of acrylic quickly for possible good candidates, but if acrylic can be found with low enough levels of trace impurities it would be a way of rapidly monitoring large amounts with a sensitivity of $(0.5\text{-}1) \times 10^{-12}\, g/g$ [94].

An α-counting method has been developed for acrylic components and more recently for bulk acrylic (Annex-14). In this method, large quantities (typically 10 kg) are reduced by vaporization in an oxygen free atmosphere. The residue is leached with HNO_3 and deposited on a planchet for α-counting in a low-background facility. The α-particles of ^{232}Th, ^{228}Th and ^{238}U are detected. The results are summarized in Table 3.8. A major advantage of this method is that it measures the activity near the end of the Th decay chain and hence it is sensitive to disequilibrium. In Table 3.8 the ^{228}Th concentration is in good agreement with expectations assuming secular equilibrium. While this does not measure directly radium-thorium disequilibrium, it can be used to reduce somewhat our ignorance about this important question. Since the parent of ^{228}Th ($T_{\frac{1}{2}}$ =1.91 y) is ^{228}Ra ($T_{\frac{1}{2}}$ =5.75 y) and since the acrylic and its components were manufactured at least a year before vaporization, the disequilibrium between ^{228}Ra and

Source	^{232}Th $(10^{-12}g/g)$	^{228}Th $(10^{-23}g/g)$	$^{232}Th^*$ $(10^{-12}g/g)$	^{238}U $(10^{-12}g/g)$	Author
R & T					
total	12±9			<28	Aardsma et al.[1]
monomer	<0.6	6	0.4	<0.23	Milton & Earle[2]
cross linker	6	70	5.2	2.9	Milton & Earle[2]
polymer	1.1	31	2.3	0.7	Milton & Earle[2]
Polycast					
total	5±6				Jagam et al.[1]
	1.9			19.5	Kelly & McDonald[3]
	0.23			0.23	Earle & McLaren[3]

Table 3.8: Radioisotope measurements on acrylic from two manufacturers. The fourth column, labelled $^{232}Th^*$, gives the concentration expected from the ^{228}Th measurement (third column) assuming secular equilibrium. Full details are given in Annex-14. A preliminary measurement is given in the last line and may need to be corrected for insoluble residues. [1]) neutron activation [2]) α-counting [3]) mass spectrometry

^{228}Th cannot have been enhanced or reduced relative to secular equilibrium by more than a factor of two.

The ^{232}Th and ^{238}U in acrylic have also been measured by mass spectrometric methods [Annex-14]. Acrylic is vaporized in an oxygen-free atmosphere and the residue is dissolved in acid and analyzed in a mass spectrometer. Kelly and McDonald obtained values of $1.9 \times 10^{-12}\ g/g$ of ^{232}Th and $19.5 \times 10^{-12}\ g/g$ of ^{238}U by this method (Table 3.8). The first sample studied by Earle and McLaren had higher levels of Th and U [Annex-14]. At these very low levels, contamination of the samples is a serious concern and a further measurement has been carried out paying strict attention to possible sources of contamination. A sheet of Polycast acrylic was trimmed and cut into strips $2.5cm \times 2.5cm \times 30cm$ using a 2500 Watt CO_2 laser cutter at NRCC. These strips were sealed in plastic bags and taken to CRNL where six strips weighing 1.3 kg were vaporized in a Suprasil quartz tube at 400°C. The residue was extracted with HNO_3 and analyzed for ^{232}Th and ^{238}U. Traces of each isotope were detected at a level corresponding to 0.23 $\times 10^{-12}\ g/g$ in the acrylic. However, it was observed that there were some

deposits which did not dissolve in HNO_3 and we consider this most recent measurement as preliminary.

The techniques for vaporizing the acrylic, extracting the residue and measuring the Th and U concentrations by α-counting and mass spectroscopy will continue to be developed with particular emphasis on hygiene and recovery efficiency. Blank runs on the Suprasil quartz tubes [Annex-14] indicate a sensitivity of better than $0.1 \times 10^{-12}\ g/g$ for mass spectroscopic detection of ^{232}Th and ^{238}U if 1 kg samples of acrylic are vaporized, and an α-counting sensitivity of about $0.5 \times 10^{-12}\ g/g$ for ^{232}Th and ^{238}U if 10 kg samples are vaporized. The α-counting technique checks for secular equilibrium. Potential suppliers of acrylic for the vessel will be asked to supply the collaboration with samples of their product. These will be checked for Th and U concentrations and a quality assurance procedure put in place to monitor Th and U in acrylic samples trimmed from each of the production panels.

In the background analysis (Section 3.4.5) we adopt values for ^{232}Th and ^{238}U in acrylic of $1.9 \times 10^{-12}\ g/g$ and $3.6 \times 10^{-12}\ g/g$, being the lowest levels found in the earlier measurements but one order of magnitude poorer than the most recent results. The adopted concentrations would produce, in secular equilibrium, about 8 neutrons per day in the D_2O. These neutrons are born within a few cm of the acrylic vessel and 93% escape the D_2O before capture [Annex-1].

Light Water

The H_2O surrounding the acrylic vessel is also a source of 2.615 MeV and 2.445 MeV γ-rays. For a uniform source of S disintegrations per unit time per unit volume spread throughout a semi-infinite volume, the flux Φ leaving an element of surface dA at the boundary is [95]

$$\Phi = SdA/4\epsilon$$

where ϵ is the γ-ray attenuation length in the water. As mentioned above, 470 γ-rays of 2.615 MeV entering the D_2O from the H_2O will produce 1 neutron in the D_2O. This implies a source strength, S, of 17 $m^{-3}d^{-1}$ of 2.615 MeV γ-rays in the water, using for dA the surface area of the acrylic vessel, 481 m^2 and $\epsilon = 4.34\ m^{-1}$ [Annex-9]. Since ^{232}Th produces 126 γ-rays of 2.615 MeV $d^{-1}\mu g^{-1}$ in secular equilibrium with its daughters, a

^{232}Th concentration of 0.13×10^{-12} g/g will produce one neutron per day in the D_2O. Using a similar argument to that for acrylic, the concentration of ^{238}U in the H_2O should be less than 1×10^{-12} g/g in order that the flux of 2.445 MeV γ-rays produce less than 1 neutron per day. The attenuation coefficient for the 2.445 MeV γ-ray is assumed to be the same as that for the 2.615 MeV γ-ray.

It is known [Annex-12] that water, after passing through a standard mixed bed resin and a distillation column, can be obtained with as little as 0.14×10^{-12} g/g ^{232}Th and 0.016×10^{-12} g/g ^{238}U. Light water with these concentrations would give only one neutron per day in the D_2O.

However, at these levels of contamination the Čerenkov light generated by β- and γ-rays, and in particular those close to the hemispherical PMTs, pose a serious background to studying the charged-current reaction events (see Section 3.4.5). Thus further filtration using Mn-coated fibres is necessary and it is assumed that the purity expected for the D_2O can also be attained for the H_2O. When this is done, the number of neutrons generated by activity in the water will be negligible. The H_2O purification system must also reduce the absorbed ^{222}Rn gas ($T_{\frac{1}{2}} = 3.8\ d$). Typical ground water contains about 30 $pCi\ \ell^{-1}$ of ^{222}Rn which would be reduced to the equivalent activity of a ^{238}U concentration of 3×10^{-15} g/g after four months in a sealed environment. The filling of the main tank is expected to take approximately four months and consideration will be given to installing a system similar to that developed for the Kamiokande II light water experiment which reduces the ^{222}Rn activity by aeration of the water. During operation of the SNO detector aged H_2O for topping up the detector will be obtained from a holding tank.

Photomultiplier Tubes

Each Hamamatsu 50 cm PMT is estimated to contain 3 to 5.4 mg of ^{232}Th and 3.0 to 5.6 mg of ^{238}U, based on measurements of the glass [Annex-11], and of ceramics, dynode structure, bakelite base and standard electronics package of three PMTs [SNO-85-3]. Using the mid-points of the ^{232}Th and ^{238}U ranges it is estimated that 10.6×10^8 of 2.615 MeV γ-rays and 1.4×10^8 of 2.445 MeV γ-rays will be emitted per day from 1955 PMTs. The number reaching the surface of the D_2O will be 1590 and 225 per day, respectively, assuming that the 2.5 m of H_2O has an attenuation factor

of 3×10^{-6} [Annex-9]. Thus the γ-rays from the PMTs will produce 1.7 neutrons per day in the D_2O from Th, and 0.1 neutrons per day from U. Because of the relatively low energy of its radiations, ^{40}K in the PMT glass at levels measured in existing PMTs, i.e. 0.7 g per PMT, will not pose a problem. A serious background due to the PMTs is from the β- and γ-rays due to radioactivity in the PMTs which cause random coincidences adding up to energies above the threshold (Section 3.4.5). The collaboration is searching for lower activity glass for PMT construction [Annex-5].

Additives

At present the only additive seriously considered for enhancing the neutral-current signal is NaCℓ (about 2500 kg). The Th and U concentrations in any NaCℓ placed in the D_2O must be three orders of magnitude lower than the concentrations so far measured, namely $1.3 \times 10^{-9}\ g/g$, at NRCC in a sample of reagent grade NaCℓ using ICPMS. However, it is known [Annex-12] that Th and Ra can be removed from brine using Mn-coated fibres. The ^{40}K in the salt is not a problem if the concentration is similar to that measured [Annex-11] in a sample of table salt (0.004% potassium).

Control of Radioactive Contamination

Cleanliness in construction is an important consideration for keeping radioactivity levels low, especially during the construction of the acrylic vessel. The rock at the mine site contains about $3.3 \times 10^{-6}\ g/g$ ^{232}Th and $1.2 \times 10^{-6}\ g/g$ ^{238}U and presumably mine dust contains similar levels. If the acrylic vessel contains 7.4 μg of ^{232}Th, one neutron per day is produced in the D_2O (Section 3.3.4). Assurance that dust on the acrylic vessel not contribute more than 7.4 μg of ^{232}Th requires that the vessel be covered with less than 2.2 g of norite rock dust. If this were spread uniformly over the inside and outside of the vessel, the dust layer would have an average thickness of $2.3 \times 10^{-7}\ gcm^{-2}$, or, assuming that it only settles on the inside at the bottom, the thickness would be about $2.3 \times 10^{-6}\ gcm^{-2}$. For comparison, in a typical building this layer of dust builds up in approximately two weeks. Hence the air in the construction zone should be filtered so as to contain less than between 1/10 and 1/100 the amount of dust in a normal building.

In the preceding sections it has been shown how important low levels of radioactive contamination are to detecting successfully both the neutral-current and charged-current reactions of solar neutrinos. In order to achieve such low levels, stringent monitoring of all the components of the detector will have to be instituted. This must begin at the raw material stage, during selection of the materials for the "Sulfurcrete", the photomultiplier glass and ceramics, the acrylic vessel, etc. Procedures for filtering and monitoring the radioactivity levels of both H_2O and D_2O will have to be developed. Procedures for checking the finished components will also have to be prepared and fitted into the construction schedule.

3.4 Simulation of the Detector Response

The physical processes taking place in a large Čerenkov detector are sufficiently complex that it is possible to predict in detail its response only by making computer simulations. This complexity is inherent in the multiple scattering and δ-ray production as the electron slows down in water. We have, therefore, carried out extensive Monte Carlo calculations to predict the response of the detector to the neutrino signals and to their backgrounds, and to guide the evolution of the detector design. A detailed report on these simulations is given in Annexes-6 and -7.

The following Monte Carlo calculations are performed to simulate an event in the detector. An electron of a given momentum at a given detector coordinate is tracked as it slows down and the Čerenkov light produced is computed. For this the proven electromagnetic shower code EGS4 [86] is used. The Čerenkov photons are then transported through the D_2O, acrylic vessel and H_2O, allowing for scattering and absorption, to the PMT plane. The PMT photocathodes are taken as hemispheres with a spectral sensitivity as quoted by the manufacturer, except that the overall sensitivity is reduced by a factor 0.585 as required by our calibration of the Kamiokande II detector [Annex-6]. The program then constructs an event in which each PMT which fired (a PMT hit) is identified and the time at which the corresponding discriminator triggered (allowing for the timing characteristics of the PMTs) is recorded. The contribution from PMT noise is included.

3.4.1 Response to Single Electrons

A histogram showing the number of PMTs hit for a set of electrons having 7 MeV kinetic energy is displayed in Figure 3.9. We see that with 40% coverage, on average 40 PMTs trigger. The spread is slightly larger than expected from statistical fluctuations ($\sigma \sim 7$ while $\sqrt{N} \sim 6.3$) due to contributions from δ-ray production and differential light attenuation. The predicted average number of PMTs hit and the corresponding σ's for electron energies up to 20 MeV are shown in Figure 3.10. Calculations for photocathode coverages of 20%, 40% and 75% are shown. We find that the response is nearly linear; the slight deviation from linearity at the highest energies is due to the chance production of multiple photoelectrons in some PMTs.

The program then tries to reconstruct the event from the observed pattern of hits. The basic principle is to search for a point source for the light which would give the correct time of arrival of the photons at the different PMT locations. This is complicated by the existence of noise hits and by the fact that up to 20% of the photons have scattered in transit to the PMTs and are delayed. How these aspects are dealt with in the fitting procedure are discussed in Annex-6. The large size of the PMTs and their timing response set a limit to the accuracy with which the reconstruction can be carried out. The reconstruction accuracy is shown in Figure 3.11. It is seen that, on average, the events can be located to within 70 cm if 40% photocathode coverage is used. The vital shrinkage of the large error tail with increasing coverage is obvious from this Figure.

Once the event vertex is known, it is possible to estimate the initial electron direction by computing the vector from the vertex to the centroid of the PMT hit locations. The accuracy of this estimate is limited mainly by multiple scattering of the electrons. The results of the simulations are shown in Figure 3.12. The error in the computed direction is about 25° and is essentially independent of the coverage.

The program has now extracted both the coordinate and momentum 4-vectors for the event. For a single electron, no further information is possible.

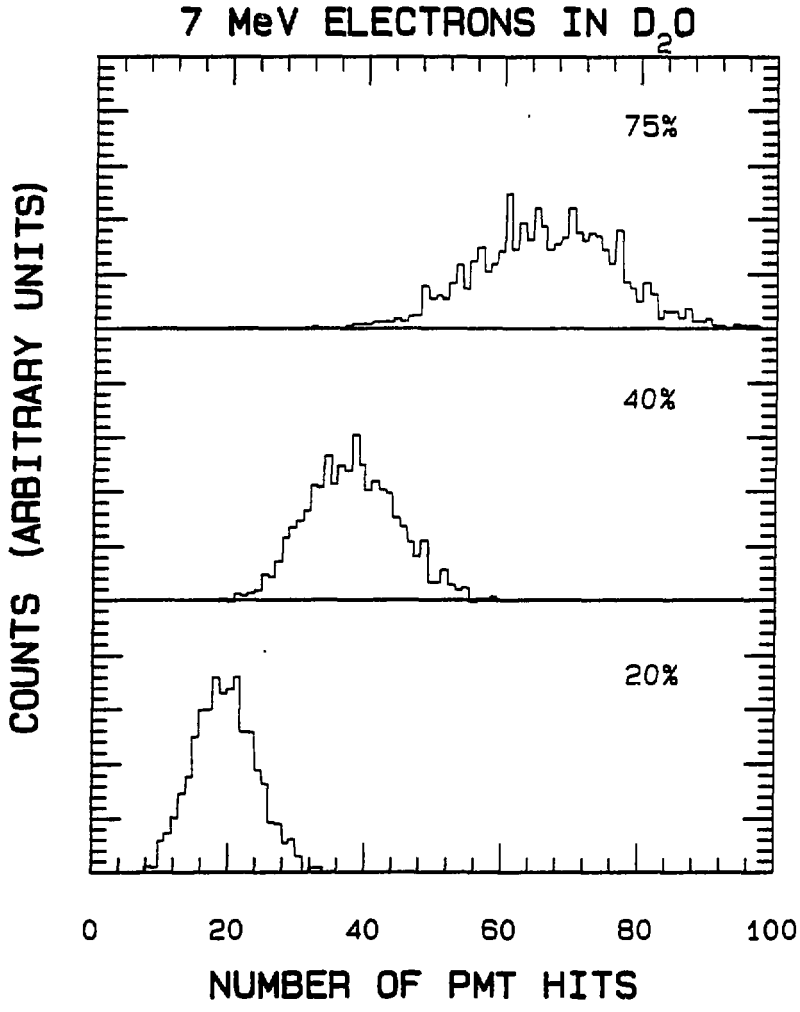

Figure 3.9: The number of PMTs hit for 7 MeV electrons randomly distributed in the D_2O are shown for 20%, 40% and 75% photocathode coverage.

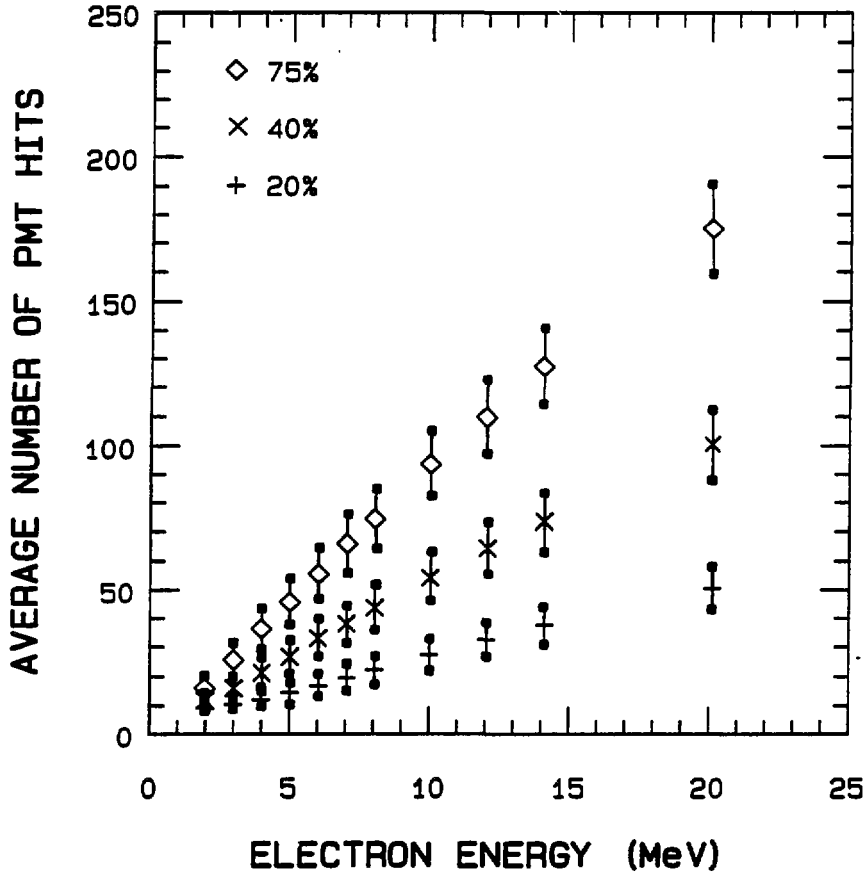

Figure 3.10: The mean numbers of PMTs hit for electrons of up to 20 MeV are shown for 20%, 40% and 75% photocathode coverage. The error bars indicate the width of the distributions.

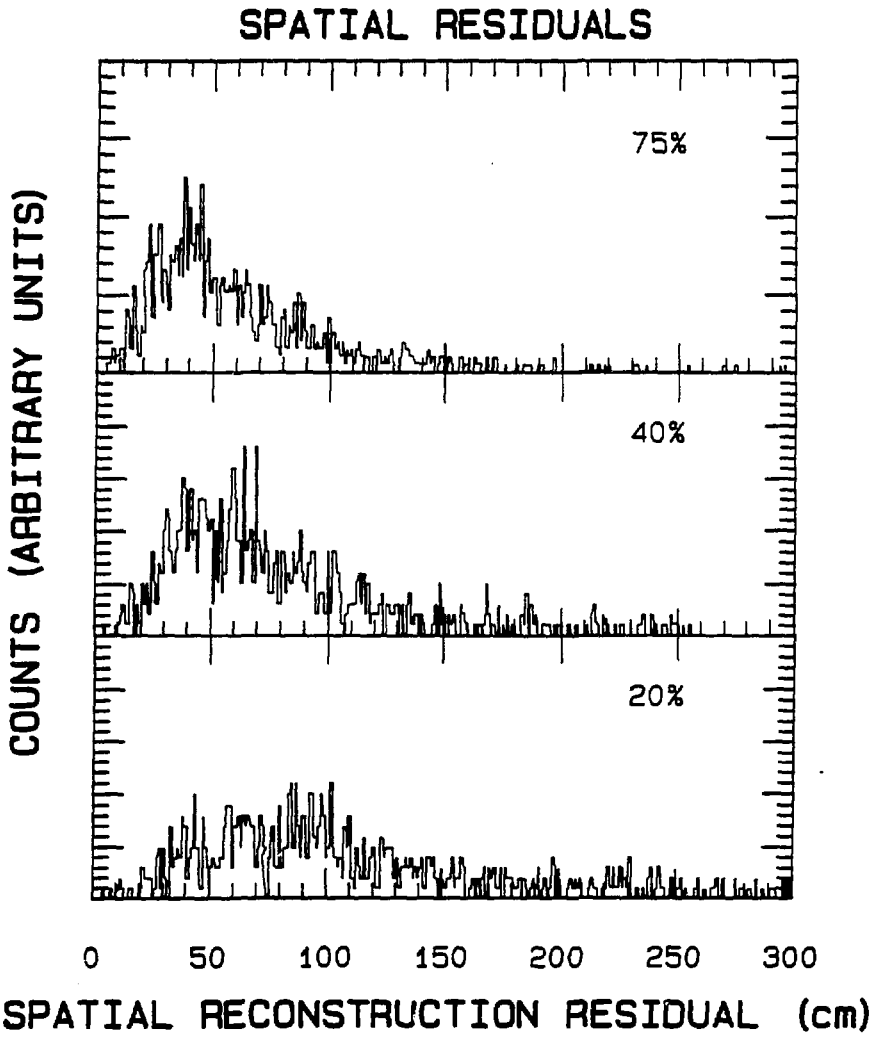

Figure 3.11: The distributions of the distance between the actual event vertex and the reconstructed vertex. With increasing photocathode coverage the position resolution is seen to improve and the large error tail becomes smaller.

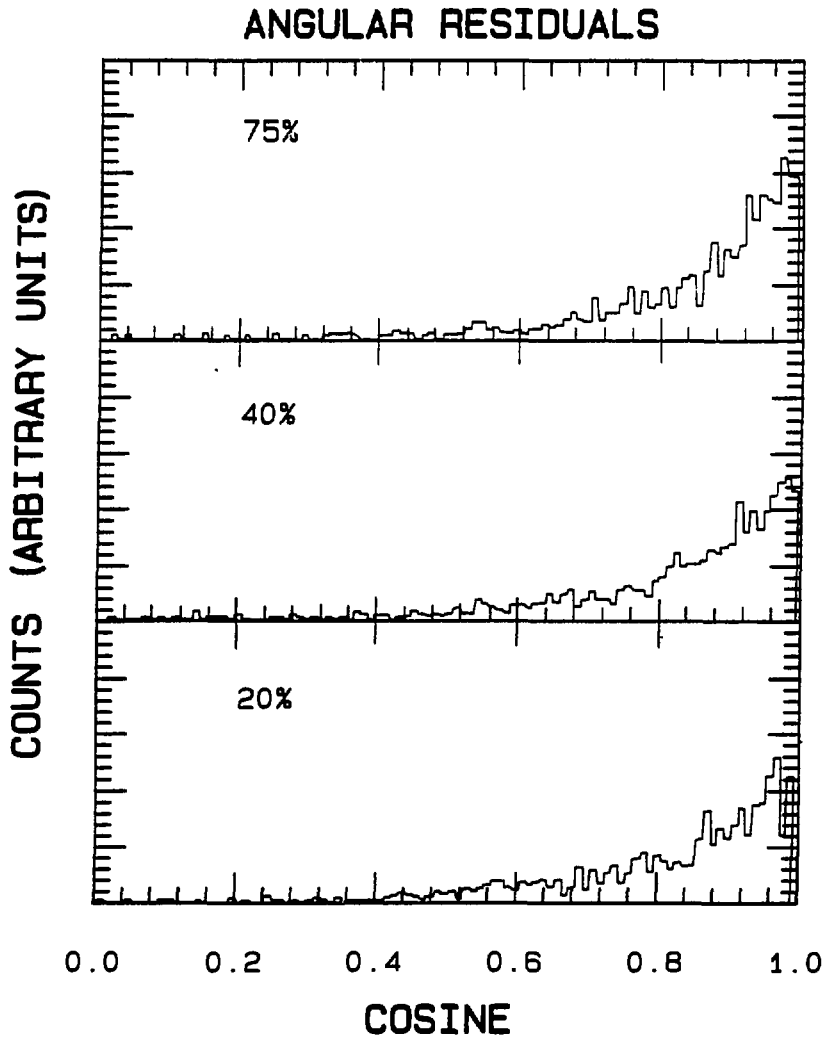

Figure 3.12: Angular accuracy of the reconstruction. The angular uncertainty is mainly due to electron multiple scattering and therefore does not depend strongly on percentage photocathode coverage.

3.4.2 Response to γ-rays

The important interactions of high-energy γ-rays in water are Compton scattering and pair production. Through these processes the γ-rays generate a shower of charged particles which in turn produce Čerenkov light. The total light production is less than that expected for a single electron having the same energy as the initial γ-ray because each charged particle ceases to produce light as soon as it drops below the Čerenkov threshold energy. Due to the spread in the number of charged particles produced in the shower, the energy resolution is poorer for γ-rays than for electrons.

In the Monte Carlo program, the γ-ray induced showers are calculated using the program EGS4 [86] and the resulting Čerenkov light is computed as in the single electron case. For γ-rays of 6 MeV we find that the mean number of PMTs hit is 18% lower and the width of the distribution of PMTs hit is 30% greater than that expected for 6 MeV electrons.

3.4.3 Effects due to the Acrylic

There is one aspect in which the simulations presented here are incomplete. The reflections and refractions of the Čerenkov photons at the acrylic-water interface have recently been incorporated into the Monte Carlo program. Sample calculations have been made with this improvement to see how the predictions are modified. The effects do not appear to be large. Signals originating in the D_2O are reduced by about 15% in light detected. The background signals due to radioactivity within the acrylic are attenuated by about 20% due to the total internal reflection of Čerenkov photons. More details on these effects are given in Annex-7. A complete reassessment of the response is in progress, but this is a major computational exercise and will require some time to complete.

3.4.4 Experiments with a Small Test Detector (STD)

Prior to undertaking the study reported on in this Section, it had not been demonstrated that Monte Carlo simulations of the performance of large-scale water Čerenkov detectors could be extrapolated with confidence

down to the low energy regime (4 - 15 MeV) of solar neutrino events. Since the validity of simulations in this energy range is central to the ultimate performance of the SNO detector, we assembled a small scale prototype detector to provide some experimental confirmation of our ability to simulate low energy events adequately. The small dimensions of the STD precluded any attempt at spatial reconstruction of events but information was obtained on the total light collection and angular distribution. A complete description of this experiment, the results and comparisons with the predictions from a Monte Carlo program, written for this detector, appear in Annex-15.

The electron linear accelerator (LINAC) at the National Research Council of Canada was used to provide the required monoenergetic beams of ultra-low intensity (10 - 100 electrons per second) in the energy range of 2 - 11 MeV. These were injected into the STD which consisted of a cylindrical water-filled steel cistern, 120 *cm* in diameter by 120 *cm* high into which was placed an array of 43 hemispherical (12.7 *cm* diameter) PMTs (borrowed from IMB) each sealed in a waterproof housing. A schematic diagram of the arrangement is shown in Figure 3.13. The PMTs, regularly spaced and supported on a tubular steel framework, looked inward onto a central cylindrical volume of water 55 *cm* in diameter and 55 *cm* high and covered approximately 38% of the surface of this inscribed cylinder. The inner surface of the water tank and supporting framework were painted black to reduce reflections. Half way up the tank a 7.5 *cm* diameter horizontal tube penetrated the wall and terminated at the centre of the tank in a 0.075 *mm* thick brass window. The beam line extended into this reentrant tube so that the electron beam was conveyed to the centre of the tank with a minimum of scattering and defocussing. A 1.6 *mm* thick, 10 *mm* diameter, plastic scintillator was mounted on the end of the reentrant tube to provide a gating signal from incident electrons from the LINAC. Amplified signals from each PMT were fed into fast multichannel CAMAC ADCs which were gated by the output of a fast discriminator triggered from the plastic scintillator signal. The pulse height response of each of the PMTs was recorded.

After calibration of the response of each PMT, as detailed in Annex-15, the data for individual events were analysed to determine N_{pe}, the total number of photoelectrons for each incident electron energy. The mean value of N_{pe} is plotted against energy in Figure 3.14. The results of computer simulation of electron events in the STD are also shown for comparison. It should be noted that the excellent agreement between the calculated and experimental energy dependence of N_{pe} comes about after the predicted N_{pe}

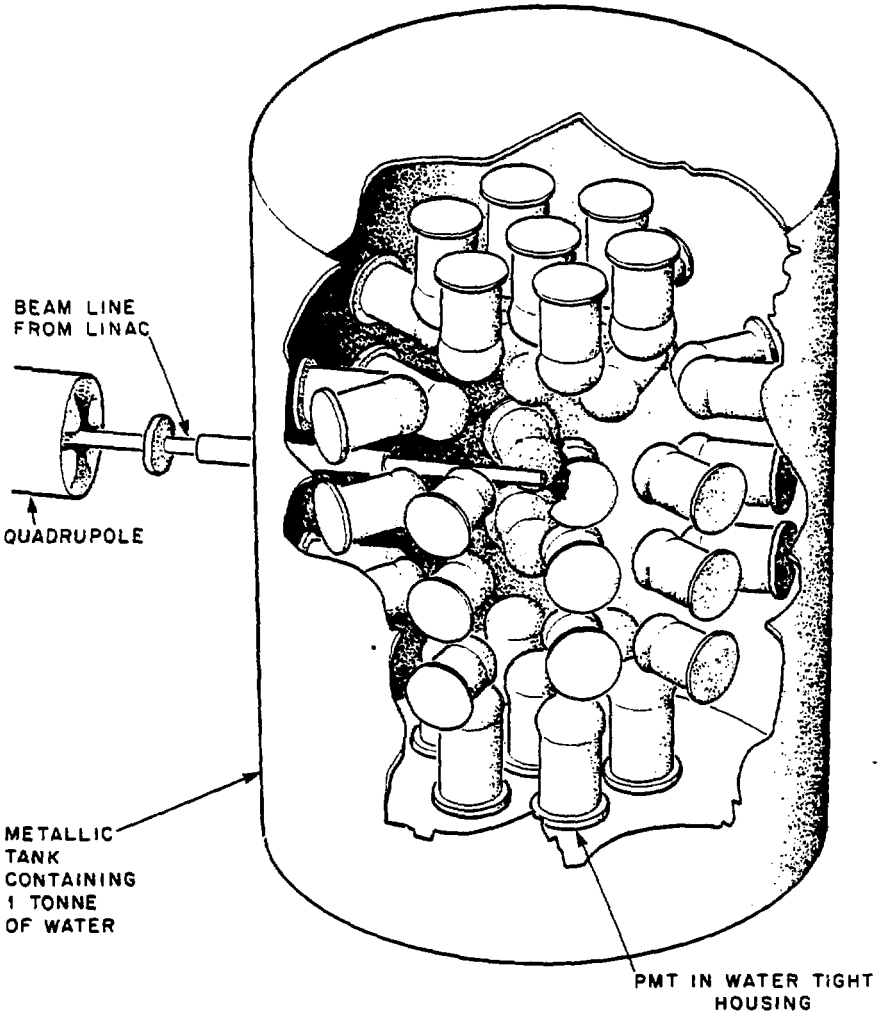

Figure 3.13: Diagram (to scale) of the Small Test Detector. The beam line from the LINAC extends into the centre of the tank. The tank has a diameter and height of 120 *cm*.

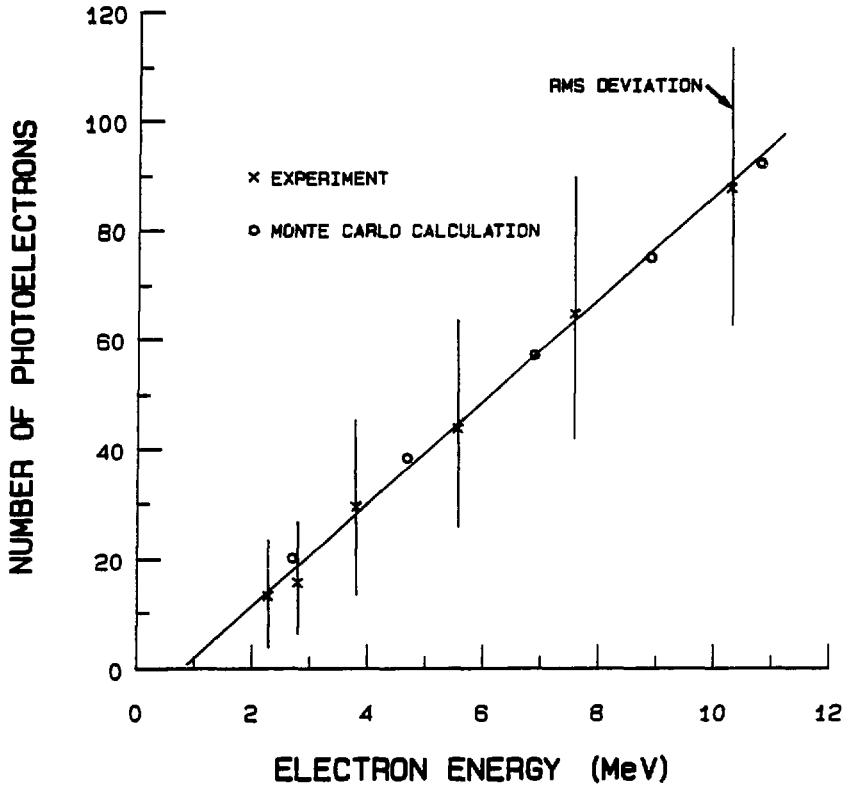

Figure 3.14: Number of photoelectrons detected with the Small Test Detector for various electron beam energies. Values calculated from Monte Carlo simulations are also shown.

numbers are normalized by a factor of 0.82. The IMB collaborators have found that they need a normalization factor of 0.53 [96] to reconcile their measurements of through-going muons with the Monte Carlo predictions.

The energy resolution achieved in the STD, indicated by the error bars in Figure 3.14, is poorer than that predicted for the SNO detector and this is understood. In the STD N_{pe} must be determined from the anode pulse heights whereas in the SNO detector it is sufficient to count the PMTs which fire. When the uncertainties in the amplitude response of the PMTs is included in a Monte Carlo calculation, reasonable agreement with the data is achieved.

In Figure 3.15 the average response of individual PMTs to 10 MeV

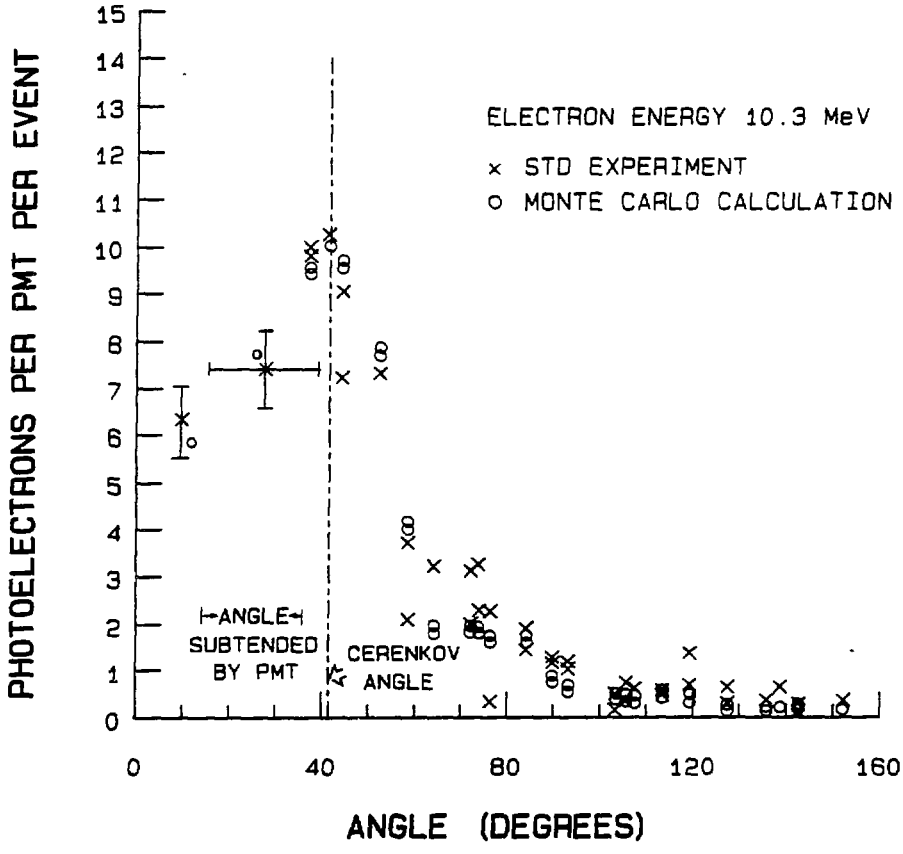

Figure 3.15: The measured and computed angular distributions of photoelectrons generated from the Čerenkov photons produced by 10.3 MeV electrons injected into the centre of the Small Test Detector. The numbers of photoelectrons are normalized for the different solid angles subtended by the PMTs at the centre of the tank.

electrons as a function of the angle between the beam direction and the line joining the centre of the PMT hit pattern and the centre of the tank is displayed. The angular dependences of the experimental and calculated values are similar, both peaking near the Čerenkov angle.

From the experience gained with the STD we can conclude that the extrapolation of the simulations of large Čerenkov detectors to low electron energies is valid, particularly with respect to calorimetry. The photon angular distributions are approximately correct but more data on the sensitivities and reflectivities of PMTs operating in water and the effect of the Earth's magnetic field on the PMTs are required for a more detailed understanding of the data.

The STD is not a scale prototype of the SNO detector since the PMT dimensions are not proportionally scaled. A single STD PMT typically covers a solid angle which, in the SNO detector, would contain 20 PMTs. For a small number of photoelectrons, say 5 - 10, the analogue response of a single PMT is substantially poorer than the 'hit' count in 20 PMTs. We propose constructing a large test detector (LTD) which will build on the experience gained with the STD to allow a more realistic simulation of the SNO detector and with which some of the problems raised in the STD data may be further explored. The LTD is discussed more fully in Section 5.4 and in Annex-16.

3.4.5 Detector Response to Backgrounds

There are several aspects of the background which must be simulated by Monte Carlo techniques. These include the response of the detector to external γ-rays, the response to radioactivities within the sensitive volume of the detector and the problems associated with neutron backgrounds to the neutral-current detection.

High-energy γ-rays

As shown in Section 3.3.3, the number of high-energy γ-rays entering the active volume of the detector is about 36 per day from outside the light water and about 120 per day from the PMTs. Two criteria can be used to

Threshold		Source		CC
PMTs hit	Energy (MeV)	PMTs	Walls	signal
20	3.69	145	211	3402
24	4.44	127	193	3090
28	5.19	92	161	2718
32	5.94	52	124	2269
36	6.69	39	88	1805
40	7.45	18	55	1425

Table 3.9: Background rates reconstructed into the D_2O (events per kt-y) for the indicated thresholds due to high-energy γ-rays from the cavity walls and the PMTs. Charged-current reaction event rates (CC) assuming a ^8B ν_e flux of $2 \times 10^{-6}\ cm^{-2}s^{-1}$ are given for comparison. A photocathode coverage of 40% is assumed.

reject these signals. First, most of them interact in the light water outside of the D_2O and hence they usually reconstruct outside of the fiducial volume. Second, they are directed towards the centre of the detector. The numbers of these events which reconstruct within the detector volume without a directional cut is given in Table 3.9 where they may be compared with the signal from the charged-current reaction. A directional cut removes 50% of the wanted neutrino events and 92% of the unwanted external γ-ray events. It is clear that, unless the ^8B solar neutrino flux is much lower than any of the solar model predictions, the external γ-ray background will not be a serious problem.

Low-energy β and γ-rays

Although our trigger threshold (expected to be near 4 MeV) is above the energies of β- and γ-rays produced in natural radioactive decay, there are three ways in which radioactive decay can give rise to backgrounds to the measurement of the solar neutrino spectrum. The combined signals from coincident β- and γ-rays (Figure 3.8) and the random coincidences of two or more decays may be above our trigger threshold and may be reconstructed

to resemble a neutrino event in the fiducial volume. In addition, γ-rays from radioactive decays may cause photodisintegration of the deuteron and the subsequent neutron capture may lead to a high-energy γ-ray event. The last of these is considered separately under the neutral-current background discussion (Section 3.5).

The highest β-decay Q-values in the ^{232}Th and ^{238}U decay chains are 5.0 MeV (^{208}Tℓ) and 3.3 MeV (^{214}Bi). The important decay branches for these nuclei are shown in Figure 3.8. The decay scheme for ^{214}Bi is complex but an important branch is the strong β-decay to the ^{214}Po ground state. This 3.3 MeV endpoint β-decay can produce more Čerenkov light than the higher Q-value ^{208}Tℓ decay where the energy is shared among a β-particle and several γ-rays. The simplified decay schemes used in the Monte Carlo calculations are given in Annex-7.

Although on average these decays give an amount of light equivalent to an electron of energy much less than the decay Q-value (because the neutrino carries off part of the energy and the low-energy γ-rays lead to little Čerenkov light) there is a tail to the response distribution which extends above our trigger threshold. This tail is primarily due to the finite energy resolution of the detector. We have calculated the background rates expected for anticipated U and Th concentrations of the various detector components. The concentrations assumed are given in Table 3.10. The calculated background rates are given in Table 3.11 for 40% coverage, and in Table 3.12 for 20% coverage. The rates tabulated are primarily due to the combined signals from coincident β- and γ-rays except for those rates in the column labelled "PMTs". The radioactive decay rate in the PMTs is about 10^8 to 10^9 per day [Annex-7]. Events resulting from these decays are rarely reconstructed into the D_2O because the PMTs are located far away from it and are shielded by the H_2O. However, this single decay rate is sufficiently high to allow multiple events from the PMTs, or from the PMTs and other materials, to occur in coincidence within the trigger time window and the resulting light pattern may result in the event being reconstructed into the D_2O. These random coincident events have been simulated and the results are included in the columns labelled "PMTs" of Tables 3.11 and 3.12. Most of these scale as the square of the concentration of ^{232}Th and ^{238}U in the glass and can be substantially lowered by reducing the radioactive contamination in the glass. In addition, any β-activity in the PMT glass will produce a large signal in that particular PMT, providing a further tool to identify and reject PMT-related events.

	PMT	H_2O	Acrylic	D_2O	$NaC\ell$
^{232}Th	3×10^5	0.022	1.9	0.011	1.0
^{238}U	3×10^5	0.015	3.6	0.011	1.0

Table 3.10: ^{232}Th and ^{238}U concentrations assumed for detector components for Monte Carlo calculations of background events. Units are in $10^{-12}\ g/g$.

Threshold		PMTs	H_2O	Acrylic	D_2O	$NaC\ell$
PMTs	Energy					
20	3.69	15085	9633	271079	17355	3944
24	4.44	5665	1501	36729	1731	393
28	5.19	37	270	4459	88	20
32	5.94	11	101	87	0	0
36	6.69	0	34	87	0	0
40	7.45	0	0	0	0	0

Table 3.11: The number of background events reconstructed into the D_2O per *kt-y* due to radioactivity in the indicated components. A photocathode coverage of 40% is used.

We observe that the background is predicted to rise sharply below 5 MeV. The dominant source in the current calculations is uranium in the acrylic. The H_2O is also an important source, particularly above 5.5 MeV, because the hemispherical photocathodes are more sensitive to the light produced close to the PMTs. Above 4.5 MeV the backgrounds are significantly worse for 20% coverage than for 40% coverage both because the energy resolution is worse with 20% coverage and because the poorer reconstruction accuracy puts more events into the D_2O.

Threshold		PMTs	H_2O	Acrylic	D_2O	$NaC\ell$
PMTs	Energy					
12	3.66	28104	17811	157090	2975	2949
14	4.54	2320	4438	37435	2188	497
16	5.42	2080	793	7696	622	141
17	5.86	2070	659	2186	135	31
19	6.74	0	0	1575	34	8
21	7.63	0	0	87	0	0

Table 3.12: The background events reconstructed into the D_2O per *kt-y*, assuming 20% photocathode coverage.

3.5 Neutral-Current Detection

The neutral-current reaction $\nu_x + d \rightarrow \nu_x + p + n$, which measures the total neutrino flux independently of oscillations, is detected by recognizing the subsequent capture of the free neutron. The signature for this capture, the detection efficiency, and the backgrounds all depend on the isotope on which the neutrons are captured. Because D_2O has a very small neutron capture cross section, it is possible to increase the capture rate and hence detection efficiency by a factor of 3 to 4 with small amounts of a suitable additive.

The three classes of background to the neutral-current signal are neutrons from photodisintegration of deuterons by γ-rays produced within the D_2O, neutrons from photodisintegration by γ-rays produced external to the D_2O, and other events which yield an equivalent amount of Čerenkov light (e.g. the charged-current signal or high-energy external γ-rays).

The only way to treat the first of these backgrounds is to measure the radioactivity in the water, as discussed in Section 3.3.4, and to subtract this contribution. Discrimination against the second source of background relies on the fact that in this case neutron production and capture occurs near the acrylic surface. If the mean free path of the neutron is long, most of these neutrons will leak into the H_2O and be lost. The remainder could be rejected by making a fiducial cut on the data. Increasing the

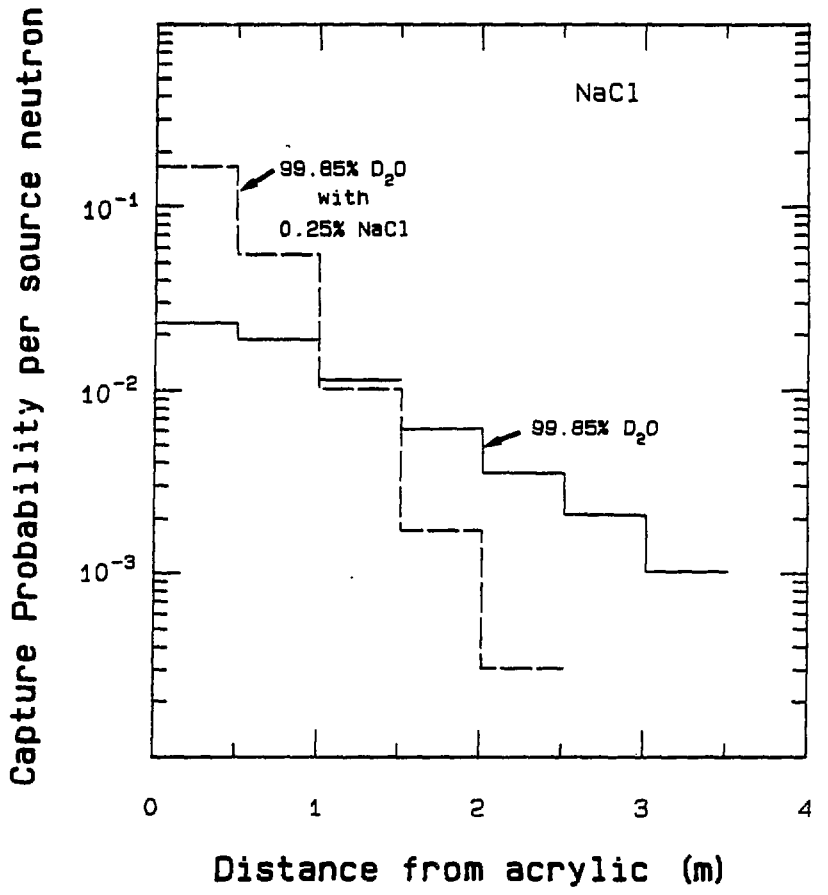

Figure 3.16: Capture position and probability in D_2O and D_2O doped with $NaC\ell$ of neutrons produced in the vessel by external γ-rays.

capture cross section by doping the D_2O shortens the distance between neutron production and its subsequent capture allowing cleaner rejection in the off-line analysis. The probability of neutron absorption in 0.5 m thick concentric spherical shells of (99.85% enriched) D_2O and D_2O doped with 0.25% $NaC\ell$ is plotted as a function of distance from the acrylic in Figure 3.16. The neutron source distribution at birth was assumed to fall off exponentially with distance as calculated for 2.615 MeV photons incident on the D_2O sphere [Annex-1].

There are several ways in which the non-neutron background can be

treated. If no additive is used then background at the high-energy side (above 6.25 MeV) of the $^2H(n,\gamma)^3H$ γ-ray signal will arise mainly from the charged-current reaction and the anisotropy of the yield from this reaction, relative to the direction of the Sun, can be used to determine the amount to be subtracted. On the low-energy side the main background is expected to come from internal radioactivity and this would require a difficult extrapolation of the background from lower energies. If a high capture cross section additive (e.g. $C\ell$ or Gd) is used, then differences in the spectra with and without the additive identifies the neutron related signal.

The final choice of additive requires both a quantitative analysis of the neutron transport and a detailed knowledge of the event signature for the capture and of the backgrounds that will be encountered. Neutron transport calculations are discussed in Annex-1. The decision on the optimum additive need not be made until measurements are performed with the detector operating with both light and heavy water. The signals from the possible neutron capture reactions will be studied using the proposed Large Test Detector (Section 5.4). Three possible detection methods are presented below, and quantified in Table 3.13 .

Capture on the deuteron is viewed as the default reaction. No additives are required and hence there is less chance of contamination. It has a low capture probability which reduces the neutrino signal but this also implies that the background due to photodisintegration by external γ-rays is greatly reduced. Neutron capture in ^2H leads to a mono-energetic 6.25 MeV γ-ray. A SSM ^8B neutrino flux would produce four such γ-rays per day in the D_2O to be compared with a background rate of one neutron capture per day, assuming the radioactive concentrations discussed in Section 3.3.4 and Table 3.10.

The introduction of $NaC\ell$ greatly increases the neutron capture probability and provides a significant increase in the yield of Čerenkov light. With 2500 kg of $NaC\ell$ in the D_2O, 83% of the neutrons from the neutral-current reaction would capture in $C\ell$ or ^2H while only 24% of the externally generated background neutrons would capture in $C\ell$ or ^2H and these captures would take place close to the acrylic so that the external background could be eliminated by reconstruction. It is also known that $NaC\ell$ can be cleansed of Th and Ra using Mn-coated fibres [89,90,91]. The neutron capture rates for neutrino-induced interactions and from background-induced radioactivities are 15 and 6 per day, respectively.

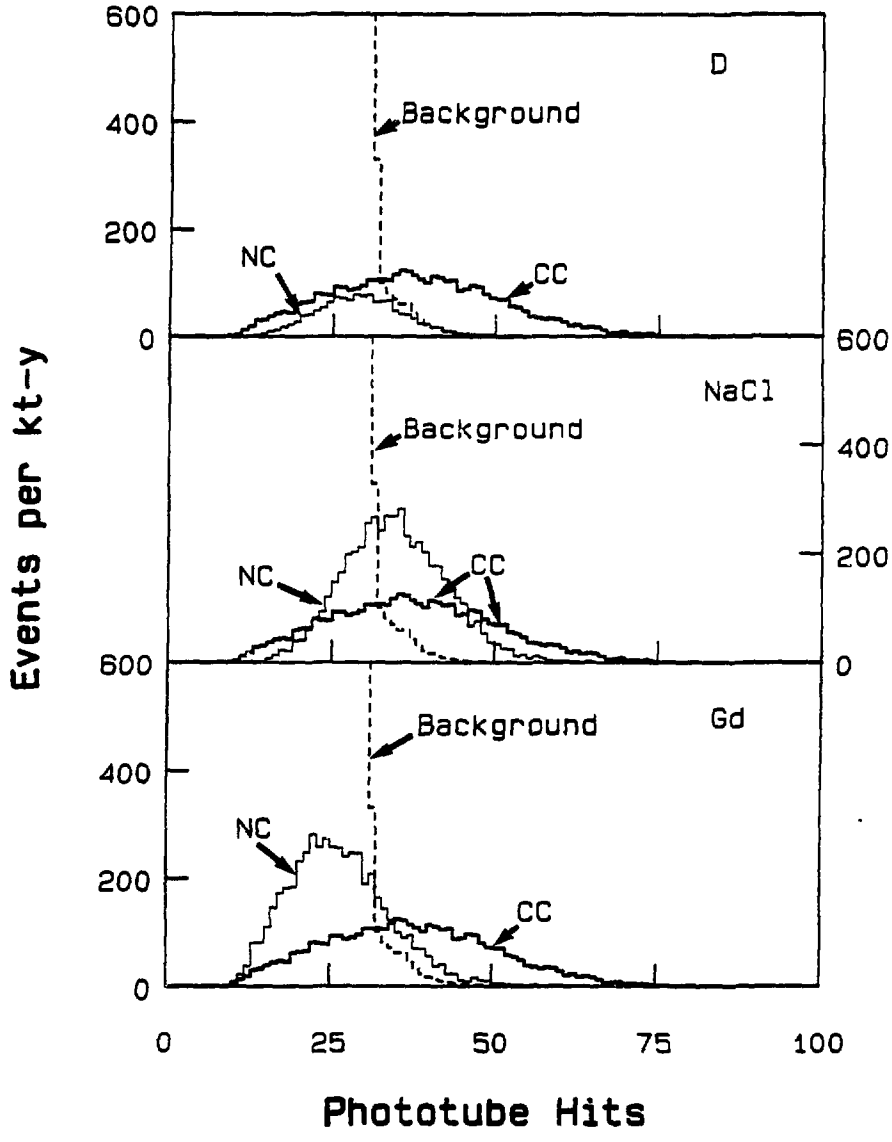

Figure 3.17: Spectra predicted for neutron capture in ^{2}H, Cℓ and Gd are shown (NC) and are compared with the spectra predicted from the charged-current (CC) reaction and from the total background. A photocathode coverage of 40% is assumed.

The addition of Gd allows very high capture probability because of its high capture cross section and offers the possibility of single event identification. This arises because the γ-ray multiplicity is high (the average is 3.4 γ-rays per capture) and hence the resulting γ-ray cascade gives rise to a much more isotropic distribution of light than is observed for single electron events. The difficulty with using Gd is that the total light from the cascade is low because multiple γ-rays are less effective at producing Čerenkov light than a single high-energy γ-ray. The addition of 4.6 kg Gd to the D_2O would give the same capture probability as 2500 kg of $NaC\ell$ and thus would have the same neutron transport properties.

The calculated response of the SNO detector to neutron capture γ-rays from these choices is displayed in Figure 3.17. The signals expected from the radioactive backgrounds and the charged-current neutrino reaction are also shown. It is evident with the present background estimates that gadolinium is inappropriate and, in spite of its advantages, at this time we do not propose to use it. This decision could be changed if the backgrounds due to activity in the acrylic and the PMT glass can be reduced. We do not wish to use the capture on deuterium because of its low efficiency and low-energy signal.

The present proposal is to use 2500 kg of $NaC\ell$ in the D_2O to detect the neutral-current generated neutrons. At this concentration the results of the neutron transport calculations show that 76% of the neutrons generated by external γ-rays leak out into the H_2O and do not constitute a background. On the other hand, 83% of the neutrons generated throughout the volume of the D_2O are captured by the $C\ell$ and ^2H. The neutral-current signal and background rates are summarized in Table 3.14. Table 3.15 summarizes the event rates and backgrounds predicted for 40% photocathode coverage and Table 3.16 does the same for 20% photocathode coverage. A ^8B ν_e flux consistent with the $C\ell$/Ar radiochemical experiment and a total neutrino flux consistent with the SSM are assumed. The event rates were calculated, as described above and in Annexes-6 and -7. The charged-current backgrounds are the sum of those listed in Tables 3.9, 3.11, and 3.12. The neutral-current signal and background are due to all neutrons captured in the D_2O as listed in Table 3.14. If desired, during data analysis, the ratio of neutral-current signal to neutral-current background could be improved with a fiducial cut on the data. Almost 50% of the neutral-current background is due to neutrons from external γ-rays. About 75% of these neutrons are captured within 0.5 m of the acrylic whereas only 25% of the neutral-current reaction events occur there.

Capture target	^{2}H	Cℓ	Gd
$\sigma(n,\gamma)$ (barns)	0.0005	33	49000
Amount of additive	0	2500 kg	4.6 kg
Capture efficiency (internal)	24%	83%	83%
Capture efficiency (external)	3.4%	24%	24%
Q-value (n,γ) (MeV)	6.25	8.6	8.0
PMTs hit (average)	28	33	25

Table 3.13: Three possible targets for neutron capture in the D_2O are listed with some of their properties. The capture efficiencies differ for neutrons generated uniformly (internal) throughout the D_2O, such as from the neutral-current signal, and for those generated near the acrylic surface (external) by γ-rays because these latter neutrons have a much higher probability of escaping into the light water (see Figure 3.16).

Source	Neutron Production Rate	Neutron Capture Rate
SSM ν flux	6380	5295
γ's in D_2O	1176	976
γ's from acrylic and H_2O	3251	780
γ's from PMTs	731	175
γ's from NaCℓ	294	244

Table 3.14: Neutron production and capture rates per kt-y leading to high-energy γ-rays are given for the SSM ν-flux and for the main background sources. D_2O with 2500 kg of NaCℓ is assumed.

Threshold		CC	ES	CC Bkgd	NC	NC bkgd
PMT	Energy					
0	0	4500	1138		5295	2167
20	3.69	3402	423	317452	3973	1063
24	4.44	3090	345	46339	3689	991
28	5.19	2718	274	5127	3122	845
32	5.94	2269	212	375	2340	641
36	6.69	1805	163	248	1497	416
40	7.45	1425	115	73	851	240

Table 3.15: Event rates for the charged-current reaction (CC), elastic-scattering reaction (ES) and the CC background for various thresholds with 40% photocathode coverage and a ^8B ν_e flux of $2 \times 10^6\ cm^{-2}s^{-1}$. Also given are the neutral-current (NC) reaction rates assuming a total ν flux of $6 \times 10^6\ cm^{-2}s^{-1}$ and that the neutrons are captured on $C\ell$. The NC background column lists the rates due to neutrons produced throughout the volume of the D_2O. All rates are in events per kt-y, and include detection and reconstruction efficiencies.

Threshold		CC	ES	CC Bkgd	NC	NC bkgd
PMT	Energy					
0	0	4500	1138		5295	2167
12	3.66	2963	327	219293	3344	881
14	4.54	2637	270	47173	2941	777
16	5.42	2299	214	11574	2330	623
17	5.86	2102	187	5321	2014	540
19	6.74	1702	144	1803	1423	385
21	7.63	1315	104	164	893	243

Table 3.16: Event rates for 20% coverage. See caption to Table 3.15.

3.6 Photocathode Coverage

The detection of solar neutrino events in a water Čerenkov detector requires the observation of light pulses of very low intensity. Thus any improvement in the light detection efficiency will lead to improvements in the detector performance. On the other hand the cost of the photomultiplier tubes is high so that the minimum coverage which allows the physics to be extracted must be identified. We argue here that this minimum is about 40% coverage.

The improvement in energy resolution with increasing coverage was demonstrated in Section 3.4.1. As we are proposing to measure the ν_e energy spectrum and to look for distortions of that spectrum from the predictions of a simple β-decay ν_e spectrum, energy resolution has to be an important consideration. Even more important, however, is the reduction in the high-energy tail of the internal radioactive background. This is clearly demonstrated in Figure 3.18 where the spectra expected for the charged-current and neutral-current reactions are shown together with the expected background for photocathode coverages of 20%, 40% and 75%. We see that the peak in the charged-current spectrum is only observed for coverages greater than 40% and that the neutral-current detection using neutron capture on $C\ell$ is only really feasible with at least 40% coverage. It would obviously be a significant advantage in going to higher coverage to extend the range over which the ν_e spectrum could be observed and to increase the neutral-current detection efficiency. More quantitative information is given in Tables 3.15 and 3.16. For example, if we set a minimum neutral-current detection efficiency of 25% or about 1400 events assuming the SSM flux, then the charged-current background with 20% coverage is about 1800 events whereas with 40% coverage it is only 200 events.

Another important consideration is that a minimum number of PMT hits required to allow a satisfactory reconstruction of an event. This reconstruction efficiency is shown in Figure 3.19 where it is seen that for 20% coverage the spectrum we wish to observe would be seriously distorted but that by 40% the efficiency is quite constant down to energies where we will be limited by backgrounds.

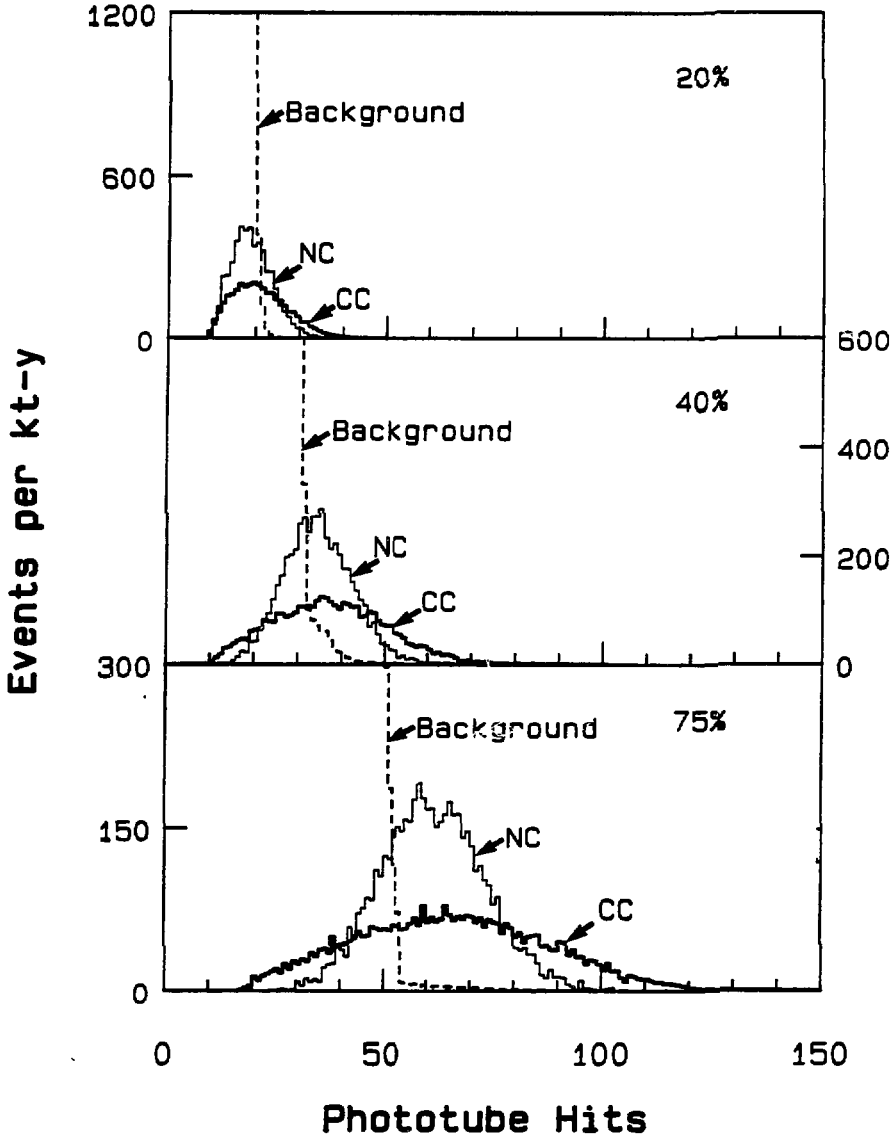

Figure 3.18: Spectra predicted for the charged-current and neutral-current reactions and for the background are shown for 20%, 40% and 75% photocathode coverages. It is assumed that the D_2O is doped with 2500 kg of $NaC\ell$.

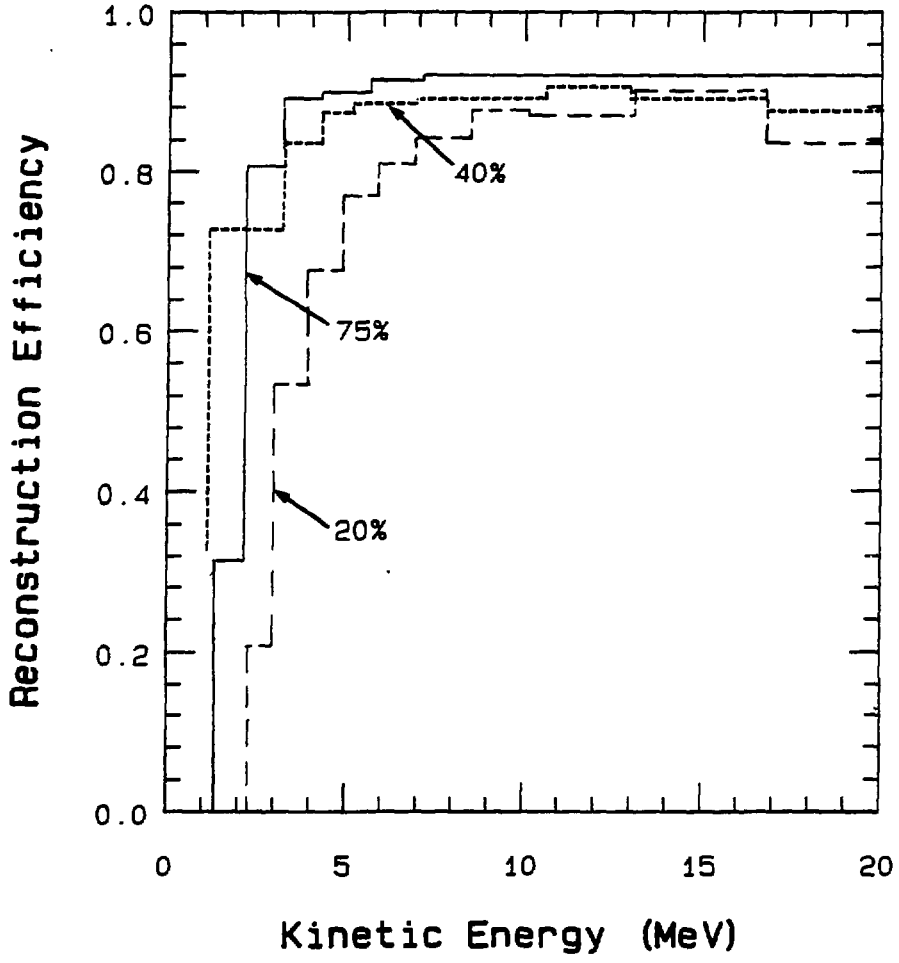

Figure 3.19: Reconstruction efficiency for 20%, 40% and 75% photocathode coverage

3.7 Experimental Program and Expected Detector Performance

The execution of the proposed physics program will require three separate runs. The detector would first be filled with light water so that all systems could be tested. Of prime importance will be the demonstration of the integrity of the D_2O containment but this period would also allow the detector operation to be checked. The time taken to fill and empty the vessel dictates a minimum 6 month period for this run. We anticipate a period of development followed by a period of at least 2 months during which the various sources of background would be identified and measured. The only neutrino signal will be the elastic scattering signal which will give events pointing away from the Sun so any other signals will be due to backgrounds. At this time the elastic scattering reaction would be studied isolated from the charged-current reaction.

We would then fill the detector with pure D_2O and collect data until a satisfactory spectrum is obtained for the ν_e (about 6 months to a year). Salt would then be added to the D_2O to enhance the neutral-current detection and data taking would continue in this mode for as long a period as possible.

If the ^8B ν_e flux is of order $2 \times 10^6\ cm^{-2}s^{-1}$, then a spectrum containing several thousand events would be obtained after running for one year. Spectra for the charged-current and elastic scattering reactions could be separated by examining the angular distributions of the electrons. Figure 3.20 gives a Monte Carlo prediction of the distribution.

As discussed in Section 2.3.4, the ^8B neutrino flux might be much smaller than the upper limit from the $C\ell/Ar$ radiochemical experiment and we must consider the minimum flux which we might be able to detect. To minimize the external backgrounds we would increase the threshold to 40 PMTs. This leaves less than 70 background events per year due to external γ-rays and this can be reduced to less than 6 per year if events directed towards the center of the detector are rejected. At these levels the neutrinos from the *hep* reaction will be the dominant background. The SSM predicts a flux of these neutrinos which would lead to about 50 events per year in the detector of which about 11 would be above the ^8B endpoint. A ^8B ν_e flux of $5 \times 10^4\ cm^{-2}s^{-1}$ would lead to 39 events detected above the 40 PMT threshold per year. This would be clearly observed if the estimated *hep*

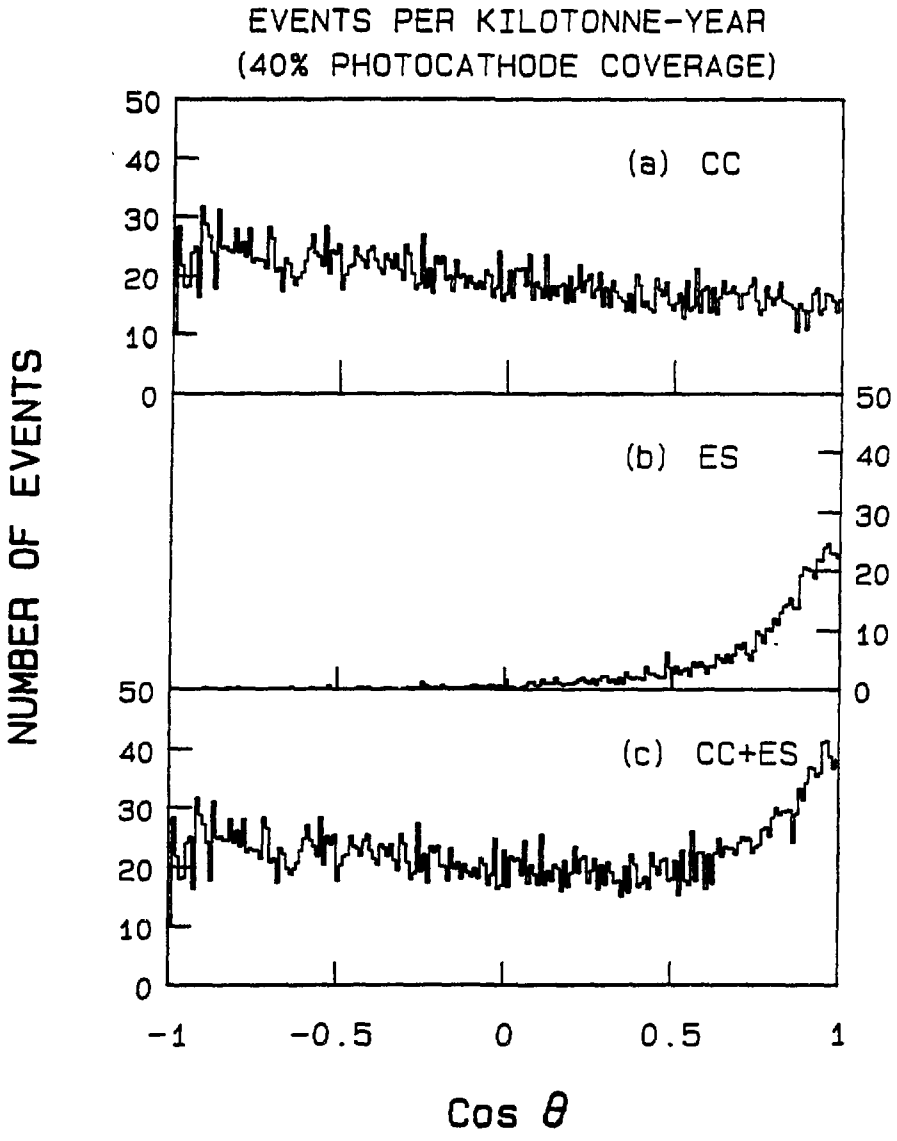

Figure 3.20: Monte Carlo prediction of the angular distribution of events after one year of data taking, with a detector with 40% photocathode coverage. A ^{8}B ν-flux of 2 $\times 10^6$ $cm^{-2}s^{-1}$ is assumed.

flux is correct.

The *hep* neutrinos should also be detectable in the SNO detector. The SSM predicts a flux of $8 \times 10^3\, cm^{-2}s^{-1}$ from this reaction which would lead to 11 events per year above 15 MeV. The largest background in this region is expected to be the tail of the ^{8}B neutrino interactions. The Monte Carlo calculations show that, if the ^{8}B ν_e flux is $2 \times 10^6\, cm^{-2}s^{-1}$, then 1.5 events per year from this source would appear above the 15 MeV (80 PMT) threshold.

The response of the detector to the various reactions and backgrounds, summarized in Table 3.15, implies that if the flux is close to the upper limit set by the Cℓ/Ar radiochemical experiment then spectra relatively free of background will be observed above a threshold of 6 MeV (32 PMTs) and a spectrum for the charged-current reaction containing a few thousand events would be expected after one year of data taking. As the detector resolution and response have been included in calculating the spectra shown in Figure 2.8, it is clear that the distortion predicted by the adiabatic oscillation solution for the SNP would be obvious in such a data set.

The neutral current signal rates expected in an energy window corresponding to PMTs hit between 32 and 44 is about 2300 events per year (Table 3.15). The corresponding charged-current and elastic scattering rate would be about 1400. The charged-current and neutral-current backgrounds would be about 350 and 640, respectively. The statistical accuracy of such a measurement of the total flux would be better than 10%, even if the flux were reduced by a factor of three as would be the case if there are no neutrino oscillations. However, the actual uncertainty would exceed this due to the difficulty in identifying the different contributions to the data. It will be particularly important to identify the sources of radioactivity in the D_2O which could lead to neutron production. This will be done in two independent ways. As discussed in Annex-12, the water will be passed over Mn-coated fibres and the activity removed will give a measure of the radium and thorium in the water. These concentrations can be confirmed by measuring the number of low-energy events within the D_2O. Data from a fiducial cut well within the acrylic tank will give a measure of the ^{208}Tl and ^{214}Bi activities. The absolute calibration for this measurement would be made by introducing well sealed Th and U sources into the D_2O.

3.8 Summary

The measurements and calculations reported in this Chapter show that the extension of large water-Čerenkov detector technology to energies low enough to allow a study of solar neutrinos is feasible. The use of heavy water in an acrylic vessel is practical.

It will be vital to monitor the radioactivity levels at all times during the construction and operation of the detector. It will be important to remove and monitor the radioactivity in the D_2O down to and below the levels assumed in this report because radioactivity contamination in the D_2O provides a uniformly distributed background similar to the solar neutrino neutral-current signal.

The importance of accurate measurements of the radioactive background will depend on the radioactivity levels ultimately achieved in the completed detector. If radioactivity levels lower than those anticipated in this report are obtained, then the necessity for accurate radioactive background measurements to obtain a reliable neutral-current solar neutrino reaction rate will be commensurately reduced.

If the solar ^{8}B ν_e flux is close to the upper limit set by the $C\ell$/Ar experiment then it should be possible to measure accurately the spectrum of these neutrinos above 5 MeV, and perhaps determine the *hep* neutrino flux. The largest backgrounds for the neutral-current reaction will be the charged-current events from solar neutrinos.

The question of unravelling the burst of events expected from a supernova has not been addressed in this Chapter. Clearly background rates are unimportant for such events but the unique sensitivity of the detector to so many components of the neutrino flux, together with the mixture of prompt and delayed signals mean that the resulting data could be quite complex to analyze. The analysis also would depend strongly on how far away the collapse occurs and a detailed discussion of various possibilities seems premature.

Chapter 4

Design of Laboratory

4.1 Site of the Laboratory

The Creighton mine of INCO Limited near Sudbury, Ontario has been selected as the site of the laboratory. At 7137′ the Creighton no. 9 shaft is the second deepest continuous mine shaft in the western world[1]. The INCO management expects to continue mining at and below the 7000′ level for the next few decades and a high level of support services will continue to be available in the mine. The neutrino detector will be located at the 6800′ level in the host rock (norite) far enough away from the mining activities that they will neither interfere with the stability of the cavity nor the detector operation. This site offers the advantages of excellent shielding from cosmic-rays, a stable homogeneous rock formation, a manageable level of background from terrestrial radioactivity and proximity to an active, fully serviced mining area. The underground laboratory will consist of a cavity 20 m in diameter and 32 m high for the heavy-water neutrino detector plus rooms and corridors for the electronics, utilities and services required to operate the detector. In addition, there will be a service building on the surface adjacent to the hoist. An artist's impression of the laboratory is shown in the frontispiece.

Relevant details of the Creighton mine are shown in the longitudinal in

[1]INCO uses British Engineering Units in mining operations and this practice will be followed to avoid confusion in descriptions of existing facilities in the mine.

Figure 4.1 and the plan of the 6800′ level in Figure 4.2. The mineralization occurs near the contact between the granite gabbro footwall rocks and the norite hanging wall. INCO is actively mining the ore body between the 6600′ and 7000′ level at the present time. The mine is dry except for water introduced in the course of the mining operations which drains down to the 7000′ level from which point it is pumped to the surface. The temperature of the virgin rock at the 6800′ level is 105 to 107°F (about 41°C) and cooling is provided by circulating 1.0 million cubic feet of air per minute through the mine. The air temperature in the mine is almost constant year round and at the 6800′ level it is 70°F (21°C).

The total underground distance to the laboratory is 3.3 *km*, 2.1 *km* down the no. 9 shaft and 1.2 *km* horizontally from the shaft. Access to the 6800′ level for personnel and material is by the hoist in the no. 9 shaft. At present, the hoist cage has two decks each 12′6″ long, 4′10″ wide and 6′2″ high: the cage entrance gate is 4′10″ wide. The load capacity of the cage is 10000 *lbs* on the top deck, 21000 *lbs* on the lower deck and the maximum combined load limit is 21715 *lbs*. There are plans to replace the hoist cage; the new cage will accommodate loads up to 10′ high. There is provision for hanging loads up to 30′ long beneath the cage. Transportation of materials and equipment at the 6800′ level is by a 24″ gauge railway, the minimum cross section on the route from the shaft to the access drift is 6′4″ wide by 6′10″ high at a ventilation door. The cage is fitted with rails and cars loaded on the surface are moved via the hoist to the rail lines underground. Transport of SNO materials and equipment will make use of these existing facilities.

The access drift, which has now been completed, starts at a point adjacent to the mining area 1 *km* from the no. 9 shaft. The drift is 180 *m* long and has a 0.4% grade sloping up from the entrance. The geotechnical survey to establish the stability of the rock, scheduled to start in October 1987, will involve test boring into the proposed site of the cavity from the end of the access drift as well as into the rock on either side . The report on the geotechnical survey enabling a refined design and cost estimate to excavate the laboratory is expected in March, 1988 [Supporting Document SD-1]. A preliminary report will be available in January, 1988.

The question of rock stability is of crucial importance to the construction of this laboratory. Excavation of a cavity of the size required for the detector at this depth is unprecedented and a final decision on cavity dimensions will follow from the results of the geotechnical survey. The only

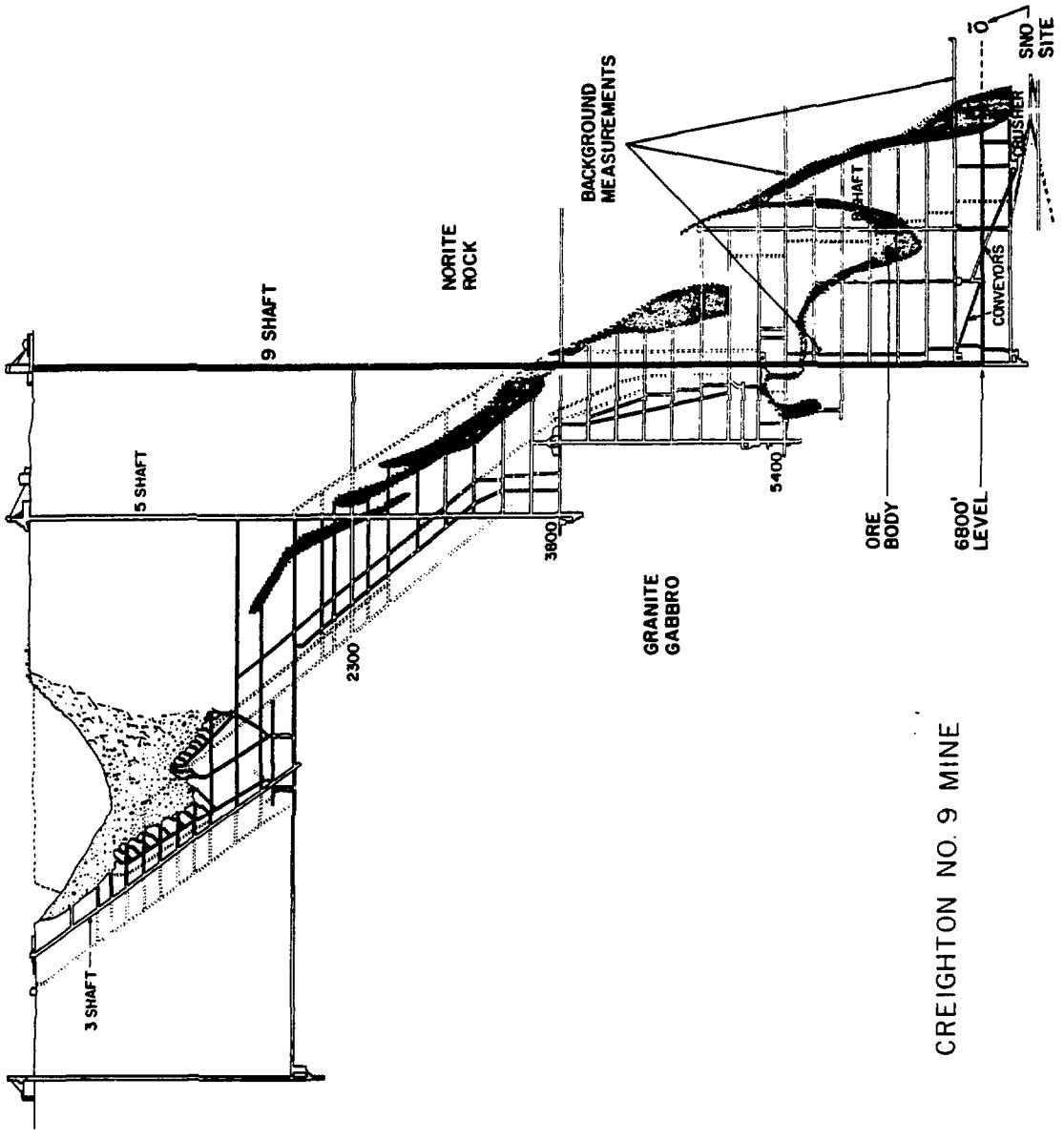

Figure 4.1: Longitudinal of the Creighton Mine showing the location of the neutrino observatory.

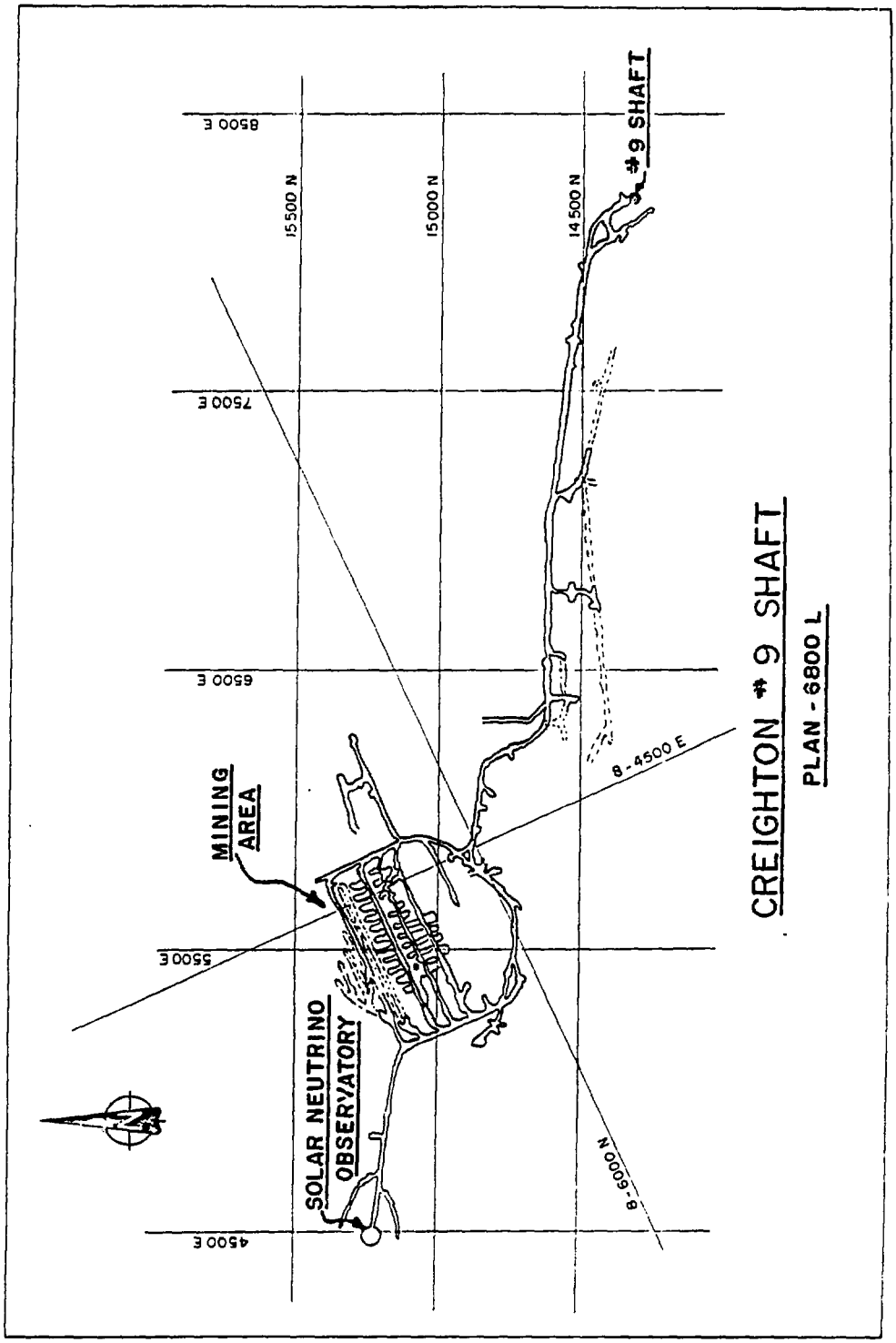

Figure 4.2: Simplified plan of the 6800′ level in the Creighton Mine showing the location of the neutrino observatory, the mining area and the no. 9 shaft.

comparable cavity at similar depth in the Creighton mine is the crusher station on the 7000′ level. Although it is located in the less stable fractured footwall rock no problems with rock instability have occurred during its 10 year life [SD-2] and a geotechnical survey of the rock surrounding the crusher station confirms the reliability of the modeling techniques used [SD-3].

4.2 Description of the Laboratory

4.2.1 The Detector

The detector will consist of 1000 tonnes of 99.92% pure D_2O (heavy water) in a transparent acrylic vessel surrounded by 5000 tonnes of H_2O (light water). The D_2O will be supplied on loan by AECL who must exchange their surplus "low trit" D_2O for virgin Ontario Hydro D_2O since the tritium content in the AECL D_2O would give an undesirable background in the experiment. The interaction of a neutrino with the D_2O/H_2O produces electrons which in turn generate Čerenkov light. The light will be detected by 50 *cm* photomultiplier tubes (PMTs), 1955 PMTs providing 40% photocathode coverage will be immersed in the H_2O. The H_2O shields the D_2O from radioactivity in the surrounding norite rock and in the PMTs. The design of the detector is driven by the need to provide an extremely low background environment for the D_2O. At this depth, backgrounds arise principally from uranium and thorium in the surrounding rock and in the materials from which the detector is constructed. Backgrounds from the rock walls of the cavity will be reduced by successive layers of increasingly clean shielding material, starting with 0.9 *m* of low activity "Sulfurcrete" followed by 4.0 *m* of ultra-pure water. Backgrounds from detector materials will be controlled by careful selection and strict monitoring. Principal sources of these backgrounds are the PMTs and the acrylic vessel. A cross sectional view of the detector is displayed in Figure 1.1. Design studies undertaken in the preparation of cost estimates by INCO TECH and Chalk River Nuclear Laboratories are described in supporting documents SD-2 and SD-4, respectively.

The overall dimensions of the cavity will be 20 *m* in diameter by 32 *m* high. The proposed method for excavation of the cavity is by drilling and blasting. Destressing will be carried out to create a relaxed zone sur-

rounding the facility, so that the possibility of violent rock failure during construction and over the life of the project will be extremely small. The rock surfaces will be secured with cable bolts 30′ in length, a continuous layer of steel screen and a 2″ covering of shotcrete. Shotcrete is a concrete composed of Portland cement and fine aggregate (in this application low radioactivity Haley dolomite) which is sprayed onto the rock surface. Monitoring drifts will be excavated on opposite sides of the cavity and two 3″ holes will be bored from each to within 3′ of the cavity at mid elevation, as shown in Figure 4.3. One hole from each drift will allow possible rock movement to be monitored by the use of extensometers while the other will be used to observe the condition of the rock with borehole cameras. It is anticipated that the monitoring will be done both during excavation and over the life of the laboratory.

"Sulfurcrete"[2] blocks will be used to form the low background concrete shield lining the cavity. "Sulfurcrete" is made of 12% sulphur with 1.2% plasticizer (SRX polymer) as the binder, and for our application, 86.8% low activity dolomite aggregate, in various gradations, obtained from the Timminco Metals quarry at Haley, Ontario. The "Sulfurcrete" blocks will be fabricated in Sudbury to the required size and delivered to the mine. Portland cement concrete also made with the dolomite aggregate will be poured to fill the void between the blocks and the shotcrete. The stainless steel (SS) liner will be made of $\frac{1}{4}$″ sheet welded to SS flat bars which will be tied into the concrete behind the "Sulfurcrete" blocks. A layer of insulation will be cast in position between the SS liner and the "Sulfurcrete" blocks to provide some thermal insulation and prevent points of high local stress from developing in the SS liner when it is filled with water. The dome of the cavity will be covered with 20″ of shotcrete (made using dolomite aggregate) and fibre mesh reinforcing.

The preferred shape of the vessel containing the D_2O is a sphere; however, pending the findings of the geotechnical survey concerning the diameter of the cavity, the vessel design is restricted to a cylindrical configuration with spherical end caps. The vessel will be constructed by bonding pre-formed slabs of acrylic sheet in the detector cavity. To achieve maximum light transmission and minimum radioactivity, no other materials will be used in the construction of the vessel.

[2] "Sulfurcrete" is the registered trade mark of Sulfurcrete Products Inc., Calgary, Alberta.

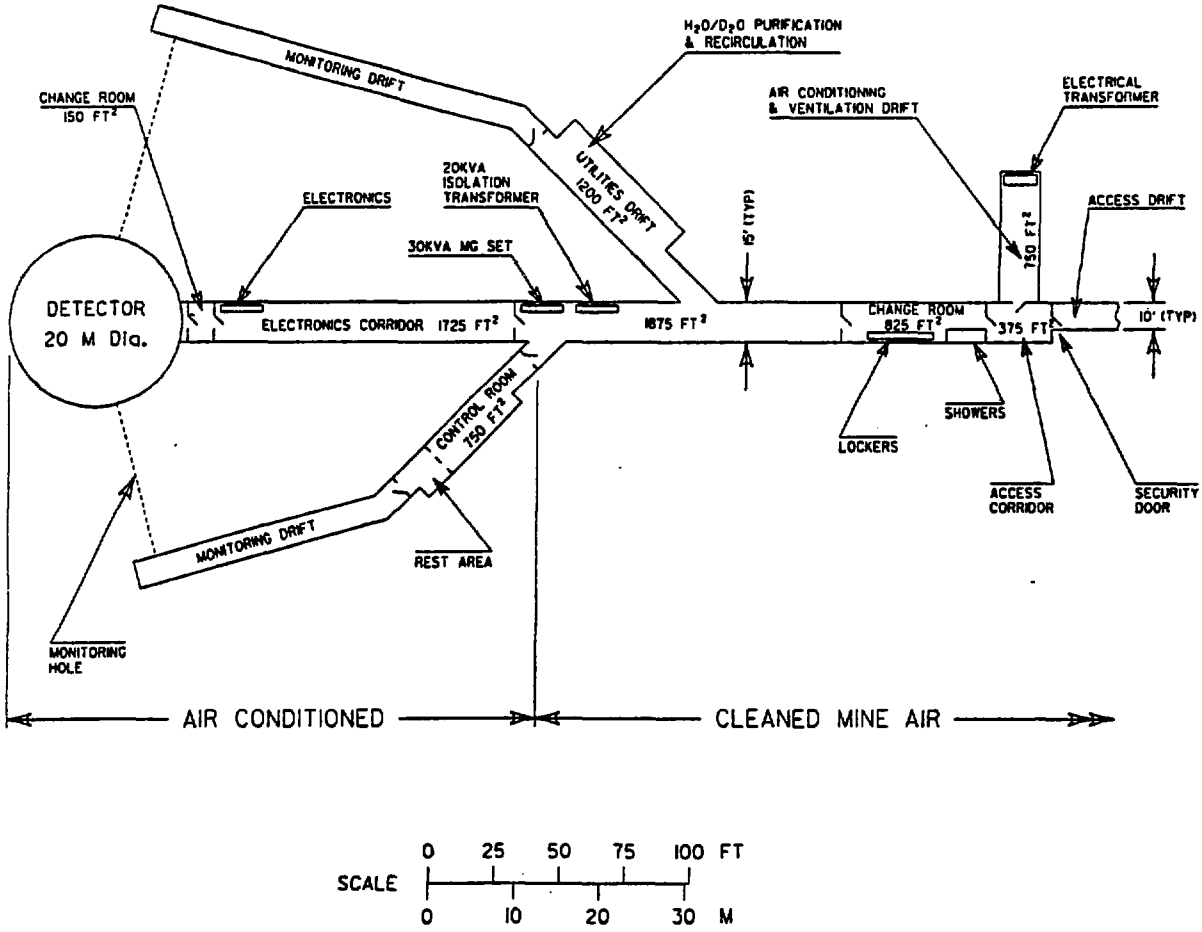

Figure 4.3: Room layout of the laboratory.

Optimization of the vessel design has been carried out by PDA Engineering under the supervision of Reynolds and Taylor Inc., Santa Ana, California, using computer aided finite element stress analysis [SD-5]. Finite element stress analysis on a spherical acrylic vessel has been independently carried out at CRNL [SD-6]. Reynolds and Taylor Inc. will also be responsible for the construction of the vessel. The goal of the analysis was to maximize the strength of the vessel, while minimizing the total mass of the acrylic which is a source of radioactive background. Acrylic sheet, manufactured by Polycast Technology Corporation, has excellent ultraviolet transmittance and low natural radioactivity and would be very suitable for this vessel.

The vessel, shown in Figure 1.1, is 10 m in diameter, with an overall height of 14 m. It is suspended by means of a collar which is made of acrylic to a point near the PMTs where light transmission is no longer necessary and a transition is made to a SS collar. This collar is in turn attached to the deck structure to be described later. The load on the deck structure is greatly reduced due to the immersion of the vessel in the H_2O and the design requires careful control of the D_2O and H_2O levels. Rising from the upper dome of the vessel and extending beyond the deck is a one metre diameter acrylic tube or neck. All penetrations into the D_2O are by way of this neck, and include the D_2O inlet/outlet acrylic pipes, fibre optic light pipes and removable calibration sources.

Since the acrylic vessel has maximum strength under tension, the hydrostatic head of the D_2O with respect to the H_2O, will be maintained so that it is in a constant state of tension. The vessel has been designed such that the life expectancy under normal operating conditions exceeds ten years. To meet this goal, the maximum stresses will not exceed 290 *psi* at any point. After this period of time, aging may become apparent with the appearance of crazing. The ultimate tensile strength of the acrylic is 9000 *psi* and bonded joints must have a strength of 4500 *psi*.

Preliminary maximum tolerable deviations in the hydrostatic heads during both normal operation and filling of the detector have been established by the stress analysis and will be refined following completion of acrylic tests now in progress. The largest anticipated seismic events, both natural and associated with mining operations, have been evaluated at the laboratory site [Annex-17]. The design studies show that these will not threaten the integrity of the vessel in either the empty or filled state.

Thermo-forming, machining and trial assembly of the acrylic vessel components will take place in California prior to shipment to the mine. Clean conditions will be established in the laboratory before assembly of the vessel. Appropriate quality controls and cleaning procedures must be defined for all stages of manufacture. The SNO collaboration will set up a quality control program to monitor thorium and uranium concentrations and light transmittance in the acrylic sheets.

A deck of the space frame type will span the cavity. It will provide a working level during and after construction, support for the acrylic vessel and form an integral part of the gas tight cover system (see Figure 4.4.). It will be supported on steel joists anchored to the rock wall of the cavity and buried in the "Sulfurcrete" blocks. The deck will consist of two parts, a ring structure outside the support collar for the acrylic vessel and a centre section that will be put in place after construction of the acrylic vessel but before its weight is transferred to the deck. The gas tight cover will keep the air above the D_2O and H_2O in the detector free of dust and radon gas. A flexible seal between the deck cover and the neck of the acrylic vessel will allow for small relative movements.

It is envisaged that an overhead crane will span the entire cavity and rotate on a track supported on the steel joists anchored to the cavity walls. Alternatively, portable hoisting equipment may be used.

The PMT support structure will be a space frame concept based on a rectangular grid illustrated in Figure 4.5. Members of this space frame will consist of pre-fabricated elements approximately 2 m long made of either SS or composite polypropylene fibre material. This structure will be anchored to reinforced points on the SS flat bars in the SS liner. The major load on this structure will be due to the buoyancy of the PMTs when the detector is filled with water, resulting in a total force of just over 1 million Newtons. The support structure for those PMTs located inside the acrylic collar will be independent of the main assembly and will be supported from the deck structure. The PMTs will be individually mounted in a restraining harness which will attach to intermediate members [Annex-18]. The harness will consist primarily of non-metallic low radioactivity materials such as polyethylene and provide for support of the watertight PMT base enclosures. The intermediate members will be non-metallic plates with holes cut to accommodate the PMTs and to allow water circulation, but they will be largely opaque to prevent light transmission from beyond the volume defined by the photosensitive surface of the PMTs. One cable per PMT

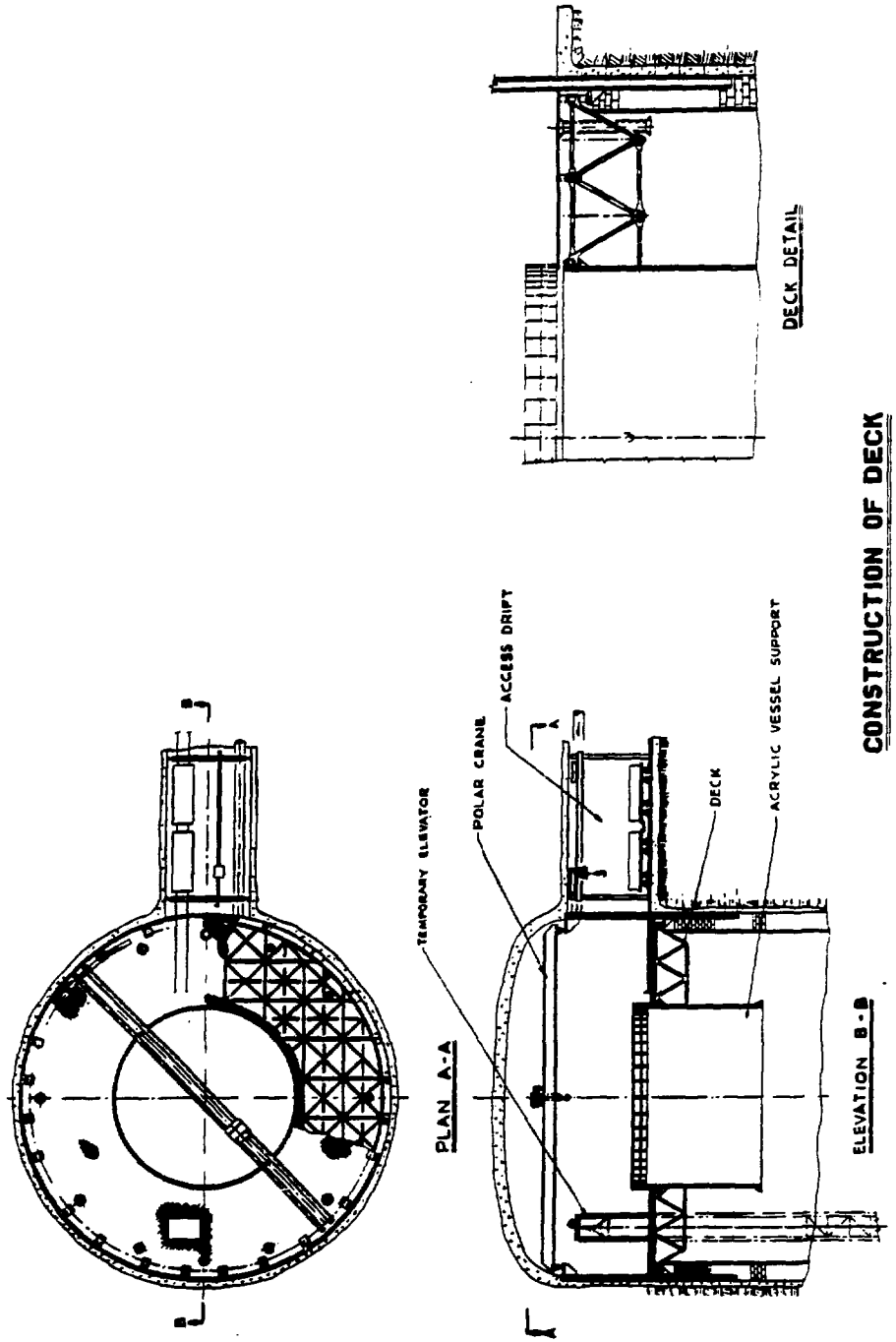

Figure 4.4: Simplified drawing of the deck structure, (a) plan and (b) elevation. The polar crane is shown and a temporary elevator to be used during construction is indicated.

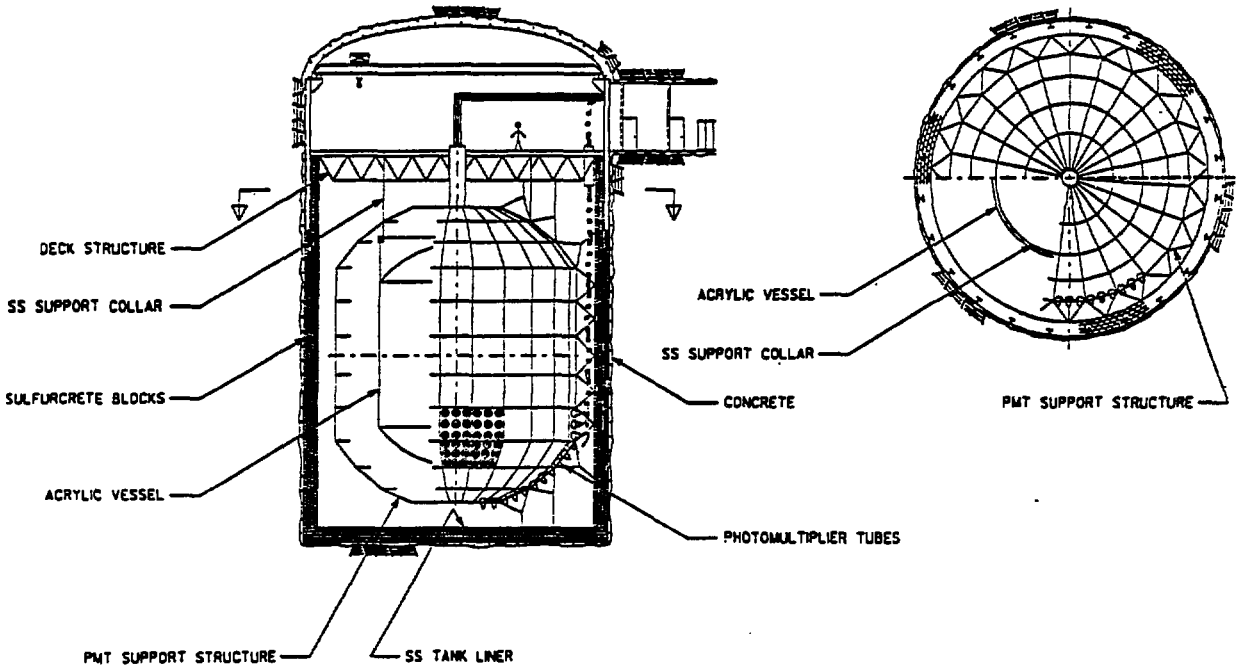

Figure 4.5: General arrangement in the detector cavity of the Sudbury Neutrino Observatory.

will be anchored to the restraining harness, will run up the inner surface of the SS liner and will pass through the gas tight cover via a U-tube air trap.

For optimum performance the PMTs must be operated in a region of low magnetic field and provision will be made to reduce the Earth's field to less than 10% of its nominal value. The compensation will be accomplished by the use of two sets of coils, with axes vertical and horizontal, embedded in the concrete shield surrounding the detector. The vertical set will consist of 79 coils each of 10 turns spaced at 30 *cm* intervals plus a pair of coils one at the top and one at the bottom to reduce fringe effects. The horizontal set will consist of 33 coils each of 10 turns, spaced 60 *cm* apart and encircling the excavated volume below the deck. Both sets of coils [Annex-4] will be anchored to the shotcrete before the "Sulfurcrete" shield is constructed. In this arrangement the coils are inaccessible once the "Sulfurcrete" shield is in place. Leads from each coil will run individually to a terminal board above the deck so that a fault in one coil can then be compensated for by increasing the current in the adjacent coils.

4.2.2 Experimental and Service Areas

The layout of the experimental and service areas of the laboratory is shown in Figure 4.3. The arrangement is governed by the need for extremely low levels of radioactivity in the detector. Thus very clean air is required in the detector cavity, with progressively reduced requirements for air quality in the electronics corridor and in the more remote service areas. These requirements will be achieved primarily by the use of air tight barriers between the various rooms of the laboratory. Change rooms and shower facilities will serve to control movement of radioactive contaminants into the detector cavity. While the electronics and data handling systems are placed closest to the detector in the electronics corridor, the service facilities required for the operation of the laboratory can be more remote. These services include H_2O purification, chilling and circulation, D_2O purification and circulation, and air filtering and conditioning. Two electrical power sources, one standard, the other free of noise from the mining operations are required. Process control, monitoring and safety systems will be interfaced to a master monitoring station operated by INCO. The drifts that will be excavated to monitor rock stability could be enlarged and shielded from the radioactivity in the norite, if necessary, to provide space for other experiments. The cost to provide such space has been estimated by INCO

[SD-2].

The access drift and the various rooms in the laboratory are shown in Figure 4.3. The access drift will be unfinished except for the usual rock bolting and screening and will be separated from the laboratory by a concrete block wall and double door [SD-2]. This wall is typical of the partitions between rooms in the laboratory. An example of a partition is shown in Figure 4.6. The cross section of most of the rooms in the laboratory will be 15′ wide by 15′ high. All room walls and ceilings will be rock bolted, screened and have a 2″ shotcrete coating applied. The surfaces will then be painted with two coats of vinyl paint to control dust and provide a surface that can be kept clean. The reinforced concrete floor will be topped with hardener suitable for waxing to control dust. A "unistrut" frame will be provided throughout to carry services overhead and to support all wall mounted fixtures and panels. A typical section through a room is shown in Figure 4.6.

The experimental electronics including computers and an area for limited electronics repair work will be located in the electronics corridor. The control room contains the instrumentation required to control and monitor the various service systems, the safety systems and interfaces with INCO's monitoring system. It will serve as office space. Facilities for the preparation and storage of food and for personnel to rest will also be located in this room. A motor generator set and isolation transformers to provide clean power to the electronics and to other circuits in the electronics corridor will be positioned opposite the entrance to the control room. The utilities room will contain the D_2O purification system and circulation pumps, the H_2O purification system, chilling and circulation pumps as well as the holding tanks associated with each system. The chiller for the air conditioning system will be in this area. There are two change rooms shown in Figure 4.3. In the one located next to the detector cavity personnel will be able to change into coveralls and special foot wear before entering the detector cavity. The larger change room adjacent to the access corridor will house showers, and facilities for changing from mining gear into conventional laboratory clothing. A chemical toilet will also be located in this area. The electrical power centre will be located in the ventilation room along with the fans required to circulate filtered air through the laboratory.

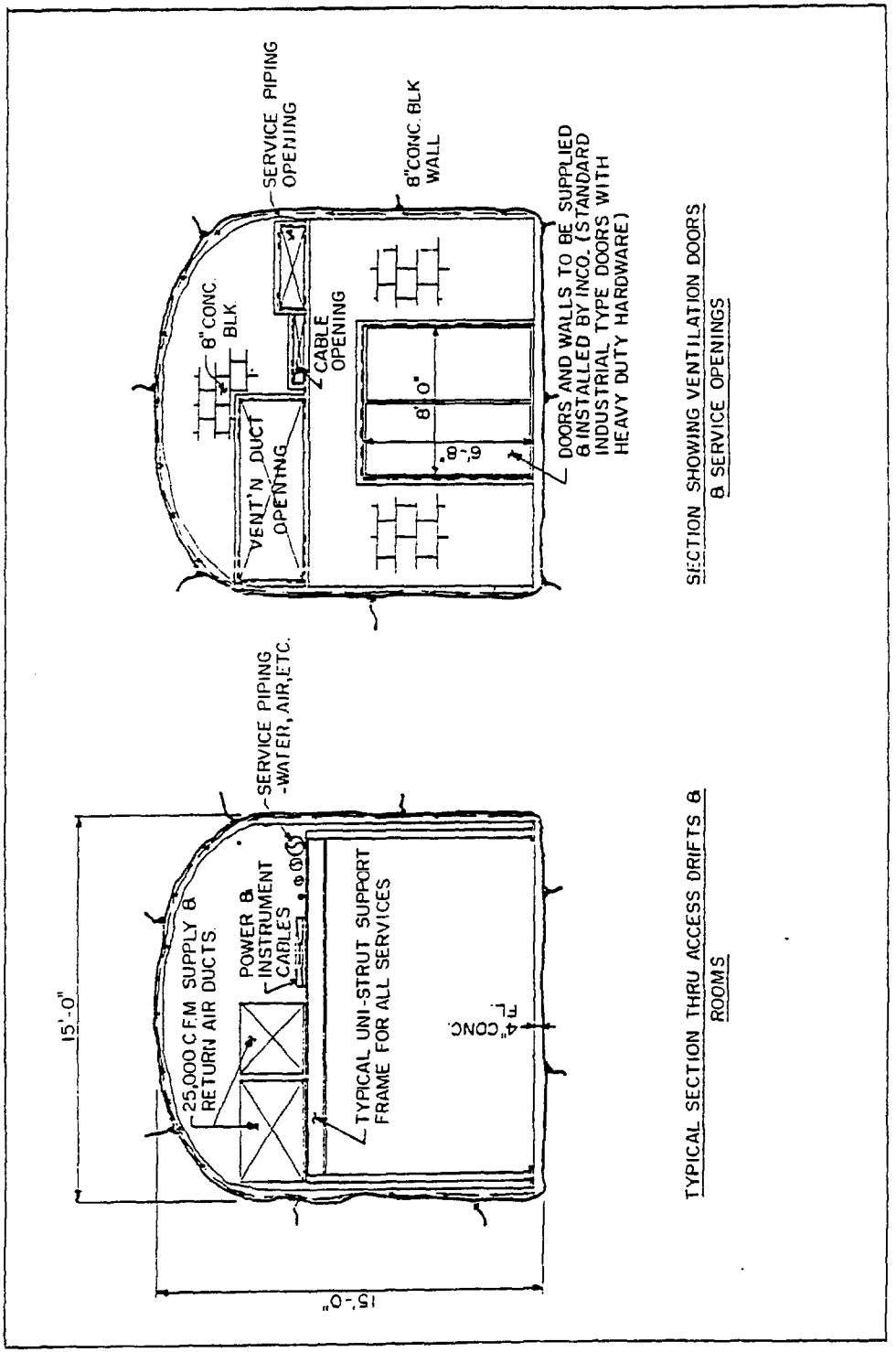

4.6: Typical section through access drifts and rooms and typical air arrier.

4.2.3 Process and Mechanical Systems

The air circulation system will provide the sink for all the heat arising from the laboratory, clean air to all of the laboratory and temperature and humidity conditioned air to the amplifier corridor, the detector cavity and the control room. A total air flow of 25,000 cubic feet per minute will be available to the laboratory, at a temperature of 21°C. The heat exchangers for the air conditioning and water chilling systems will be located in the access drift and the large flow of air required for this purpose will be unfiltered. There will be two stages of filtering; the primary filter for all the air circulating through the laboratory and a secondary filter plus air conditioner for the air supplying the electronics corridor, detector cavity and the control room. The air pressure will be highest in the cavity and lowest in the access corridor to prevent back flow of air from the less clean areas into those rooms where cleanliness has to be of the highest possible standard.

The principle of the water circulation system is indicated on the flow sheet Figure 4.7 [SD-4]. The source of H_2O is the mine water system which draws from the Copper Cliff municipal water supply. The primary purification of the incoming water will be a 5.0 micron filter and the reverse osmosis (RO) process. The second stage of purification will employ ion exchange resins, special filters designed to reduce uranium and thorium concentrations to the required level and a 0.2 micron filter. Ultraviolet sterilization will be used to kill biological organisms. The second stage will handle a total flow of 130 litres per minute (ℓ/min), during filling 38 ℓ/min will come from the primary system and 95 ℓ/min will be recirculated from the detector. The heat exchangers provide for raising the temperature of the intake water to approximately 27°C to optimize the efficiency of the RO process. The H_2O decay tank allows radon dissolved in the intake water to decay before the water is added to the operating detector. After the detector has been filled, the water will be recirculated continuously through the secondary stage at up to 130 ℓ/min. The H_2O in the detector will be kept at 10°C to reduce PMT noise. This will also retard biological growth in the water. To maintain this temperature, heat will be removed by the heat exchanger in the recirculation loop.

The D_2O will be delivered to the laboratory in specially-designed rail cars and transferred into the D_2O holding tank. The acrylic vessel will be filled from the holding tank by passing the D_2O through the filtration sys-

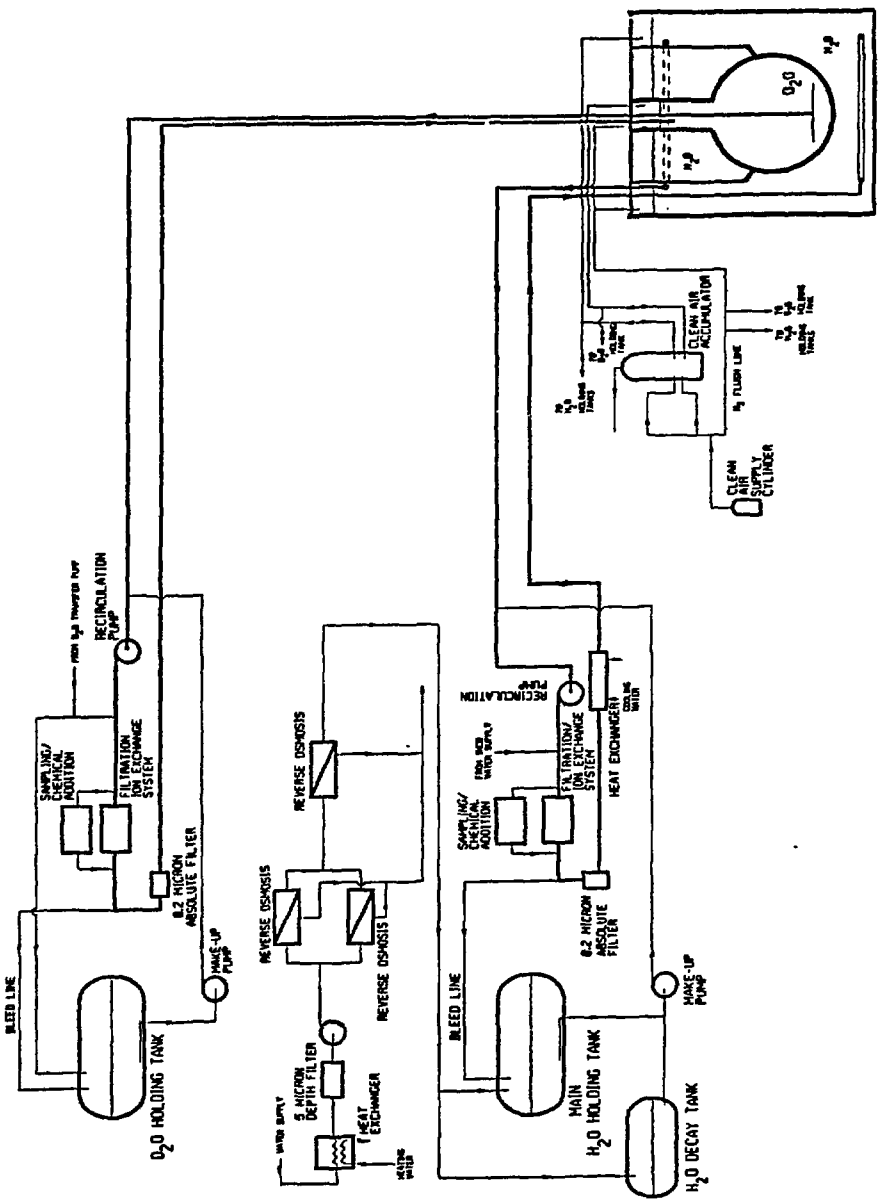

Figure 4.7: Simplified flow diagram of D_2O/H_2O circulation systems.

tem which will be similar to the second stage of the H_2O filtration system. When the detector is in operation the D_2O will be recirculated through the filtration system as required. This will only be done under direct supervision of the operating personnel. The filling of the detector will involve raising the levels of both D_2O and H_2O simultaneously to maintain stresses on the acrylic vessel within prescribed limits. Control of the temperature will be required during the filling to minimize thermal shock to the PMTs and other components. The levels of the D_2O and H_2O will be monitored and controlled at all times to prevent excursions that would overstress the acrylic vessel and support structure.

The gas cover system is designed to prevent dust which may carry radioactivity and radon gas which has evolved from the rock from reaching the detector and to prevent D_2O loss by evaporation. Clean air which has been stored for sufficient time to allow any radon to decay will be used. The gas cover for the D_2O and H_2O will be isolated from each other to prevent D_2O/H_2O exchange and a D_2O recovery system will be provided in the exhaust line from the gas cover for the D_2O.

4.2.4 Electrical and Instrumentation

Electrical power for the laboratory will be supplied through a portable mine power centre rated at 500 kVA and a portable mine distribution centre rated at 400 A, 600 V. These are standard items at INCO and will be used during the construction of the laboratory. It is estimated that the power requirements of the operating laboratory will be about 300 kVA. The power centre will have a more than adequate capacity and the distribution centre can be modified to suit the power requirements of the laboratory. A block diagram of the electrical system is shown in Figure 4.8. The rock at the 6800′ level is dry and is not an effective electrical ground; the electrical ground in the mine is provided by a heavy wire which runs down the no. 9 shaft from the surface. There is substantial noise on the mine ground due to many sources and it will only be used for circuits supplying power to the utilities (eg. pumps, blowers, heat pumps, etc.). The electronics must be well isolated from the electrical noise generated in the mining operations as signal levels in the millivolt range are used at the output of the PMTs. This will be accomplished by providing the power for the electronics from a motor alternator set. A local isolated ground will consist of the SS tank and the wire screening and rock bolts surrounding the detector cavity and

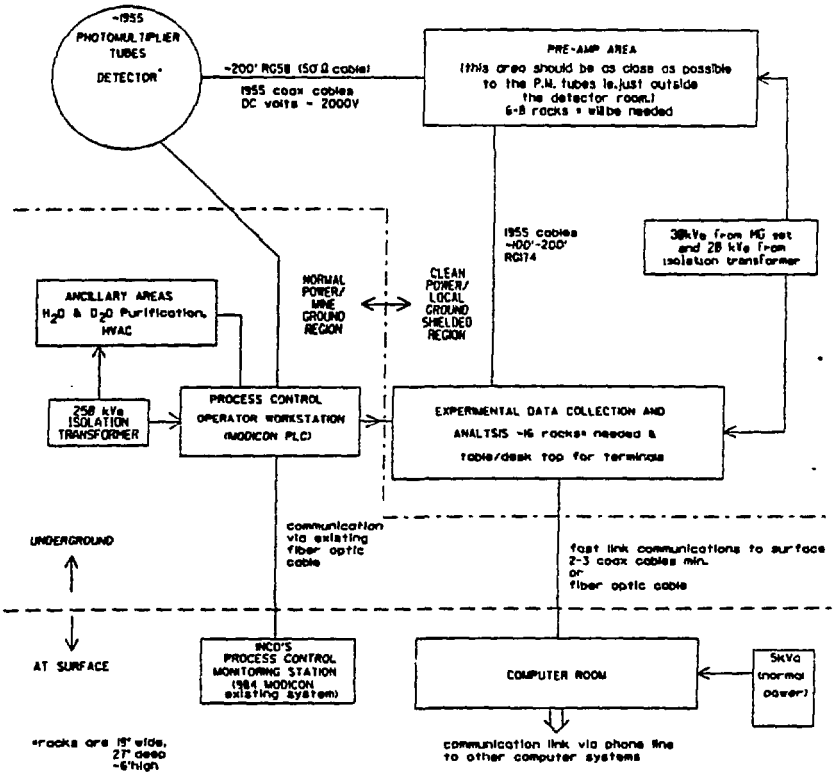

Figure 4.8: Electrical block diagram.

the amplifier corridor. The screening will be isolated from the screening in the rest of the laboratory and should serve to provide electrical shielding for the detector. Other power used in the isolated part of the laboratory such as for lights and for compensating coils for the Earth's field will come from special isolation transformers. Water lines, ventilation ducts and other services will have insulating sections to prevent coupling in of noise on the mine ground. Power lines required for services that are only used when the detector is not operating (e.g. crane) will be supplied from conventional sources and disconnected from the source and connected to the local ground when not in use.

The control centre for the process systems will be located in the control room. It will include the instrumentation required to control and monitor the air circulation and conditioning system, power supplies, the H_2O and D_2O systems and the gas cover system. These will include measurements of pressures, temperatures, currents, water levels and water quality (i.e., resistivity and pH). Many of these signals will be available to the experimental instrumentation system and an estimated 30 process alarm points will be monitored by INCO's "PC annunciator" system. Triplicate alarms may be provided on critical systems such as water level indicators.

The link to the surface for data and for communication with INCO's process control monitoring centre will be provided by 6 pairs of fibre optic cables.

4.3 Surface Building

A surface building, 60′ x 80′, with 12′ overhead clearance, will be constructed [SD-2] close to the collar of the no. 9 shaft as indicated in Figure 4.9. This building will be used to provide services and storage facilities for the laboratory when it is in operation as well as providing handling and loading facilities during construction. It is anticipated that materials and components required for the construction of the underground laboratory will be delivered to this building where they will be stored temporarily until required. Peak storage requirements will be met by renting storage space in Sudbury as required. The handling of D_2O is particularly critical and the building, which will be heated, will be large enough to accommodate a 22 ton tanker truck that will deliver the D_2O to the site as well as four rail cars designed to transport the D_2O to the laboratory. Alternatively, the D_2O may be shipped in SS barrels, in which case the transfer to the rail cars would also take place inside the building. A 24″ gauge track will connect the surface building to the collar house. A weigh scale will be provided to allow full and empty rail cars to be weighed and thereby a careful inventory of D_2O to be maintained.

The floor of the area where the D_2O is transferred from the tanker or from the SS barrels to the rail cars will be designed to permit collection of any spilled D_2O. A concrete pad adjacent to the building will provide a clean storage area for dolomite aggregate.

When the laboratory is in operation the surface building will provide a base from which the SNO personnel can operate independently of the INCO facilities. Thus clothing and safety equipment required to enter the mine will be stored in the building and shower and change facilities will be included. A computer will be installed in the building and will be connected to the underground laboratory by a fibre optic link. A small shop for electronics, testing and repair will be provided. Provision will be included for parking several trailers beside the building.

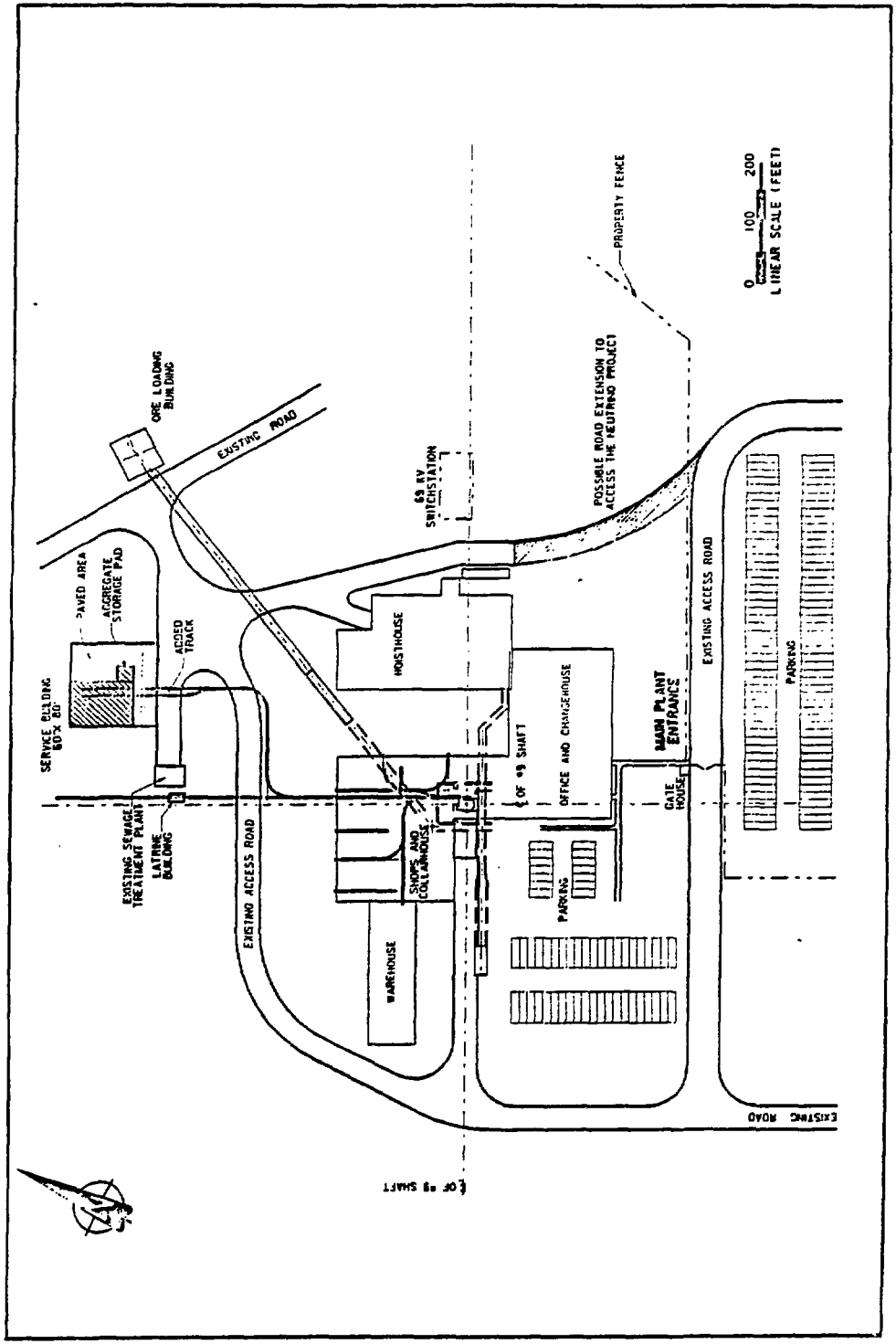

Figure 4.9: Surface plan of Creighton no. 9 shaft showing the Sudbury Neutrino Observatory surface building at top centre.

4.4 Quality Control

Cleanliness will be essential during critical stages of the construction; the closer the location of the components to the D_2O the more stringent the control of radioactive contamination must be. Thus standard mining and underground construction techniques can be used during the excavation and ground control work on the laboratory. An initial clean up will be required before construction of the "Sulfurcrete" and SS liner to prevent inclusion of large quantities of norite in the wall. Before the construction of the acrylic vessel can begin the cavity and the auxiliary rooms and corridors of the laboratory must be cleaned up and the various measures to control transport of dust put in place. In particular, the air filtration system and the barriers with air tight doors must be in operation. The acrylic panels, packaged by Reynolds and Taylor Inc. for shipment, will be transported to the laboratory and only unwrapped after they are inside the clean environment. They will then be cleaned in an ultrasonic bath and moved into the cavity for assembly. Personnel will be required to shower and change out of mining clothes when entering the laboratory. The clean environment must be maintained and cleaning techniques developed for all stages of construction starting with the assembly of the acrylic vessel. For example, it was shown in Section 3.3.4 that the air must be filtered to contain 1/10 to 1/100 the amount of dust in a normal building in order that the activity due to dust settling out on the acrylic does not exceed the activity in the acrylic.

The discussion in Chapter 3 shows how important low levels of radioactive contamination are to successful detection of solar neutrinos. In order to achieve such low levels, stringent monitoring of all the components of the detector will be instituted. This must begin at the raw material stage, during selection of the materials for the "Sulfurcrete", the photomultiplier glass and ceramics, and the acrylic vessel. Procedures for checking the finished components will also be prepared and fitted into the construction schedule. The D_2O and H_2O circulation systems will include facilities for sampling the water and techniques for monitoring radioactivity will be developed.

4.5 Security Systems

Security systems will be required both on the surface and underground to protect both equipment and the D_2O. A security barrier will be provided to separate all the underground facilities of the laboratory from the mine. The security barrier will be a wire mesh barrier with security doors that can be locked, positioned some distance along the access drift. The barrier will be equipped with an alarm and may have a television surveillance system. The surface building will be equipped with secure locks and the outside of the building will be well lit at night. When D_2O is present, security guards will be stationed at the surface building and they will accompany the rail cars when they are transported through the mine to the laboratory. An educational program will be organized to inform the miners and the general public about the value of the D_2O and the fact that it is not a readily marketable commodity.

4.6 Facility Operating Procedures

Standard procedures will be established for the operation of the facility. Improper operation or failure to maintain relative water levels within required limits could result in damage to the acrylic vessel and the possibility of mixing the D_2O and H_2O. Strict attention must be paid to procedures for material and personnel access, water quality maintenance, etc., so that any additional radioactivity is excluded from the detector. The operations instrumentation which will control and monitor the process systems will operate independently of the experimental instrumentation. Although the experimental instrumentation will access information from the operations system, it will not in any way control the process instrumentation.

A trained technical operations group will be set up which will be responsible for the system at all times. During off-shifts, weekends and holidays the monitoring and response activities will be transferred to INCO's operations group. A system will be put in place which will clearly identify when a member of the SNO operating group is in charge of the process systems and when the staff of INCO would be expected to respond to a critical alarm, such as one involving the integrity of the acrylic vessel. A member of the SNO operations group will be on call 24 hours per day. Requests

for changes in the system conditions must be made through the designated operations group.

4.7 Safety

All SNO personnel will be trained in safety and other mine procedures by INCO. Combustible materials will be kept to a minimum underground and smoking will not be permitted. Fire protection will be provided by a "Halon" system, where two simultaneous alarm signals are required to start "Halon" release and shut off ventilation flow. Fire alarms will be monitored at INCO's control centre and communication by telephone will be provided. Emergency lighting will be provided by battery lighting units.

Chapter 5

Program Plan

5.1 Introduction

In order to construct the proposed detector a variety of tasks must be performed or sub-contracted to others by the SNO collaboration. Much of the sub-contracted work of an engineering nature forms the basis for Chapter 4 on the detector design. The engineering documentation for that part of the program plan is referred to in Chapter 4 and summarized in Section 5.2. The development work required to be performed primarily by the SNO collaboration in order to optimize the performance of the Observatory and to bring it into operation efficiently is detailed in Section 5.3. This section summarizes the jobs, the institutions responsible and the time to complete this development work. The costs associated with these responsibilities are summarized in Chapter 7. It is proposed that a large test detector (LTD) be constructed at the NRCC LINAC to simulate in some respects the response of the SNO detector and to act as a test bed for SNO prototypes. The LTD program is discussed in Section 5.4.

5.2 Engineering Documentation

A scope of work document [SD-4] has been prepared by design engineers at CRNL. This document details the many jobs that must be done to

construct the observatory and, in particular, indicates which organization is responsible for each job. It suggests a division of labour which includes INCO Limited, Reynolds and Taylor Inc., CANDU Operations, the SNO physicists, other contractors and CRNL. It suggests, for illustrative purposes, that CRNL act as co-ordinator of the construction of the project. We have used this document as a basis for design requests to the various organizations.

INCO's responsibilities cover engineering review, mining design, excavation, construction and provision of services to the underground laboratory and the surface facilities, and are detailed in a supporting document [SD-2] compiled by E. Armitt, INCO TECH. INCO will excavate the laboratory and install the "Sulfurcrete" and stainless steel liner. They will also provide labour for the assembly of the acrylic vessel and PMTs. In addition to drawings showing how they will carry out these responsibilities, INCO TECH has provided a cost estimate for their responsibilities and a time schedule for the project. Selected items on the INCO TECH time schedule are shown in Figure 5.1. Each item is identified by the INCO number assigned in SD-2.

Reynolds and Taylor Inc. are responsible for designing, supplying and installing the acrylic vessel and their documentation [SD-5] includes cost and time schedule estimates for this. Reynolds and Taylor will fabricate the sections of the vessel from acrylic sheets manufactured by a suitable supplier, probably Polycast Technology Corp.[75] or CY/RO Industries [97]. After 'dry' assembly of the vessel in California it will be dismantled and shipped to Sudbury for installation.

CRNL has prepared a construction sequence [SD-4] continuing from where INCO had completed its construction commitments to commissioning of the facility. This sequence includes installing the acrylic vessel, the PMTs, the water handling equipment, etc. The CRNL document also includes cost estimates of all materials not included in the INCO and Reynolds and Taylor documents except for the PMTs and electronics. CRNL has also considered in a preliminary way the project management and quality control management costs. These latter estimates are supported by a preliminary project execution manual prepared at CRNL [SD-7] which details appropriate procedures for controlling the cost and scheduling of the project and ensuring that the many phases of the project are co-ordinated.

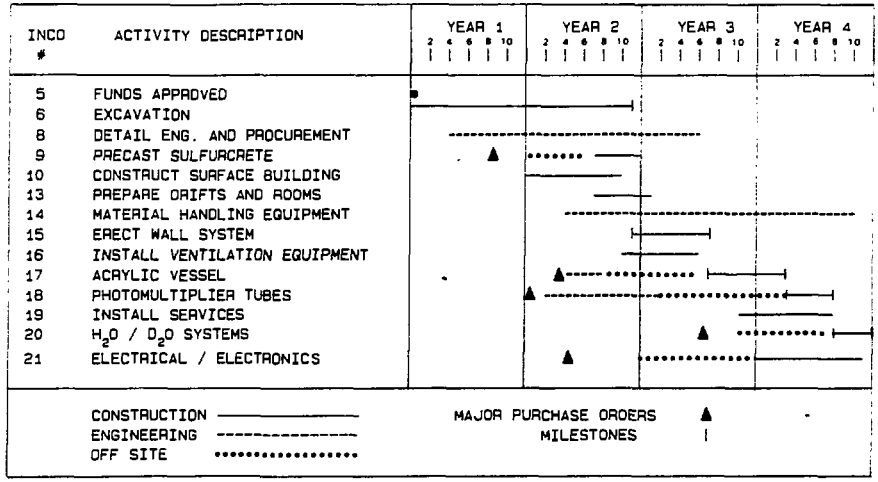

Figure 5.1: Project schedule.

CANDU Operations are responsible for the exchange of AECL and Ontario Hydro heavy water and the delivery of the latter to the mine site. They must ensure that our handling of the heavy water is correct and that the heavy water asset is protected. They have supplied cost estimates and delivery schedules for the D_2O handling together with acceptance of the design to this stage [SD-8].

Queen's University is responsible for the design, construction and testing of the electronics in the data acquisition system as well as for the testing and calibration of the PMTs. Detailed cost estimates and time schedules for these activities have been documented [Annex-4]. Hamamatsu Photonics K.K. in Japan has indicated the cost and delivery schedule for the 50 *cm* PMTs.

A schedule for the completion of the observatory has been prepared by INCO TECH and forms the critical path sequence in Figure 5.1. After funding approval at the beginning of Year 1, there will be 23 months of excavation followed by eight months to erect the "Sulfurcrete" wall and stainless steel liner. Reynolds and Taylor estimate that installation of the acrylic vessel will take eight months and this will be followed by installation of the PMTs (five months) and the water fill (four months). Commissioning of the observatory would begin four years after the approval of funding.

5.3 Development Program

In order to meet these construction dates there are many decision points which must be addressed by the SNO collaboration and in some cases important information is required for the decisions. This information can only be obtained by a strong development and experimental program by the SNO collaboration. A master construction schedule has been prepared [SD-7] which includes the fabrication and delivery times of the observatory components as provided by the engineering firms. Some of these times are indicated in Figure 5.1 by dotted lines. The times to issue purchase orders for "Sulfurcrete" blocks, acrylic vessel, PMTs, water purification system and electronics are indicated by triangles in Figure 5.1.

5.3.1 "Sulfurcrete" Blocks

CRNL has estimated a cost for 90.000 "Sulfurcrete" blocks [SD-4] and a Sudbury construction firm has independently detailed the fabrication procedures and costs. Laurentian University will be responsible for coordinating this activity. Shielding calculations to optimize the design of the cavity wall and ingredients of the blocks will be performed at CRNL and Queen's University. The design and installation of a quality control system for checking that the ingredients of the blocks have the required low levels of Th and U is the responsibility of the University of Guelph. These jobs must be completed eight months after funding.

5.3.2 Acrylic Vessel

While Reynolds and Taylor may have been selected to fabricate the vessel, the vessel design and acrylic suppliers have not been finalized. U.C. Irvine is the institution that will take responsibility for design decisions and procurement of this vessel.

Acrylic from several suppliers has been studied (Chapter 3). The choice of acrylic will depend on its radioactivity, and on its optical and mechanical properties. Measurements of acrylic properties have been and will continue to be carried out at NRCC, CRNL and NBS [Annexes 2,3,14]. To date acrylic samples have been obtained from five manufacturers and the light transmittance and radioactivity of these samples have varied significantly. Two large slabs of Polycast acrylic closely resembling those to be used in the manufacture of the vessel have recently been purchased by the collaboration. The first tests of radioactivity on one slab are very encouraging. The collaboration intends to ask potential suppliers to make samples optimized to our requirements and to test these samples in our facilities. On the basis of these tests, radioactivity and optical specifications will be set for the purchase of the 194 sheets required for the vessel. A quality assurance (QA) program will monitor an appropriate sampling of these sheets. This work will be performed primarily at NRCC and CRNL (see Section 3.3.4 for details). The QA program must be in place 15 months after funding when the vessel should be ordered.

The vessel design in this proposal is conservative as regards the amount

of external shielding provided. It is intended to continue to explore other designs to optimizing the physics potential and cost of the project. In particular, the advantages of a spherical design for the acrylic vessel require that it be given careful consideration. The advantages are thinner acrylic (approximately 2.5 *cm* instead of 5 *cm*), fewer PMTs (approximately 1660), and better detector response since the average D_2O-acrylic distance is increased. The main disadvantage is higher external background if we are constrained to a 20 *m* diameter cavity. The shielding calculations planned for the "Sulfurcrete" blocks will also include various acrylic vessel designs. The vessel design must be finalized in time to obtain CANDU Operations approval before placing the acrylic sheet order, or about ten months after funding. Monte Carlo calculations of the background signal in all designs will be performed at U.C. Irvine.

5.3.3 Photomultiplier Tubes

Since radioactivies in PMT glass is a major constraint in the design and performance of the detector, NRCC and University of Guelph, in collaboration with Hamamatsu Photonics K.K. and Burle Industries, are exploring sources of low activity glass. Burle Industries Inc. in the USA is designing a low cost 20 *cm* PMT to compete with the Hamamatsu 50 *cm* PMT. A prototype should be available in 12 months. To meet the project schedule, a purchase order for the PMTs must be placed 12 months after funding for the improved 50 *cm* PMTs or 18 months after for the new 20 *cm* PMTs. As soon as prototypes are available, sample 50 *cm* and 20 *cm* PMTs will be purchased and tested at Queen's University. The performance of the detector with the different PMT types will be computed by U.C. Irvine.

5.3.4 Water Purification

As detailed in Chapter 3 low radioactivity water is of paramount importance and the levels of activity required dictate removal and analysis techniques on the forefront of this science [Annex-12]. Oxford University is the lead institution in developing these techniques particularly with respect to the Th chain, while Princeton University and University of Guelph are studying the feasibility of monitoring the U chain using γ-ray counting. The time available for solving this problem depends on the installation of

purification equipment in the mine and is about 30 months after funding.

5.3.5 Electronics

The construction and testing of the electronics, from PMTs to data handling, is a major activity. Much of the design and prototyping must be completed 16 months after funding to allow sufficient time for production and testing of individual and assembled components before installation. The present design calls for 1955 50 *cm* PMTs, two flash ADCs per channel and surface mounted components. In this design the front end board is such that it can readily be modified to incorporate a custom made analogue store integrated circuit. A development program is planned to design and test a CMOS analog store system at Queen's University. If successful, this modification to the front end will allow for the multiplexing of the timing and charge signals, reducing the number of ADCs and the capital cost of the electronics. This aspect would be especially important if 12,200 20 *cm* PMTs are used in the final design.

The data acquisition hardware and software will be the responsibility of U.C. Irvine and Princeton University. To operate the detector at low threshold, on-line analysis will be needed to filter the data before storage. The U.C. Irvine will be responsible for developing the necessary software and hardware required for this purpose from the Advanced Computer Project (ACP)[77]. Such a system should be completed within 36 months after funding.

5.3.6 Detector Details

Many details of the observatory have not yet been finalized. The exact dimensions of the cavity must await the INCO TECH geotechnical report. The exact floor area of auxiliary space depends on details of the equipment required for our detector and other experiments. The process equipment for servicing the experiment and laboratory, the alarm and safety monitors and many other incidentals detailed in the scope of work [SD-4] all require input by the collaboration. Queen's University, Laurentian University and CRNL supported by all members of the collaboration will have to oversee these details which will not be forthcoming before significant design funds

have been obtained.

The collaboration will continue to investigate the properties of suitable additives to enhance the neutral-current signal (U.C. Irvine), to measure backgrounds in the mine (Queen's and Laurentian Universities) and to test potential calibration methods (Queen's University). The dimensions of the vessel neck must be fixed 12 months after funding and all calibration options should be explored by that time.

5.4 Large Test Detector

The SNO detector will operate in a low-energy regime which has not yet been explored to any extent by existing large water Čerenkov detectors. The collaboration recognized this problem early on and constructed the small test detector described in Section 3.4.4 to investigate operation at low energy. A much better appreciation of the response of the SNO detector can be achieved through the construction of a large-scale, well-instrumented, test detector of dimensions more nearly approaching those of the proposed detector.

There are several practical reasons why we wish to develop a large test detector (LTD). First, the use of D_2O and the levels of cleanliness required for low-energy operation preclude access to the detector once it is in operation. As it will be imperative to make the SNO detector function with as complete reliability as possible at start-up, we regard the LTD as an indispensable test bed for prototyping many of the component systems which will ultimately be used at the mine. Second, we will have to rely on calibration sources as discussed in Section 3.2.4. To fully understand the calibration we must know how the light production from these sources compares with that of electrons of known energy. A large detector is required to contain the showers from the high-energy γ-ray sources. Third, we wish to study the Čerenkov light produced by the neutron capture processes by which we expect to detect the neutral-current reaction. This again requires a large fiducial volume to contain the γ-rays. Fourth, we wish to test the water purification and monitoring systems to ensure that we can maintain the radioactive purity levels in a system containing PMTs, cables and stainless steel.

It is proposed therefore that a large water-filled test detector (LTD) consisting of a stainless steel right cylindrical vessel, 5 m high by 6 m in diameter, be mounted at one of the beamlines of the NRCC LINAC. This system, containing about 140 tonnes of H_2O, would be of sufficient size to provide a central fiducial volume, about 3 m high and 4 m in diameter, in which γ-ray and bremsstrahlung events are completely contained and full reconstruction of events is possible. PMTs of the type chosen for the SNO detector will be installed to cover 40% of the surface area. Accurate calibration of the system will be achieved by injection of single electrons from the LINAC, as outlined in Annex-15. More details about the LTD can be found in Annex-16.

The main responsibility for constructing the LTD and the electron beam transport system will rest with NRCC and Carleton University. The other groups within the collaboration will be responsible for those items which they will eventually provide for the final detector. Thus Queen's University will provide the electronics and calibration sources, U.C. Irvine will provide a light pulser, U.C. Irvine and Princeton will be responsible for data acquisition and Oxford will provide the water filtration system necessary to remove and monitor the Ra and Th levels.

The LTD is viewed as the main test bed for the systems being developed for the proposed detector. It would operate initially with borrowed PMTs to check out its operation. These would be replaced by PMTs ordered for the SNO detector as they become available. If these photomultiplier tubes are the last to be installed in the underground detector, then more than one year's operation of the fully instrumented LTD would be possible without compromising the SNO assembly schedule. The additional equipment cost to build the LTD is \$75,000 [Annex-16].

Chapter 6

Administration

We propose that the Sudbury Neutrino Observatory (SNO) be operated as a National Facility under procedures similar to those already in place for existing facilities which report through the National Research Council of Canada. As the funding of SNO will in all likelihood involve the participation of provincial and federal bodies, as well as agencies in the United States and the United Kingdom, final administrative and reporting structures will have to be worked out later. In addition, the location of the Observatory in a working mine, contiguous to the commercial operation of a private corporation, will impose unusual constraints on the operation and development of the facility.

The prime focus of the facility is the one kilotonne heavy-water neutrino detector. The scope of this project, and the institutional involvement justify its designation as a National Facility. Once the Observatory exists, proposals will come forward to install projects of smaller scale in the available space, as will proposals for a future generation of large underground detectors. All such proposals must be subject to the approval of INCO Limited, and consistent with the execution of the scientific program associated with the heavy-water detector.

We anticipate that the granting bodies will collectively require reporting mechanisms and a management structure consistent with their own practices. The administrative structure discussed below is put forward as a reasonable basis for future discussion. It is based on the formation of an Institute of Neutrino Physics to administer and exploit the research poten-

tial of the Neutrino Observatory. Its purpose would be first and foremost to implement and execute the experimental program of this proposal, but provision is being made to encompass further experiments related to the neutrino detector or, indeed, new research projects elsewhere in the mine. Membership of the Institute would be open to scientists active in its area of interest - at present the SNO project and proposals for experiments made possible by a low background, deep underground, laboratory.

INCO has indicated that, before participating, it would require a signed agreement with an institution or consortium of institutions which would assume the final fiscal and legal reponsibility for contracts, insurance, etc. We propose setting up an Institute made up of a consortium of participating organizations, duly constituted under the laws of Ontario. A Board of Management would be appointed by institutions with fiscal responsibility for the operation of the Institute and by INCO. This Board would represent the interests of the above institutions and would be responsible for the Institute. They would appoint a director who would be responsible for the day-to-day operation of the Institute. A possible organizational structure is outlined in Figure 6.1 and described below.

The Director would have responsibility for all work of the Institute, and would report to the Board of Management. In particular, the Director would be responsible for the development of the laboratory, beginning with the construction and commissioning of the heavy-water detector and continuing with a consideration of other underground experiments including use of the SNO detector after completion of the heavy-water experiment. Program Committees, and such other committees as may be deemed appropriate, would be appointed by the Director, on either an *ad hoc* or a standing basis.

A Scientific Advisory Council, composed primarily of active scientists of the participating laboratories, would advise the Director on matters affecting the scientific program of the Observatory. This group would also meet from time to time with the Board of Management to assure close communication between the two groups.

The Director would be appointed by the Board of Management, representing the Principal Officer(s) of the responsible institution(s), on the advice of a Search Committee including members of the Board of Management and Scientific Advisory Committee. The Director would normally be appointed for a five-year term and be eligible for reappointment. He or

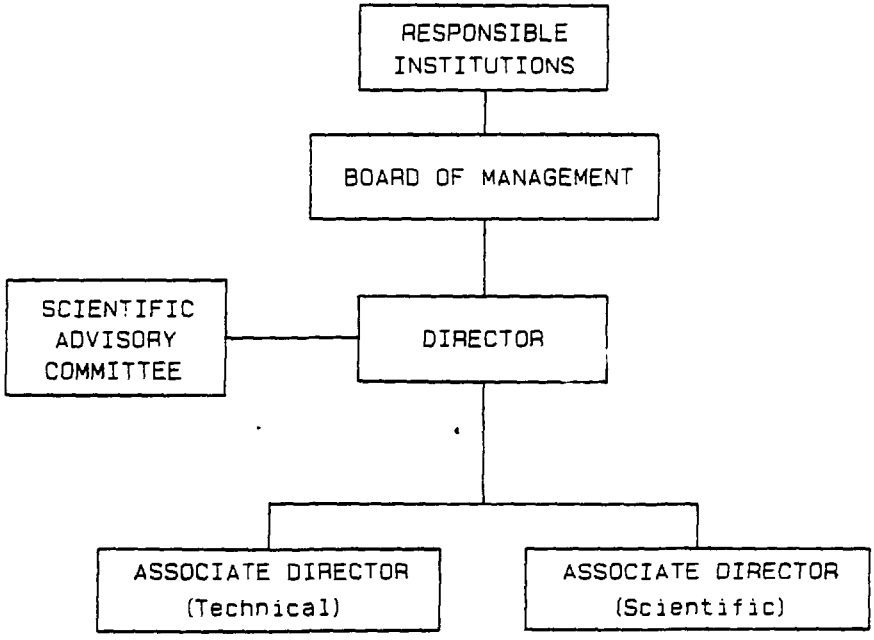

Figure 6.1: Organizational structure of the Institute of Neutrino Physics.

she could appoint Associate Directors to assist in running the laboratory. An Associate Director (Technical) would be responsible for the technical aspects of construction and of running the laboratory and detector. An Associate Director (Scientific) would ensure that the scientific goals for the heavy-water detector are achieved.

The excavation of the cavern and laboratory space, the installation of services, the installation of shielding and the stainless steel tank will be carried out by INCO under contract to the Institute. Upon completion of that phase of the work the installation of the detector and ancillary apparatus will begin. The engineering design of the detector, save for the acrylic vessel, is being carried out by Chalk River Nuclear Laboratories. The engineering design of the acrylic vessel is being carried out by Reynolds and Taylor Inc. We propose that the Institute contract out the management of the construction phase of the project. The Associate Director (Technical) would be responsible for working out, with the INCO Project Manager and the management firm, the logistics of the construction. He or she would be responsible for day-to-day liaison with management at the Creighton mine. Scheduling, procurement, and sub-contracting would be carried out by the firm managing the construction in consultation with the Associate Director (Technical). During the construction phase the Associate Director (Scientific) would be responsible for ensuring that the work of the collaboration as detailed in Chapter 5 is carried out and that the detector is assembled according to the requirements of the scientific program.

During the commissioning of the detector and the subsequent operational phase of the Observatory there will be a continuing need for the Associate Director (Technical) to direct the technical staff, to set priorities for day-to-day activities and to provide liaison with mine management and AECL which has the responsibility for the security of the heavy water. A major responsibility will rest in overseeing the water purification procedures and monitoring the heavy water containment. The Associate Director (Scientific) would oversee the data collection and recommend the scheduling of the phases of the experiment involving light water, heavy water, and heavy water with additives. He or she would assess and co-ordinate other experimental proposals.

We propose that the capital funding for the construction of the Observatory from Canadian sources be administered through the Institute. Funds which originate outside Canada will be administered through the institutions involved in the project in accordance with the practices of those

countries.

The Institute would coordinate the capital funding for construction of the laboratory and the heavy water detector. Funds will be sought from sources inside Canada for the laboratory. Funds for the detector would be sought both inside and outside Canada and contracts arranged for the provision of specific items for the detector. The Institute would submit an infrastructure and operating grant on behalf of the Canadian collaboration while the international collaborators, to fulfil their responsibilites, would request funds through their own agencies. When new experiments are proposed the Institute would continue to be responsible for operating the laboratory but new capital and operating funds for the experiments would be the responsibility of the proponents.

The incorporation of an Institute involving a consortium of participating institutions can require lengthy consultations. In view of the urgency of starting construction of the laboratory as soon as possible Queen's University has been approached to act as the institution with legal and fiscal responsibility until such time as joint responsibility is established. This has been discussed informally with INCO officials and the administrative officers of Queen's University and has been accepted in principle. The provision of indemnification for INCO is still under negotiation. The acceptance in principle by Queen's University of the role proposed above is made on the assumption that these issues can be resolved through consultation with the agencies involved.

Chapter 7

Costs

7.1 Introduction

In this Chapter we outline the capital costs for the detector, the operating costs and a cash flow scenario for the construction phase. The detailed documentation to support the capital estimates has been provided by Chalk River Nuclear Laboratories (CRNL) [SD-4], INCO Limited [SD-2], Reynolds and Taylor Inc. [SD-5], CANDU Operations [SD-8] and Queen's University [Annex-4]. The operating costs of the collaboration during the construction and post-construction phases have been estimated by the various institutions participating in the project and are based on a knowledge of the sophistication of the project and experience in running other research institutions. These estimates are based on the assumption that an Institute of Neutrino Physics be established as discussed in Chapter 6. The cash flow for the capital has been determined with assistance from INCO TECH and project management personnel at CRNL. It is based on a master schedule [SD-7] and a knowledge of the usual practices in the construction industry.

7.2 Capital Costs

The project's capital costs are listed in Table 7.1 in units of millions of Canadian 1987 dollars. The numbers in Table 7.1a are from the INCO

TECH Document [SD-2] and their contingency estimate is listed in Table 7.1g. In addition, INCO will charge the SNO collaboration indirect costs, amounting to $4.16M, associated with the mining and construction services provided. The disposition of these indirect costs, which include depreciation, amortization and overhead, is still under discussion and they are listed at the bottom of Table 7.1.

Table 7.1b lists the estimates from Reynolds and Taylor [SD-5] for the acrylic vessel. Their numbers have been converted to Canadian dollars by assuming a 1.35 exchange rate between U.S. and Canadian funds.

The electronics estimate given in Table 7.1c was prepared by Queen's University personnel and forms part of Annex-4. It includes the cost of the Hamamatsu PMTs as provided to us by Hamamatsu and assumes an exchange rate of 0.00923 between Canadian and Japanese currencies.

The entries in Table 7.1d entitled MATERIALS are the estimates by CRNL design engineers for various materials and detector components not included in the earlier sections of the Table. These estimates, detailed in SD-4, are based on correspondence with suppliers of "Sulfurcrete", boron, spacedecking, process systems, etc. and do not include the 30% contingency suggested by CRNL as appropriate at this stage of a design. This contingency is reported in Table 7.1g.

CANDU Operations are responsible for the exchange of AECL and Ontario Hydro heavy water and the delivery of the latter to the mine head. Their cost estimates and delivery schedules for the D_2O handling are detailed in SD-8.

In addition to the material, labour and similar costs listed in Tables 7.1a to 7.1e each group has indicated design, management and development costs in their respective documents. These costs are summarized in Table 7.1f.

INCO and CRNL have included in their cost estimates contingency costs (Table 7.1g) intended to reflect the uncertainties in the present estimates which are based on the design work to date. In order to reduce these contingency costs significantly more detailed design must be performed. This design work is scheduled for the first year following funding and will require significant engineering effort. The design work and cavity excava-

Table 7.1: Capital Costs (Millions of 1987 Canadian dollars)

7.1a	LABORATORY PREPARATION [SD-2]		
	Excavation of cavity and rooms	2.16	
	Construction of walls and liner	3.59	
	Installation of services	0.51	
	Labour for acrylic and PMT assembly	0.58	
	Surface building site preparation	0.32	
	Electrical installations	1.26	
	Underground handling charges	0.50	
	Dedicated transportation system	0.40	9.32
7.1b	ACRYLIC VESSEL [SD-5]		
	Tooling fabrication	0.38	
	Material cost (Polycast sheet)	0.86	
	Fabrication & labour (California)	0.44	
	Testing requirements and certification	0.05	
	Miscellaneous equipment	0.11	
	Preassembly	0.09	
	Scaffolding	0.14	
	Crating, packaging	0.07	
	Transportation	0.03	
	Mine construction (supervisors & technicians)	0.34	2.51
7.1c	ELECTRONICS [Annex-4]		
	Surface electronics & computer	0.184	
	Experimental electronics	0.718	
	Monitor & safety electronics	0.044	
	Installation supplies & spares	0.144	
	2000 Hamamatsu PMTs	6.590	
	Shipping of PMTs	0.134	7.81

7.1d	MATERIALS [SD-4]			
	"Sulfurcrete", concrete, boron	1.27		
	Insulation, liner	0.59		
	Crane	0.15		
	Deck, PMT support	0.81		
	Underground miscellaneous	0.15		
	Surface building, etc.	0.44		
	H_2O/D_2O handling system	0.48		
	Ventilation	0.17		
	Power supplies	0.04		
	Magnetic field compensation	0.06		
	Safety, security, lighting	0.16		
	Monitoring systems	0.31	4.63	
7.1e	D_2O HANDLING [SD-8]			
	Transportation to the mine	0.5		
	D_2O exchange	0.5	1.0	
7.1f	DESIGN & MANAGEMENT			
	INCO engineering [SD-2]	1.0		
	INCO process development [SD-2]	2.5		
	Reynolds & Taylor design [SD-5]	0.11		
	Electronics design [Annex-4]	0.2		
	Detector design [SD-4]	1.92		
	Project management & control [SD-4]	0.85	6.58	
7.1g	CONTINGENCIES			
	From [SD-4]	2.22		
	From [SD-2]	1.32	3.54	
	TOTAL			35.39
	Indirect costs (under negotiation)		4.16	

tion are the two major expenses during the first year of the project. As discussed in Chapter 5, the purchase orders for the acrylic vessel, the PMTs, the electronics and water handling systems are all to be issued after Year 1.

7.3 Operating Costs

During the construction phase of the project the collaboration will be executing the program plan outlined in Chapter 5 and, in some respects, the "Project management & control" entry in the capital cost table (7.1f) could be considered as an operating cost. An estimate of the operating costs of each participating institution next year (Year 1 of the project) are detailed in Table 7.2. It is assumed that an Institute of Neutrino Physics will be incorporated and a Director and Associate Director (Technical), with administrative support, will be funded from the SNO project operating funds. During Years 2–4 there will be a transfer of technical support from the universities to the Institute, such that by Year 5 the Institute's staff will consist of six technicians and an Associate Director (Scientific) in addition to the two professionals appointed earlier. It is anticipated that at least two of these technicians would be stationed in the Sudbury area and the others would be stationed in the participating institutions but employed by the Institute. The annual operating costs after the construction phase are anticipated to be \$1.4M, of which half is in salaries for the administrative staff, research associates and technicians, and the other half for materials, services and INCO charges (see [SD-2] for INCO's charges). In addition, the cost estimate for insurance against loss or downgrading of the heavy water is \$0.4M per year [SD-8].

The operating cost estimates from the non-Canadian institutions listed in Table 7.2 have been determined by those institutions using procedures applicable in their respective countries for research grant applications. In particular, the U.S. institutions have included the customary salary and total overheads.

Institutions	Year 1	Years 2,3,4
Queen's	$485	$400
Guelph	125	64
Laurentian	36	47
Carleton	82	110
NRCC	192	97
CRNL	250	200
Institute	150	250
Canadian Total	1320	1168
UCI	544	544
Princeton	362	362
U.S. Total	906	906
Oxford	62	66
U.K. Total	62	66

Table 7.2: Annual operating costs during construction in thousands of 1987 Canadian dollars.

7.4 Capital Cash Flow

The proposed project will require the co-operation and co-ordination of several companies and the procurement and delivery of materials from diverse sources. A project execution manual is in preparation detailing accounting, scheduling, and control procedures appropriate for the SNO project [SD-7]. A master schedule has been prepared incorporating the INCO schedule (outlined in Fig 5.1), including appropriate dates for purchase order placements and scheduling the construction and procurement of materials not covered in the INCO document. On the basis of this schedule and the capital costs detailed in section 7.2 a cash flow estimate for the project has been prepared. A breakdown of the anticipated semiannual expenditures is given in Table 7.3. Figure 7.1 shows the cash flow information in graphical form. The INCO indirect costs and the SNO collaboration operating costs have not been included.

	INCO	R&T	Electronics and PMT	Materials and Design	D_2O Handling	Totals
Year 1	0.860			0.97		1.83
	0.910			1.54		2.45
Year 2	2.390	0.11	1.34	2.11		5.95
	3.251	0.50	1.00	0.87		5.62
Year 3	3.270	0.76	1.66	1.49		7.18
	1.665	0.75	1.66	1.42		5.49
Year 4	1.347	0.50	2.35	0.87	0.5	5.57
	0.447			0.35	0.5	1.30
Total	14.140	2.62	8.01	9.62	1.0	35.39

Table 7.3: Semiannual capital cash flow schedule.

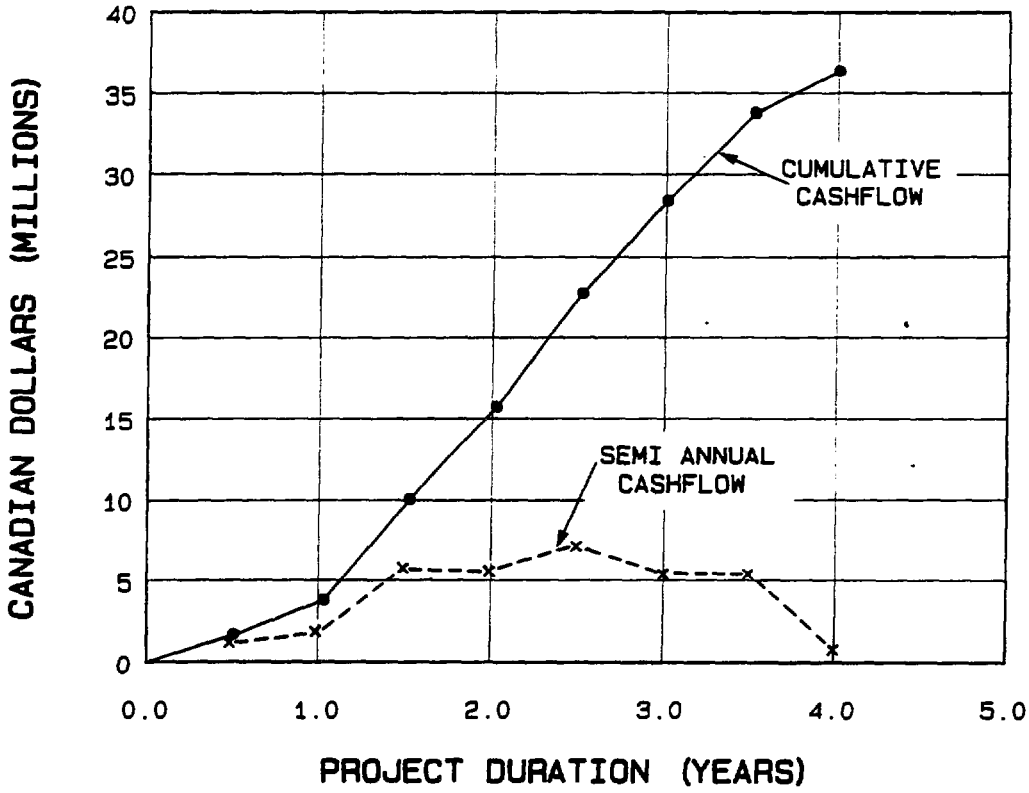

Figure 7.1: Semiannual capital cash flow schedule.

Bibliography

[1] R. Davis Jr. *et al.*, Phys. Rev. Lett. 20, 1205 (1968).
J.K. Rowley *et al.*, in *Solar Neutrinos and Neutrino Astronomy*, ed. M. L. Cherry, W. A. Fowler, and K. Lande (AIP Conf. Proc. No. 126, New York, 1985), p. 1.

[2] J.N. Bahcall, Rev. Mod. Phys. 50, 881 (1978).
J.N. Bahcall *et al.*, Rev. Mod. Phys. 54, 767 (1982).
J.N. Bahcall and R.K. Ulrich, tc be published.

[3] B. Kuchowicz, Rep. Prog. in Phys. 39, 291 (1976).

[4] B. Pontecorvo, Zh. Eksp. Teor. Fiz. 53, 1717 (1967) [Sov. Phys. JETP 26, 984 (1968)];
V. Gribov and B. Pontecorvo, Phys. Lett. 28B, 495 (1969).

[5] S.P. Mikheyev and A. Yu. Smirnov, Nuovo Cimento C9, 17 (1986); Yad. Fiz. 42, 1441 (1985) [Sov. J. Nucl. Phys. 42, 913 (1985)].

[6] L. Wolfenstein, Phys. Rev. D17, 2369 (1978) and Phys. Rev. D20, 2634 (1979).

[7] S. Weinberg, Int. J. Mod. Phys. A 2, 301 (1987).

[8] J.A. Frieman *et al.*, SLAC-PUB-4261, to be published.

[9] M.B. Voloshin *et al.*, Yad. Fiz. 44, 677 (1986) [Sov. J. Nucl. Phys. 44, 440 (1986)];
L.B. Okun' *et al.*, Yad. Fiz. 44, 847 (1986) [Sov. J. Nucl. Phys. 44, 546 (1986)].

[10] F.J. Kelly and H. Überall, Phys. Rev. Lett. 16, 145 (1966).

[11] S. Nozawa *et al.*, J. Phys. Soc. Japan 55, 2636 (1986).

[12] S.D. Ellis and J.N. Bahcall, Nucl. Phys. A114, 636 (1968).

[13] R.C. Allen *et al.*, Phys. Rev. Lett. 55, 2401 (1985).

[14] L.A. Ahrens *et al.*, Phys. Rev. Lett. 51, 1514 (1983); Phys. Rev. Lett. 54, 18 (1985).

[15] H.H. Chen, Phys. Rev. Lett. 55, 1534 (1985).

[16] This is described in many texts, e.g. D.D. Clayton, *Principles of Stellar Evolution and Nucleosynthesis*, McGraw-Hill (1968).

[17] C.W. Allen, *Astrophysical Quantities*, The Athlone Press (1973), p. 161.

[18] J.W. Leibacher *et al.*, Scientific American 253, no. 3, p. 48 (1985); J. Christensen-Dalsgaard *et al.*, Science 229, 923 (1985).

[19] J.N. Bahcall and R. Davis Jr., in *Essays in Nuclear Astrophysics*, ed. C.A. Barnes, D. D. Clayton, and D. N. Schramm, Cambridge University Press (1982), p. 243, and references therein.

[20] J. Rapaport *et al.*, Phys. Rev. Lett. 47, 1518 (1981).

[21] J.N. Bahcall, Phys. Rev. Lett. 17, 398 (1966).

[22] M. Nakahata, reported at the *Workshop on Physics with Solar Neutrinos*, University of California, Santa Barbara (1987).

[23] P.D. Parker, in *Physics of the Sun*, edited by P.A. Sturrock, D. Reidel Publish. Co. Vol 1, (1986), p. 15 (1986); and C. Rolfs *et al.*, Rep. Prog. Phys. 50, 233 (1987).

[24] R.N. Boyd *et al.*, in *Solar Neutrinos and Neutrino Astronomy*, ed. M. L. Cherry, W. A. Fowler, and K. Lande (AIP Conf. Proc. No. 126, New York, 1985), p. 145.

[25] E.E. Salpeter, Nature 225, 165 (1970).

[26] R. Gilliand *et al.*, Ap. J. 306, 703 (1986).

[27] J. Grifols and J. Sola, Phys. Lett. 182B, 53 (1986); M. Fukugita and T. Yanagida, Phys. Rev. Lett. 58, 1808 (1987).

[28] D.H. Perkins, *Introduction to Elementary Particle Physics*, Addison-Wesley Pub. Co. Inc., Third edition (1987), p. 253.

[29] H. Kwon *et al.*, Phys. Rev. D24, 1097 (1981);
J. L. Vuilleumier *et al.*, Phys. Lett. 114B, 298 (1982);
F. Reines, Nucl. Phys. A396, 469c (1983).
K. Gabathuler *et al.*, Phys. Lett. 138B, 449 (1984).

[30] F.W. Bullock and R.C.E. Devenish, Rep. Prog. Phys 46, 1029 (1983);
G. Bernardi *et al.*, Phys. Lett. B181, 173 (1986);
E.B. Brucker *et al.*, Phys. Rev. D34, 2183 (1986);
N. Ushida *et al.*, Phys. Rev. Lett. 57, 2897 (1986).

[31] H.A. Bethe, Phys. Rev. Lett. 56, 1305 (1986).

[32] A.J. Baltz and J. Weneser, Phys. Rev. D35, 528 (1987);
M. Cribier *et al.*, Phys. Lett. B182, 89 (1986).

[33] D.V. Nanopoulos and K.A. Olive, Nature 327, 487 (1987).

[34] S.P. Rosen and J.M. Gelb, Phys. Rev. D34, 969 (1986);
W.C. Haxton, Phys. Rev. Lett. 57, 1271 (1986);
E.W. Kolb *et al.*, Phys. Lett. 175B, 478 (1986);
V. Barger *et al.*, Phys. Rev. D34, 980 (1986).

[35] A.J. Baltz and J. Weneser, *BNL Neutrino Workshop*, 4-7 February (1987), BNL Report 39629.

[36] G. Friedlander and J. Weneser, Science 235, 760 (1987);
J. Weneser and G. Friedlander, Science 235, 755 (1987).

[37] D. Cline, reported at the *Workshop on Physics with Solar Neutrinos*, University of California, Santa Barbara (1987);
J. N. Bahcall *et al.*, Phys. Lett. 178B, 324 (1986).

[38] I.R. Barabanov *et al.*, in *Solar Neutrinos and Neutrino Astronomy*, ed. M. L. Cherry, W. A. Fowler, and K. Lande (AIP Conf. Proc. No. 126, New York, 1985), p. 175.

[39] T. Kirsten in *Proc. 12th Int. Conf. Neutrino Physics and Astrophysics*, Sendai, Japan, June 1986, ed. T. Kitagaki and H. Yuta, World Scientific (1986), p. 317.

[40] K. Wolfsberg *et al.*, , in *Solar Neutrinos and Neutrino Astronomy*, ed. M. L. Cherry, W. A. Fowler, and K. Lande (AIP Conf. Proc. No. 126, New York, 1985), p. 196.

[41] I. Shelton, International Astronomical Union (IUA) Circular No 4316, Feb. 24 1987.

[42] K. Hirata *et al.*, Phys. Rev. Lett. 58, 1490 (1987);
R.M. Bionta *et al.*, Phys. Rev. Lett. 58, 1494(1987);
M. Aglietta *et al.*, Europhys. Lett. 3, 1315 (1987);
A. A. Pomansky, Rencontre de Moriond, in press (1987).

[43] R. Bowers and J.R. Wilson, Ap. J. 263, 366 (1982) and Ap. J., Suppl., 50, 115 (1982).

[44] R. Mayle *et al.*, Ap. J. 318, 288 (1987).

[45] A. Burrows, Ap. J. 283, 848 (1984).

[46] E.W. Kolb *et al.*, Phys. Rev. D35, 3598 (1987);
W. Arnett and J.L. Rosner, Phys. Rev. Lett. 58, 1906 (1987);
J. Bahcall and S.L. Glashow, Nature 326, 476 (1987);
K. Sato and H. Suzuki, Phys. Rev. Lett. 58, 2722 (1987).

[47] M. Aguilar-Benitez *et al.*, Phys. Lett. 170B, 1 (1986);
H. Harari and Y.Nir, Phys. Lett. B188, 138 (1987);
S. Csorna *et al.*, Phys. Rev. D35, 2747 (1987);
S. Abachi *et al.*, Phys. Rev. D35, 2880 (1987);
S. Boris *et al.*, Phys. Rev. Lett. 58, 2019 (1987);
J.F. Wilkerson *et al.*, Phys. Rev. Lett. 58, 2023 (1987).

[48] J.N. Bahcall and T. Piran, Ap. J. 267, 177 (1983).

[49] S.E. Woosley and T.A. Weaver, Ann. Rev. Astron. Astrophys. 24, 205 (1986).
D. Sugimoto and K. Nomoto, Space Science Rev. 25, 155 (1980).

[50] A. Burrows and J.M. Lattimer, Ap. J. 307, 178 (1986).

[51] D.Z. Freedman *et al.*, Ann. Rev. Nucl. Sci. 27, 167 (1977).

[52] S. Shapiro, in *Gravitational Radiation*, edited by L. Smarr, Oxford University Press, (1978).

[53] S.W. Bruenn, Ap. J. Suppl. 62, 331 (1986).

[54] D.K. Nadezhin and I.V. Otroshchenko, Sov. Astron. 24, 47 (1980).

[55] A. Burrows, Ap. J. 318, L57 (1987).

[56] E. N. Alexeyev *et al.* in *Proc. 12th Int. Conf. Neutrino Physics and Astrophysics*, Sendai, Japan June 1986, ed. T. Kitagaki and H. Yuta, World Scientific (1986), p. 270 ;
M. Aglietta *et al.*, Nuovo Cimento 9C, 185 (1986).

[57] D.B. Cline *et al.*, Comments Nucl. Part. Phys. 17, 145 (1987).

[58] P. Langacker, Phys. Rep. 72, 285 (1981).

[59] H. Georgi and S.L. Glashow, Phys. Rev. Lett. 32, 438 (1974).

[60] H.S. Park *et al.*, Phys. Rev. Lett. 54, 22 (1985);
G. Blewitt *et al.*, Phys. Rev. Lett. 55, 2114 (1985).

[61] K. Arisaka *et al.*, J. Phys. Soc. Japan 54, 3213 (1985).

[62] E. Fiorini in *Proc. XXII Int. Conf. High Energy Phys.*, Leipzig, July, 1984, ed. A. Meyer and E. Wieczorek, Vol. I, p. 246; Akad. Wiss. DDR.

[63] F.E. Dix, Ph.D. Thesis, Case Western Reserve University (1970);
F. Reines, Proc. Neutrino '77 2, 327 (1978), Baksan Valley.

[64] E.L. Fireman, Proc Neutrino '77 1, 53 (1978), Baksan Valley.

[65] V.A. Rubakov, Nucl. Phys. B203, 311 (1982).

[66] C.G. Callan Jr., Phys. Rev. D26, 2058 (1982).

[67] L. Arafune *et al.*, Univ. of Kyoto pre-print RIFP-531 (1987).

[68] R.N. Mohapatra and R.E. Marshak, Phys. Rev. Lett. 44, 1316 (1980) and Phys. Lett. 94B, 183 (1980).

[69] C.B. Dover *et al.*, Phys. Rev. D27, 1090 (1983).

[70] M. Takita *et al.*, University of Tokyo pre-print, ICEPP-86-04 (1986).

[71] H. H. Staub in *Experimental Nuclear Physics*, vol. 1 , edited by E. Segrè, John Wiley and Sons, New York, (1953), p. 72.

[72] *Stopping Powers for Electrons and Positrons*, International Commission on Radiation Units and Measurements, Bethesda, Md, Report 37, (1984).

[73] T. I. Quickenden and J.A. Irwin, J. Chem. Phys. 72, 4416 (1980);
M. Hass and J.W. Davisson, J. Opt. Soc. Amer. 67, 622 (1977);
S.A. Sullivan, J. Opt. Soc. Amer. 53, 962 (1963);
A. C. Tam and C.K.N. Patel, Appl. Opt. 18, 3348 (1979);
H. Larzul *et al.*, C. R. Acad. Sci. Paris 261, 4701 (1965).

[74] L. P. Boivin *et al.*, Appl. Optics 25, 877 (1986).

[75] Polycast Technology Corporation, Stamford, Connecticut.

[76] H. Kume *et al.*, Nucl. Instrum. Meth. 205, 443 (1983).

[77] T. Nash *et al.* in *Computing in High Energy Physics*, ed. L. O. Hertzberger and W. Hoogland, Elsevier Science Publishers, North Holland, (1986).

[78] K. Arisaka, Ph.D. thesis, Department of Physics, University of Tokyo, (Report No. UT-ICEPP-85-01), 1985.
T. Kajita, Ph.D. Thesis, Department of Physics, University of Tokyo. (Report No. UT-ICEPP-86-03), 1986.

[79] R. M. Bionta *et al.*, Phys. Rev. Lett. 51, 27 (1983).

[80] R. W. Zurmühle *et al.*, Phys. Rev. 132, 751 (1963).

[81] D. G. Madland and J. R. Nix, Nucl. Sci. Engin. 81, 213 (1982).

[82] E. W. Beier in *Proc. of the Seventh Workshop on Grand Unification/ICOBAN '86*, Toyama, Japan, (April 1986).

[83] W. W. Engle Jr. , Oak Ridge National Lab, K-1693 (1967).

[84] H. M. Colbert, Sandia Laboratories, SLL-74-0012 (1974).

[85] M. A. Lone *et al.*, Nuclear Data Tables 26, 511 (1981).

[86] W. R. Nelson *et al.*, SLAC-Report-265, Stanford Linear Accelerator Center, December 1985.

[87] A. A. Pomansky, Nucl. Instrum. Meth. Phys. Res. B17, 406 (1986).

[88] *Engineering Compendium on Radiation Shielding*, vol. II, edited by R. G. Jaeger, Springer Verlag, (1975), p. 54.

[89] W. S. Moore and L. M. Cook, Nature 253, 262 (1975).

[90] W. S. Moore, Deep Sea Research 23, 647 (1976).

[91] W. S. Moore *et al.*, J. Geophys. Res. 90, 6983 (1985).

[92] J. F. Todd *et al.*, Marine Chemistry, in press.

[93] G. Aardsma *et al.*, J. Radioanal. Nucl. Chem. 111, 111 (1987).

[94] P. Jagam *et al.*, private communication.

[95] *Radiation Shielding*, B. T. Price, C. C. Horton and K. T. Spinney, Pergamon Press, (1957), p. 223.

[96] R. C. Svoboda, Ph.D. Thesis, University of Hawaii, 1985.

[97] CY/RO Industries, Wayne, New Jersey.

Acknowledgments

First and foremost, the proposed Sudbury Neutrino Observatory described in this document would never have reached this stage had it not been for the unstinting help and enthusiastic cooperation of the staff of INCO Limited. Over the four years that has elapsed since the first members of the collaboration visited the Sudbury region to explore with INCO staff the possibility of using a deep underground site for physics research we have been treated with great courtesy and interest at all levels of INCO Limited, whether it be in discussions with senior management or interacting with the miners at Creighton mine or working out the complex engineering details with the staff at INCO TECH.

We extend our special gratitude to :

— Dr. W. Curlook (Executive Vice President, INCO Limited).

— Dr. M. D. Sopko (President, Ontario Division).

— M. C. Kossatz (Vice President Mining, Ontario Division).

— E. Armitt, P. Eng. (Superintendent Design, INCO TECH).

— M. Friesen (Manager, Creighton Complex).

— F. W. Jay (Director, Mines Engineering, INCO Gold).

— J. G. Kelly (Manager, Mines Research, Copper Cliff North Mine).

— P. H. Oliver (Supervisor, Rock Mechanics).

— C. K. Park (Superintendent, Mines Technical Services, Creighton Complex).

— P. W. Pula, P. Eng. (Manager, General Engineering, INCO TECH).

— G. W. Ross (Director Safety, Occupational Health and Environment Control, Ontario Division).

The SNO collaboration gratefully acknowledges financial support provided through the auspices of the Natural Sciences and Engineering Research Council of Canada, the National Research Council of Canada, Atomic Energy of Canada Limited, and the United States Department of Energy.

The SNO collaboration would like to express their gratitude to the President of the National Research Council of Canada, the Principal of Queen's University, and the Dean of Science at the University of California at Irvine for their timely, bold and imaginative initiative in collectively raising some $370,000, thereby permitting the excavation of the dedicated access drift to the proposed site of the laboratory.

In bringing this proposal to fruition the authors have benefitted greatly from the professional assistance of many specialists in disparate fields of expertise. It is a pleasure to acknowledge specifically:

— Drs. J.W. McLaren, S.S. Berman, D. Beauchemin, R.E. Sturgeon and S.N. Willie of the Analytical Chemistry Section, Division of Chemistry, NRCC for developing analytical techniques, among them ICPMS, for the determination of Th and U concentrations at ultra-trace levels in H_2O, D_2O and acrylic.

— Drs. J.J. Beaudoin, V.S. Ramachandran and P. Grattan-Bellew of the Institute for Research in Construction, NRCC for discussions and assistance in identifying a suitable concrete for the shielding of the SNO detector.

— Dr. L.P. Boivin, C.X. Dodd, and Dr. J. Zwinkels of the Photometry and Radiometry Section, Division of Physics, NRCC for spectrophotometry of samples of acrylic, H_2O and D_2O; and for absolute measurements of PMT spectral response.

— W.J. Wells and Z. Jennings of the Manufacturing Technology Centre, Division of Mechanical Engineering, NRCC for cutting acrylic samples using a 2500W CO_2 laser.

— Dr. C.K. Ross and A. Nowak of the Ionizing Radiation Standards Section, Division of Physics, NRCC for operating the LINAC and contributing to the Small Test Detector (STD) project.

— Dr. K.R. Shortt of the Ionizing Radiation Standards Section, Division of Physics, NRCC for provision of ultra-pure water samples and for help in tests associated with immersion of acrylic specimens in liquids.

— Dr. D. J. Worsfold, High Polymer Chemistry Section, Division of Chemistry, NRCC for discussions and measurements related to the leaching of acrylic.

— P. L'Abbe of the Division of Electrical Engineering, NRCC for production of quartz vessels required for acrylic tests.

— S.K.L. Lee, P.C. Gaudert and R.F. Scott of the Structures and Materials Laboratory, National Aeronautical Establishment, NRCC for advice on ASTM engineering tests on bonded acrylic joints.

— M. Kotler, Mrs. A.-L. Thompson and Mme M. C. Léonard, Design Office, Division of Physics, NRCC and Dr. D. S. Ritchie, Divisional Computer Service, Division of Physics, NRCC for design work related to the SNO proposal.

— Drs. R. Cassidy and L. Green, General Chemistry, CRNL, for extensive consultation on analytical analysis techniques for trace analysis of acrylic and D_2O, for supervising acrylic measurements and document preparation.

— Drs. A. Miller, D. Spagnolo, and A. Borodin, Chemical Engineering Branch, CRNL, for discussions and memoranda on D_2O processes, handling and diffusion through acrylic.

— Mr. P.Y. Wong, Mathematics and Computation Branch, CRNL, for shielding calculations and neutron transport calculations utilizing the extensive library of programs at CRNL.

— Mr. L. Howie, Mr. K.M. McFarlane, Mrs. N. Howden and Mr. H. Hatton, Design Division, CRNL, for engineering and technical discussions, document preparation and project cost estimates.

— Mr. K. Ruhland, Project Management, CRNL, for documentation on project management procedures appropriate to the SNO project and Mr. J. Williams, Quality Systems, CRNL, for documentation on appropriate quality assurance procedures.

— R. Deal, Neutron and Solid State Physics, CRNL, for developing an acrylic vaporization technique and vaporizing large quantities of acrylic.

— Mr. A. Middleton and Mr. D. Connelly, Process Systems Design, CRNL, for graphic arts material depicting the proposed facility.

— J. Miller, J. McKenzie and B. Simmons, Ontario Hydro, for their co-operation in supplying the collaboration with D_2O from the Bruce Heavy Water Plant.

— E. Romaniszyn, W. Ward, D. Doering, and N. Elliot, CRNL, for their technical expertise in obtaining information on D_2O and acrylic.

— K. Hafner and J. Sliwka of the Physics Department, Carleton University for help in construction of the Small Test Detector (STD).

— Dr. G. Aardsma of the Institute for Creation Research, San Diego; and Mr. L. Hahn and Mr. R. Lewis at the University of Guelph for their contributions to low-level radiometric measurements.

— Drs. V. Trimble of UC Irvine and A. Burrows of the University of Arizona, for discussions on the topic of stellar collapse.

— Dr. J. A. Bahcall, Institute for Advanced Study, Princeton, for discussions and comments on the SNO proposal.

— Members of the IMB and Kamiokande II collaborations for their comments, suggestions, words of encouragement, and other contributions.

— The IMB Collaboration for the loan of 52 5″ photomultiplier tubes for use in the Small Test Detector (STD).

— Dr. H.W. Sobel and Dr. W.R. Kropp of the IMB Collaboration for discussion about IMB operations.

— Dr. D. A. Sinclair of the IMB Collaboration for the hospitality shown to members of the SNO collaboration during visits to the IMB detector site.

— Dr. W. Gajewski of the IMB Collaboration for discussions about the IMB point fitter.

— The staff of LAMPF, Los Alamos National Laboratory, for loan of scintillator amplifiers for the Small Test Detector.

— Drs. D.W. Davis and T.E. Krogh of the Jack Satterly Geochronology Laboratory, Royal Ontario Museum, Toronto for developing a program using Thermal Ionization Mass Spectrometry for the determination of ultra-low levels of Th and U in D_2O.

— Drs. W.R. Kelly and J.D. Fassett, Center for Analytical Chemistry, National Measurement Laboratory, NBS, Washington for determinations of Th and U by Isotope Dilution Thermal Ionization Mass Spectrometry.

— Dr. P.G. Killen of the Geological Survey of Canada, and Dr. J.A. Soles of the Canada Centre for Mineral and Energy Technology for help in identifying low radioactivity aggregate.

— Dr. J. Pathak of the Canada Centre for Mineral and Energy Technology for discussions on mining techniques.

— Allan Froats, Chief Metallurgist at Timminco Metals, Haley, Ontario for assistance in identifying dolomite as aggregate in the SNO shielding.

— Dr. A.H. Vroom, President of Sulfurcrete Products Inc., Calgary for numerous discussions about the use of "Sulfurcrete" as the shielding material for SNO.

— Dr. T. J. Katsube, Mineral Resources Division, Geological Survey of Canada for a report on possible transport of heavy water through rock.

— H.M. Van Alstyne, CANDU Operations for discussions regarding the provision of the heavy water.

— A. Boothroyd, CANDU Operations for detailed and critical assessment of the design during its development.

— Dr. W. S. Moore of the Department of Geological Sciences, University of South Carolina, Columbia for advice on water purification using Mn-coated fibres.

— Dr. P. Macedo of the Catholic University of America, Washington, D. C. for discussions on water purification.

— The Directors of Science North Museum in Sudbury for their interest in making the aims of the SNO project known in the community.

— F. Miksch, The Minnor K. S. Company in Oslo, Norway;
B.C. Schafer, the U. S. Borax Company, Los Angeles; Dr. R. Meikle, Alcan Ltd., Kingston, Ontario; L. Heymann, G. Gerritse, Indusmin Ltd., Toronto, Ontario for kindly and freely providing the SNO collaboration with constituent high-purity materials for research into a customized PMT glass.

— P. Werner of Quartz Scientific, Fairport, Ohio for advice on producing customized PMT glass.

— P. N. Gaskin and B.B. Hope of the Civil Engineering Department, Queen's University for discussions about sulphur-loaded concretes.

— A. H. Clark and R. J. Uffen of the Geology Department, Queen's University and O. Vogt and M. Wojechowski of the Canada Centre for Mineral and Energy Technology, for helpful discussions about the locations of low activity shielding materials.

Supporting Documents

SD–1 Geotechnical Report from INCO Limited: scheduled for March 1988 (preliminary letter scheduled for January 1, 1988)

SD–2 Sudbury Neutrino Observatory Creighton Mine No. 9 Shaft 6800′ Level, INCO TECH Scope, Job No. 725-101, compiled by E. Armitt, P. Eng., Project Coordinator

SD–3 Preliminary Evaluation of the Stability of the Proposed Neutrino Observatory Excavation at Creighton Mine, P. Oliver, Mines Research, INCO Limited, Copper Cliff, Ontario, February 11, 1986

SD–4 Sudbury Neutrino Observatory Scope of Work-Atomic Energy of Canada Limited Technical Specification 13575-SP-02, Prepared by N.E. Howden, A.L. Howie and K.M. McFarlane

SD–5 Report on the SNO Acrylic Vessel prepared by Reynolds and Taylor Inc., Santa Ana, California 92707, USA

SD–6 Analysis of Spherical D_2O Acrylic Vessel for the Sudbury Neutrino Observatory by H. Hatton and K.M. McFarlane, Process Systems Design Branch, Chalk River Nuclear Laboratories, Chalk River, Ontario, KOJ 1JO (February 1987)

SD–7 SNO Project Management by K. Ruhland, Chalk River Nuclear Laboratories, AECL, Chalk River, Ontario

SD–8 Memoranda from CANDU Operations concerning Heavy Water by A. Boothroyd and H.M. Van Alstyne

Annexes

Reports and Publications

CUL-84-1 **A National Underground Physics Laboratory in Canada**, W.F. Davidson, P. Depommier, G.T. Ewan, and H.-B. Mak, in Proc. of the International Conference on Baryon Non-Conservation (ICOBAN '84), Park City, Utah, 1984, p. 273.

SNO-84-1 **Electronic Detectors for the Study of ^{8}B Solar Neutrinos**, H. H. Chen, AIP Conference Proceedings, No. 126 (American Institute of Physics, New York, 1985), p. 249.

SNO-85-1 **Proposal to Build a Neutrino Observatory in Sudbury, Canada**, D. Sinclair, A.L. Carter, D. Kessler, E.D. Earle, P. Jagam, J.J. Simpson, R.C. Allen, H.H. Chen, P.J. Doe, E.D. Hallman, W.F. Davidson, R.S. Storey, A.B. McDonald, G.T. Ewan, H.-B. Mak, and B.C. Robertson, Il Nuovo Cimento C9, 308 (1986).

SNO-85-2 **A Direct Approach to Solve the Solar Neutrino Problem**, H. H. Chen, Phys. Rev. Lett. 55, 1534 (1985).

SNO-85-3 **Feasibility Study for a Neutrino Observatory Based on a Large Heavy Water Detector Deep Underground**, G.T. Ewan, H.-B. Mak, B.C. Robertson, R.C. Allen, H.H. Chen, P.J. Doe, D. Sinclair, W.F. Davidson, R.S. Storey, E.D. Earle, P. Jagam, J.J. Simpson, E.D. Hallman, A.B. McDonald, A.L. Carter, and D. Kessler.

SNO-85-4 **Determination of the Attenuation Coefficients of Visible and Ultraviolet Radiation in Heavy Water**,

L.P. Boivin, W.F. Davidson, R.S. Storey, D. Sinclair, and E.D. Earle, Appl. Optics 25, 877 (1986).

SNO-85-5 **Modelling the Response of Water Čerenkov Detectors for 3-50 MeV Electrons and Gammas,** R.C. Allen, H.H. Chen, P.J. Doe and K. Roemheld.

SNO-86-1 **SNO: The Sudbury Neutrino Observatory**, J.J. Simpson, G.T. Ewan, H.-B. Mak, B.C. Robertson, R.C. Allen, H.H. Chen, P.J. Doe, D. Sinclair, W.F. Davidson, R.S. Storey, E.D. Earle, P. Jagam, E.D. Hallman, A.B. McDonald, A.L. Carter, and D. Kessler, Proc. VIth Moriond Workshop on Massive Neutrinos in Astrophysics and Particle Physics, Tignes, France, January 1986 (Editions Frontières), p. 151.

SNO-86-2 **A D_2O Čerenkov Detector for Solar Neutrinos**, E.D. Earle, G.T. Ewan, H.W. Lee, H.-B. Mak, B.C. Robertson, R.C. Allen, H.H. Chen, P.J. Doe, D. Sinclair, W.F. Davidson, C.K. Hargrove, R.S. Storey, G. Aardsma, P. Jagam, J.J. Simpson, E.D. Hallman, A.B. McDonald, A.L. Carter, and D. Kessler, Proc. Second Conference on the Intersections between Particle and Nuclear Physics, Lake Louise, 26-31 May, 1986; AIP Conference Proceedings, No. 150 (American Institute of Physics, New York, 1986), p. 1094.

SNO-86-3 **The Sudbury D_2O Neutrino Detector**, E.D. Earle, G.T. Ewan, H.W. Lee, H.-B. Mak, B.C. Robertson, R.C. Allen, H.H. Chen, P.J. Doe, D. Sinclair, W.F. Davidson, C.K. Hargrove, R.S. Storey, G. Aardsma, P. Jagam, J.J. Simpson, E.D. Hallman, A.B. McDonald, A.L. Carter, and D. Kessler, Proc. International Symposium on Weak and Electromagnetic Interactions with Nuclei, Heidelberg, 1-5 July, 1986, (Springer-Verlag), p. 737.

SNO-86-4 **Canadian Underground Project - Sudbury Neutrino Observatory**, G.T. Ewan, H.-B. Mak, B.C. Robertson, R.C. Allen, H.H. Chen, P.J. Doe, D. Sinclair, W.F. Davidson, C.K. Hargrove, R.S. Storey, E.D. Earle, G. Aardsma, P. Jagam, J.J. Simpson, E.D. Hallman, A.B. McDonald, A.L. Carter, and D. Kessler, Proc. Seventh Workshop on Grand Unification ICOBAN '86, Toyama, Japan, April 1986.

SNO-86-5 **A Heavy Water Čerenkov Detector to Study ^8B Solar Neutrinos**, H.H. Chen, R.C. Allen, P.J. Doe, H.C. Evans,

G.T. Ewan, H.W. Lee, J.R. Leslie, J.D. MacArthur, H.-B. Mak, *W. McLatchie, B.C. Robertson, P. Skensved, D. Sinclair*, J.D. Anglin, M. Bercovitch, W.F. Davidson, C.K. Hargrove, R.S. Storey, G. Aardsma, P. Jagam, J.J. Simpson, E.D. Hallman, A.B. McDonald, A.L. Carter and D. Kessler, Proc. Snowmass Summer Workshop, July 1986, (AIP Conf. Proc.), in press.

SNO-86-6 **Sudbury Neutrino Observatory**: Update to Feasibility Study SNO-85-3 (Supplement to grant request), October 1986.

SNO-86-7 **A Heavy Water Detector to Resolve the Solar Neutrino Problem**, G. Aardsma, R.C. Allen, J.D. Anglin, M. Bercovitch, A.L. Carter, H.H. Chen, W.F. Davidson, P.J. Doe, E.D. Earle, H.C. Evans, G.T. Ewan, E.D. Hallman, C.K. Hargrove, P. Jagam, D. Kessler, H.W. Lee, J.R. Leslie, J.D. MacArthur, H.-B. Mak, A.B. McDonald, W. McLatchie, B.C. Robertson, J.J. Simpson, D. Sinclair, P. Skensved, and R.S. Storey, Physics Letters 194, 321 (1987).

SNO-87-1 **Shielding calculations for the SNO Detector**, E. D. Earle and P. Y. Wong, February 1987 (AECL 9393).

SNO-87-2 **Sudbury Neutrino Observatory Scope of Work for INCO**, K. McFarlane, March 1987 (AECL Technical Specification 13575-SP-02).

SNO-87-3 **Operation of the NRC Linear Accelerator with Average Electron Currents less than 10 Attoamperes**, C.K. Ross, A. Nowak, R.S. Storey, M. Bercovitch, and W.F. Davidson, March 1987.

SNO-87-4 **A Heavy Water Solar Neutrino Detector**, E. D. Earle, Lake Louise Winter Institute, February 1987.

SNO-87-5 **The Sudbury Neutrino Observatory**, W. McLatchie and E.D. Earle, 12th Science Teachers Seminar at CRNL, April 2-4, 1987.

SNO-87-6 **The Sudbury Neutrino Observatory**, W. McLatchie and E.D. Earle, August 1987.

SNO-87-7 **Operation and Performance of a Water Čerenkov Test Detector at Low Electron Energies**, M. Bercovitch, J.D. Anglin, W.F. Davidson, S. Fukui, C.K. Hargrove, R.S. Storey,

J.R. Leslie, H.-B. Mak, P. Skensved, D. Kessler, R.C. Allen, H.H. Chen and D. Sinclair, August 1987.

SNO-87-8 **A Monte Carlo Simulation of the Sudbury Neutrino Observatory Heavy Water Čerenkov Detector**, R.C. Allen, G. Bühler, H.H. Chen, H.-B. Mak and K. Roemheld, September 1987 (UCI-Neutrino-87-35).

SNO-87-9 **Simulation of the SNO Heavy Water Čerenkov Detector: Response to Low Energy Phenomena**, R.C. Allen, G. Bühler and H.H. Chen, September 1987 (UCI-Neutrino-87-36).

SNO-87-10 **Sudbury Neutrino Observatory**, G.T. Ewan, H.C. Evans, H.W. Lee, J.R. Leslie, J.D. MacArthur, H.-B. Mak, W. McLatchie, B.C. Robertson, P. Skensved, R.C. Allen, H.H. Chen, P.J. Doe, D. Sinclair, J.D. Anglin, M. Bercovitch, W.F. Davidson, C.K. Hargrove, R.S. Storey, E.D. Earle, P. Jagam, J.J. Simpson, E.D. Hallman, A.B. McDonald, A.L. Carter, D. Kessler, Proc. Int. Conf. on Nuclei Far from Stability, Rosseau Lake, Ontario, Canada, September 1987, in press.

SNO-87-11 **The Sudbury Heavy Water Neutrino Detector**, W.F. Davidson, J.D. Anglin, M. Bercovitch, C.K. Hargrove, R.S. Storey, E.D. Earle, H.C. Evans, G.T. Ewan, H.W. Lee, J.R. Leslie, H.-B. Mak, W. McLatchie, B.C. Robertson, P. Skensved, R.C. Allen, G. Bühler, H.H. Chen, P.J. Doe, D. Sinclair, N.W. Tanner, P. Jagam, J.J. Simpson, E.D. Hallman, A.B. McDonald, A.L. Carter and D. Kessler, Proceedings of the Second International Symposium on Underground Physics, Baksan, Caucasus, U.S.S.R., August 1987.

SNO-87-12 **Sudbury Neutrino Observatory Proposal**, G.T. Ewan, H.C. Evans, H.W. Lee, J.R. Leslie, H.-B. Mak, W. McLatchie, B.C. Robertson, P. Skensved, R.C. Allen, G. Bühler, H.H. Chen, P.J. Doe, D. Sinclair, N.W. Tanner, J.D. Anglin, M. Bercovitch, W.F. Davidson, C.K. Hargrove, H. Mes, R.S. Storey, E.D. Earle, G.M. Milton, P. Jagam, J.J. Simpson, E.D. Hallman, A.B. McDonald, A.L. Carter and D. Kessler, October 1987.